Evolutionary Multi-objective Optimization for Bulldozer and its Blade in Soil Cutting

Thesis Submitted
In Partial Fulfillment of the Requirements
for the Degree of
Doctor of Philosophy

by

Nada Barakat
(Roll No. 136103042)

to the

DEPARTMENT OF MECHANICAL ENGINEERING
INDIAN INSTITUTE OF TECHNOLOGY GUWAHATI
November 2018

CERTIFICATE

It is certified that the work contained in the thesis entitled "***Evolutionary Multi-Objective Optimization for Bulldozer and its Balde in Soil Cutting***", by "*Nada Barakat*", has been carried out under my supervision and that this work has not been submitted elsewhere for a degree.

(Signature with date)

Dr. Deepak Sharma

November, 2018.

Department of Mechanical Engineering,

I.I.T. Guwahati, Assam, India

Declaration

I declare that this written submission represents my ideas in my own words and where others' ideas or words have been included, I have adequately cited and referenced the original sources. I also declare that I have adhered to all principles of academic honesty and integrity and have not misrepresented or fabricated or falsified any idea/data/fact/source in my submission. I understand that any violation of the above will be cause for disciplinary action by the Institute and can also evoke penal action from the sources which have thus not been properly cited or from whom proper permission has not been taken when needed.

(Signature with date)

Nada Barakat

Roll number: 136103042

Department of Mechanical Engineering,

I.I.T. Guwahati, Assam, India

DEDICATED TO

MY BELOVED MOTHER NOUHAD DAYOUB,

MY BELOVED FATHER MARWAN BARAKAT,

MY LOVELY HUSBAND MAHRAN ALGHADA,

MY BELOVED SISTERS RASHA AND NOURA

Abstract

A bulldozer is one of the construction equipment, which has a tractor/engine for supplying power and a metallic blade in its front for soil cutting. A bulldozer experiences enormous resistance due to adhesion, cohesion, and friction between soil and blade. Many studies in the literature focused on determining the cutting force on a blade and observing effect of various input parameters on the force. Except for a few handful studies, an effort has not been made to make the soil cutting operation by bulldozer and its blade economical and productive. In this thesis, the soil cutting operation is modeled as an optimization problem in which the operating conditions of a bulldozer and dimensions of a blade are chosen as decision variables.

Three multi-objective optimization formulations are proposed chronologically by making them realistic and practical in every attempt. In the first attempt, the cutting force is minimized and the volume capacity of a bulldozer blade is maximized with a constraint on the remaining power. In the second attempt, the optimization formulation is made more realistic by simultaneously minimizing the power requirement from a bulldozer to overcome resistance due to the cutting force, and the time required to fill a bulldozer blade with soil. Three problem-specific constraints are also included in this formulation. In the last attempt, the power required from a bulldozer, the time to fill a bulldozer blade, and the number of passes to cut a fixed volume of soil are minimized simultaneously so that different sizes of bulldozer blade can be evolved that can be operated at different operating conditions.

For solving the proposed multi-objective formulations, the existing evolutionary multi-objective (EMO) techniques are used. The classical multi-objective optimization method, that is, the $\epsilon-$constraint method is also used to generate the Pareto-optimal (PO) solutions. The post-optimal analysis is performed among the objectives and decision variables of the obtained PO solutions to develop important relationships among them. For improving convergence of the exiting EMO techniques, a hybrid

procedure is proposed in which three challenges for the local search on `frequency`, `choice`, and `number` of solutions are addressed by using the idea of decomposing the objective space into the structured reference points.

The results demonstrate different nature of the obtained PO solutions for the proposed optimization formulations. The results of the $\epsilon-$constraint method, the perturbation analysis and comparison with the experimental results from the literature suggest that the obtained PO solutions are converged to or very close to the true PO front. The post-optimal analysis deciphers useful and non-intuitive relationships among the objectives and decision variables, which otherwise are difficult to obtain. Some common design principles and dissimilar relationships are extracted that are responsible for trade-off among the PO solutions. The guidelines are then suggested for selecting an appropriate solution and its optimal decision variable values from the set of PO solutions so that a practitioner can choose input parameters for the optimal soil cutting. The results of a hybrid procedure demonstrate that the convergence can be made faster as twice as compared to the exiting EMO technique.

The originality of this work lies in formulating realistic multi-objective optimization formulations, validating the obtained PO solutions through various analysis and from the experimental results, deciphering important relationships from the obtained solutions that can be used for making the guidelines, and a hybrid procedure for improving convergence of the exisiting EMO techniques.

Acknowledgment

I would like to express my deepest appreciation to every single individual who contributed in making this thesis come to its finalized copy.

For the people who mean a lot to me, my parents, **Nouhad Dayoub** and **Dr. Marwan Barakat**, for showing faith in me and giving me liberty to choose what I desired. I salute you all for the selfless love, care, pain and sacrifice you did to shape my life. I would never be able to pay back the love and affection showered upon by my parents.

For timely guidance, extreme patience, support and enthusiasm, I must convey my utmost gratitude to my supervisor **Dr. Deepak Sharma**. Sir, I am in debt to you for all that you have done ever since I met you. I have been extremely fortunate to have had such a genuine, keen and devoted individual as yourself by my side.

My extended gratitude also goes to the Honorable Director of IITG, **Prof. Gautam Biswas** and **Prof. Uday S. Dixit** for their unlimited support.

Very special thanks go to the DC members **Dr. Sukhomay Pal** and **Dr. Ashish Anand** for their presious support. I express my gratitude to all teaching staff of the Mechanical Engineering Department in Indian Institute of Technology-Guwahati for their invaluable support during my PhD program.

I also would like to thank all the members in Syrian High Education Ministry. My greatful thanks go to the Head of Vehicles and Heavy Equipment Engineering Department in Damascus University **Dr. Saeed Alsabek** for being such a true, punctual and particular person.

Last but not least, lots of thanks are granted to my precious husband **Mahran Alghada**, sisters **Rasha Barakat** and **Noura Barakat**, friends and teachers both in India and Syria.

Nada Barakat
IIT Guwahati
November, 2018

Publications

Journal

- N. Barakat and D. Sharma,(2017), "Modeling and Bi-Objective Optimization of Soil Cutting and Pushing Process by Bulldozer", *Journal of The Institution of Engineers (India): Series C*, pages 1-15. https://doi.org/10.1007/s40032-017-0421-7

- D. Sharma and N. Barakat,(2018), "Evolutionary Bi-Objective Optimization for Bulldozer and its Blade in Soil Cutting", *Journal of The Institution of Engineers (India): Series C*, pages 1-16. https://doi.org/10.1007/s40032-017-0437-z

- N. Barakat and D. Sharma, "Evolutionary Multi-Objective Optimization for Bulldozer and its Blade in Soil Cutting", *International Journal of Management Science and Engineering Management*. pages 1-11. https://doi.org/10.1080/17509653.2018.1500953

- N. Barakat and D. Sharma, "A hybrid Evolutionary Multi-Objective Procedure for Continuous Optimization Problems". (Under preparation).

Conference

- N. Barakat and D. Sharma, "Evolutionary bi-objective optimization of soil cutting by bull-dozer: A real-world application," 2017 International Conference on Advances in Mechanical, Industrial, Automation and Management Systems (AMIAMS), Allahabad, 2017, pp. 80-87. doi: 10.1109/AMIAMS.2017.8069193

- N. Barakat and D. Sharma, "Towards Optimal Soil Cutting Process Using a Multi-objective Genetic Algorithm", In Proceedings of the National Conference on Sustainable Mechanical Engineering: Today and Beyond, 24-25 March, 2017, Tezpur University, India

- N. Barakat and D. Sharma, "Multi-Objective Optimization Framework and its Experimental Validation for Bulldozer in Soil Cutting"", In Proceedings of the Indian Geotechnical Conference 2017 GeoNEst, 14-16 December 2017, IIT Guwahati, India

Contents

List of Figures

List of Tables

Nomenclature

α	Angle of cutting blade (radians)
β	Angle that the rupture plane makes with horizontal (radians)
γ_o	Cut soil density (Kg/m^3)
γ	Uncut soil density (Kg/m^3)
θ	Blade curvature angle (radians)
δ	Soil-metal angle friction (radians
φ	Angle of internal friction of soil (radians)
φ_o	Angle of accumulation of cut soil (radians)
μ	The frictional factor between the dozer crawlers and the soil
A_d	Soil adhesion factor (N/m^2)
B	Blade width (m)
C_o	Cohesion of cut soil (N/m^2)
C	Cohesion of uncut soil (N/m^2)
CF_1	Cohesion force on the rupture plane (N)
CF_2	Cohesion force on the sides (bcd) and (nmk) of soil wedge (N)
D	Cutting depth (m)
F_{ad}	Adhesion force between soil and cutting edge (N)
F_{c1}	Cohesion force between soil pile and ground (N)
F_{f1}	Frictional force between soil pile and ground (N)
F_x	The horizontal component of resultant cutting force (N)
F_y	The vertical component of resultant cutting force (N)
F	The resultant cutting force (N)
G	Force acting normal to the face (bcd) and (nmk) of soil wedge (N)
G_1	The weight of dozer equipment (KN)
H	Blade height (m)
L	The cut distance at which the blade is fully loaded (m)
m_1g	Weight of soil pile moving on the ground (fgde) (N)
m_2g	Weight of cut soil (abdgf) sliding up on the surface of the blade (N)

$m_3 g$	Weight of soil wedge (bcdnmk) (N)
N	The number of passes to cut a fixed volume of soil
P	The power required from a bulldozer to overcome resistance
P_{ad}	Adhesion force between blade and cut soil (N)
P_{bull}	The flywheel power of dozer equipment ($KN.m/sec$)
P_{c1}	Cohesion force between soil pile and cut soil (N)
P_{ce}	Force acting on the cutting edge of blade (N)
P_{f1}	Frictional force between soil pile and cut soil (N)
P_{f2}	Frictional force between blade and cut soil (N)
P_F	The power required to overcome the cutting force ($KN.m/sec$)
P_R	The remaining power ($KN.m/sec$)
Q	Normal force on the rupture plane (N)
R	Blade curvature radius (m)
SF_1	Frictional force on the rupture plane (N)
SF_2	Frictional force on the sides (bcd) and (nmk) of soil wedge (N)
T	The time required to cut maximum volume of soil per one pass (sec)
v	The travel speed of dozer equipment (m/sec)
V	The blade capacity (m^3)
V_1	The volume of (fde) of the soil pile (m^3)
V_2	The volume of (afg) of the soil pile (m^3)
V_3	The volume of (abdg) of the soil pile (m^3)
V_4	The volume of the soil pile in the curvature area (ab) (m^3)
W	Force acting normal to the face (bdkn) of soil wedge (N)

Chapter 1

Introduction

A bulldozer is one of the construction equipment, which is mainly used for cutting soil. It consists of a tractor that supplies power to the metallic blade attached at its front. During soil cutting the blade of a bulldozer is inserted in soil up to a certain depth and then starts moving. In this soil cutting operation, a blade experiences a large amount of resistance due to friction, cohesion, and adhesion between a blade and soil.

1.1 Motivation

In this thesis, the soil cutting operation is modeled for a bulldozer and its blade, wherein an emphasis is given to make the operation economical and productive. The operation can be made economical when its variable cost can be reduced. The variable cost depends on the operating conditions which involve many parameters, such as power required from a bulldozer, speed of a bulldozer, depth of a blade inserted in soil, dimensions of a blade, etc. The operation can be made productive when a bulldozer can finish the soil cutting operation as early as possible. However, any productive soil cutting operation with a large size blade operating at a larger speed and a higher cutting depth requires more power from a bulldozer.

In the literature, most of the earlier studies focused on determining the cutting force on a bulldozer blade at different cutting depths (McKyes 1985). For example, many analytical and numerical models have been developed that can determine the cutting force with the desired accuracy. The numerical models were developed using

finite element methods and discrete element methods which were found to be efficient by considering the effect of parameters, such as blade dimensions, cutting depth and cutting angle, etc. on the cutting force. However, the numerical models always demand higher computation time. On the other hand, the analytical models can determine the cutting force quickly on a blade with a decent accuracy. Experimental studies have also been done to determine the accurate cutting force on a bulldozer blade. However, such studies need more time and economic support.

In the past, studies focused on determining the cutting force accurately during the soil cutting by changing a few parameters, such as cutting depth, velocity of bulldozer etc. However, to make the soil cutting operation economical and productive the optimal input parameters have to be chosen. This leads to the motivation of this thesis in which the soil cutting operation by bulldozer and its blade is modeled as an optimization problem. Moreover, the real-world problems often consist of multiple objectives that are to be optimized simultaneously (Deb et al. 2002). When such problems are solved using any evolutionary multi-objective (EMO) technique, a set of Pareto-optimal (PO) solutions are generated that show trade-off among the objectives. These PO solutions provide multiple choices to a practitioner that can be used for a relative comparison and also, for an appropriate selection of a solution. Furthermore, the post-optimal analysis (Deb and Srinivasan 2006) can be done to decipher important relationships among the objectives and decision variables. With those remarks, the objectives of the thesis are stated in the following section.

1.2 Objectives of the Thesis

The aim of the thesis is to make economical and productive soil cutting operation. The aim is achieved by modeling the operation as an optimization problem in which the operating conditions of a bulldozer and dimensions of a blade have been chosen as decision variables. The optimization formulation can help the practitioner/user to choose an appropriate blade and the corresponding optimal operating conditions for the economical and productive soil cutting operation for a given bulldozer-type and soil-type. Followings are the main objectives of this thesis,

- Developing realistic multi-objective optimization formulation for a bulldozer and

its blade in soil cutting to make the operation economical and productive simultaneously.

- Validating the obtained PO solutions through various analysis, and also from the experiment results from the literature.
- Deciphering relationships among the objectives and decision variables from the obtained PO solutions for a better understanding of the problem.
- Preparing guidelines for a practitioner based on the evolved relationships.
- Developing a hybrid EMO technique for better convergence.

1.3 Organization of the Report

The thesis report is organized in five chapters. Chapter 2 presents the relevant literature survey on soil cutting operation. Chapter 3 presents three multi-objective optimization formulations that have been developed chronologically. The results evolved by existing EMO techniques are presented and discussed is put forward in terms of advantages and limitations of the proposed formulations. Chapter 4 presents a hybrid EMO technique. Various strategies of local searches are discussed and their results are compared. The thesis is concluded in chapter 5 with future work.

Chapter 2

Literature Survey

2.1 Introduction

A bulldozer is the main equipment in construction that is mainly used to cut soil. A bulldozer consists of a tractor/engine for supplying power and a blade in its front for cutting soil. The blade acts like a tool which is inserted in soil for a certain depth. When power is supplied to a bulldozer, the blade starts cutting soil. The interaction between the blade and soil has been referred as the soil-blade interaction in the literature. During this interaction, the blade experiences enormous forces due to cohesion, adhesion and friction between the blade and soil. The resultant force on the blade is generally referred as the cutting force. The literature has been focusing in determining the cutting force for so long. Early studies performed experiments to determine the cutting force by using sensors. Thereafter, the analytical models were developed that were based on certain assumptions. These models can predict the cutting force with a desired accuracy. The numerical models have also been developed in which finite element methods and discrete element methods were used. All the models targeted to incorporate multiple parameters so that effect of these parameters on the soil-blade interaction can be determined. In the following sections, the studies are discussed based on the approaches for determining the cutting force on a bulldozer blade.

2.2 Experimental Studies

The soil-blade interaction was determined earlier through experiments. In those experiments, soil was cut either by wide blades, which are generally used with bulldozer, or by narrow blades, which are used for tillage. The effect of few parameters on the soil-blade interaction was also observed. Bagster and Bridgwater (1967) found that the parameters, such as weight, size, and power of a bulldozer influenced the cutting force. It was concluded that these parameters can be selected carefully to overcome the cutting force without slippage between soil and a bulldozer. Wislicki (1969) investigated effect of types of soil on the soil-blade interaction. It was observed that the hard soil indeed generated more resistance than the soft soil. Therefore, more power was required to cut hard soil. Qinsen and Shuren (1994) performed the experiments by considering different sizes of blade that were operated at different cutting depths. The study suggested that the cutting force got increased at a higher cutting depth when a bulldozer was running at a constant speed. The cutting force was determined experimentally when the blade was fully loaded with soil. Karmakar and Kushwaha (2006) investigated effect of different bulldozer blades in soil cutting. It was concluded that the size, shape, and volume capacity affected the forces due cohesion, adhesion, and friction thereby affecting the cutting force on a bulldozer blade. Xia (2008) performed experiments on different terrains, such as flat, downward or upward hilly area. In downward sloppy areas, the power requirement was found to be less because the weight of a bulldozer acted against the cutting force. However, effect was totally opposite when soil cutting was done in upward hilly area for which a bulldozer had to supply power to overcome the cutting force and weight of a bulldozer, which generally in many tons. King et al. (2011) performed experiments on Lunar and Ottawa soils which were relatively soft. The experiments were performed by using a narrow blade, which was operated at different cutting depths. More cutting force was observed at higher cutting depths.

Experimentally, a different attempt was made to reduce the cutting force by introducing convex shaped-bodies on the blade surface. It was referred as bionic technology because the shape was inspired from the insect found in soil (Ren et al. 1995, 2002). Due to such small and multiple convex shaped-bodies, the adhesion between a blade and soil was decreased thereby reducing the cutting force up to 13%.

The experimental studies successfully investigated effect of various parameters on the cutting force. Indeed many parameters have been taken, however, it is not always feasible to perform multiple experiments for quantifying the cutting force. For example, every experiment involves costly setup thereby making the soil cutting operation expensive. Moreover, certain terrains and soil conditions may not allow to perform multiple experiments for determining the cutting. It is also to understand that the soil cutting operation can be made economical and productive when an optimal set of input parameters are chosen.

2.3 Analytical Studies

The analytical models have been developed almost parallel with the experimental studies. It was found that these models are not as accurate as numerical methods, but they can reasonably quantify the soil-blade interaction by involving many important parameters related to soil cutting operation, such as cutting depth, cutting angle, inclination of job site, and also dimensions of blade, such as height, and width of a blade. The models have been developed based on specifying the soil failure zone from which various force equations can be derived (McKyes 1985, Kushwaha et al. 1993). The failure zone in these models were developed by constructing a soil wedge. In two-dimensional (2D) soil failure zone, a soil wedge was considered specially for wide blades (Perumpral et al. 1983, Qinsen and Shuren 1994). However in three-dimensional (3D) soil failure zone, a center wedge with two circular side crescents were considered mainly for narrow blades (Hettiaratchi and Reece 1967, McKyes and Ali 1977).

Terzaghi (1943) proposed a 2D analytical model to simulate interaction between soil and a wide blade using the passive earth pressure theory and semi-empirical failure zone. The soil failure zone in the 2D analytical model consisted of Rankine passive zone and shear zone bounded by a part of logarithmic spiral curve. Reece (1964) proposed a fundamental equation of earthmoving mechanics in which resistance forces due to shear, cohesion, adhesion and surcharge pressure were considered. Hettiaratchi and Reece (1974) later found that the adhesion force had a negligible impact on the passive force, thus components of adhesion and cohesion forces were combined. Luengo et al. (1998) included the job site inclination angle in the fundamental equation of

earthmoving mechanics. Qinsen and Shuren (1994) used a 2D analytical model in which various forces due to friction, cohesion and adhesion were considered on a soil wedge. Forces due to soil pile on the ground and soil accumulated in a blade were also taken into consideration for a wide blade of a bulldozer. King et al. (2011) compared various analytical models with the experimental cutting force that was conducted on Lunar and Ottawa soil. The experiments were conducted using a narrow blade that was operated at different cutting depths. It was found that the model of McKyes (1985) predicted the cutting force closer to the experiment results. The models developed by Swick and Perumpral (1988) and by Qinsen and Shuren (1994) over predicted the cutting force.

Many attempts have been made in the past to develop 3D failure zone of soil for accurately determining the cutting force on a metallic blade. Hettiaratchi and Reece (1967) developed the fundamental equation of earthmoving mechanics for a 3D soil wedge considering a center wedge and two side crescents for narrow blades. The cutting force was determined for a wide range of depth/width ratio, which showed a good closeness of results with the experimental cutting force. Godwin and Spoor (1977) proposed a model that suggested two different ratios, that are, crescent ratio and aspect ratio. In the procedure, the shear plane was not considered for calculating the cutting force. Perumpral et al. (1983) developed a model that was based on limit equilibrium analysis to predict behavior of narrow blades and soil by including cohesion and adhesion effects, and the parameters affecting the performance of a blade. The results showed a good agreement between the predicted and observed forces. However, the proposed model under predicted the force at a high value of blade's cutting angle. Gupta et al. (1989) developed a model to predict the force acting on a convex blade. The model consisted of four components related to the weight of soil acting on a blade, shear force, surcharge pressure of soil on a blade, and soil-blade friction force. The model concluded that the predicted force on a convex blade showed a close agreement with the experimental results. While these models were generated, Kushwaha et al. (1993) presented a survey on the analytical models mainly focused on failure zones and equations derived from them.

The analytical models were also developed to include dynamic conditions in which acceleration (Karmakar and Kushwaha 2006) and velocity (Swick and Perumpral 1988,

Gupta et al. 1989) were considered. Mainly, the inertia force was considered either in term of velocity or acceleration. These models predicted the cutting force with respect to the experiments and investigated effect of extended angles on the side crescent of the failure zone, rupture distance, rupture angle, and rake angle (Swick and Perumpral 1988). It is found that the models have under or over predicted the cutting force at the high cutting depths (Obermayr et al. 2011).

2.4 Numerical Studies

The studies using the numerical methods, such as finite element method (FEM) and discrete element method (DEM) were conducted in which soil was modeled using these numerical methods. In those studies, different parameters were considered so that the soil-blade interaction, behavior of soil, and cutting force can be observed.

The studies based on FEM used the concepts of soil mechanics and the failure zone by using various models like constitutive equations of soil failure (Karmakar and Kushwaha 2006, Obermayr et al. 2011, Armin et al. 2014), hypo-plastic constitutive model (Abo-Elnor et al. 2003, 2004), elasto-plastic constitutive model (Bentaher et al. 2013) to name a few. Abo-Elnor et al. (2003) investigated the dynamic effect of soil-blade interaction. The effect of velocity and acceleration of a bulldozer was considered in the FEM model by using ABAQUS software. It was found that the cutting force was increased for a larger velocity and acceleration. Eventually, the power requirement from a bulldozer engine also got increased that affected efficiency of bulldozer in soil cutting. Also, when a larger velocity and acceleration were considered, the power required to drag weight of a bulldozer also increased. Abo-Elnor et al. (2004) extended the study and investigated effect of blade width, certain boundary conditions and mesh density with FEM model for soil. Bentaher et al. (2013) investigated effect of inclination angle and lifting angle during the soil-blade interaction by modeling soil using FEM. It was observed that both the parameters influenced the interaction and thus, the cutting force got changed. Armin et al. (2014) conducted the study for improving design of blades by modeling soil using the Durker-Prager and Mohr-Coulomb constitutive law. The rake angle and blade curvature were taken as input parameters. It was found that both parameters were sensitive to the FEM model and increased the cutting force when

their values were increased.

DEM was used for modeling soil in which the simulating motion was modeled for a large number of small particles of soil. Shmulevich et al. (2007) used DEM model for soil in which effect of blade geometry was investigated. The soil particles were modeled as disk clumps and their interaction was modeled by using some softening model. It was found that as a blade of a bulldozer moved forward, the horizontal component of the cutting force got increased. It was due to soil pile accumulated in front of a bulldozer. Zhang et al. (2008) used the morphology of earthworm and a wavy non-smooth shape was designed for the blade plate. DEM was used to simulate contact between the soil particles and bulldozer plate. It was similar to the bionic technology that reduced the cutting force due to stronger clod-crushing ability. Bentaher et al. (2013) successfully setup a model for predicting the cutting force for a large industrial simulation. DEM model was used with equations of contact law, equations of normal and tangential stiffness and equations of particle rotation. Tsuji et al. (2012) developed a three-dimensional parallel DEM simulation model by using the top-down cohesive bond model. The mathematical model adopted in this study depended on Newton translational and rotational equations of motion for individual particles.

From these handful studies, it is found that the numerical models are capable to predict accurate cutting force. Every study included some input parameters to observe their effects on the cutting force. If these models are used for determining the optimal input parameters for soil cutting, the procedure can become computationally expensive. Since many parameters affect the soil-blade interaction, a complex model is required that can include various input parameters.

2.5 Closure

In this chapter, the studies focusing on the cutting force through experiments, analytical, and numerical models were discussed. The experimental studies indeed are the best to determine the cutting force on a bulldozer blade. However, it is impractical to perform many experiments for observing effects of various input parameters on the soil-blade interaction. As presented in the literature, the analytical and numerical models are the best to predict the cutting force. Early studies in the literature survey

focused on developing soil failure zones for 2D and 3D analytical models. Generally, a soil-wedge formed by a bulldozer blade in 2D was modeled and various forces due to adhesion, cohesion and friction were considered. Such 2D soil-wedges were useful for wide blades which are used with the bulldozer for cutting as well as pushing soil. The soil-wedge was then extended to make 3D soil cutting zone in which a soil-wedge with two side-crescent were considered. Such 3D failure zones exist in tillage operation in which narrow blades are used. The numerical models have been proposed to model soil. FEM models were developed for soil cutting and the cutting force was predicted by incorporating various models like constitutive equations of soil failure, hypo-plastic constitutive model, elasto-plastic constitutive model, and Newton transnational and rotational equations of motion of particles. DEM models were used for simulating the soil-blade interaction by considering motion and effect of a large number of small particles. The major outcome from these studies are accurate cutting force calculation and effect of various parameters on the force.

In the literature, the numerical and analytical studies on the soil-blade interaction were validated using the experiments. In those studies the operating conditions, such as cutting depth, cutting angle, velocity are kept fixed and the cutting force was predicted by using one bulldozer blade. In practice, a user decides these input parameters based on the experience targeting better soil cutting operation. However, it is not true for every user who can decide values of these parameters to achieve economical and productive operation. To the best of author's knowledge, a setting for optimal input parameters for soil cutting operation has not been reported in the literature. These remarks lead to the motivation of this thesis in which the soil cutting operation is formulated as an optimization problem. In the next chapter, the optimization formulations are discussed in detail.

Chapter 3

Multi-Objective Optimization Formulations for Bulldozer and its Blade

3.1 Introduction

In this chapter, the soil cutting operation is modeled for a bulldozer and its blade, in which an emphasis is given to make the operation economical and productive. The operation can be made economical when its variable cost can be reduced. The variable cost depends on the operating conditions which involve many parameters, such as power required from a bulldozer, speed of a bulldozer, depth of a blade inserted in soil, dimensions of a blade, etc. The operation can be made productive when a bulldozer can finish soil cutting operation as early as possible. However, any productive soil cutting operation with a large size blade operating at a larger speed and higher cutting depth requires more power from the bulldozer. Since optimal soil cutting operation involves multiple parameters related to the operating conditions and blade dimensions, three multi-objective formulations are developed chronologically by making them realistic and practical for usage in every attempt.

A systematic approach is adopted in this chapter for presenting results and discussion in which the statistical performance of evolutionary multi-objective (EMO) techniques are presented followed by presenting trends of the obtained non-dominated

solutions. The perturbation analysis is also done to observe the hierarchical sequence of decision variables over the change in the objective function values. The post-optimal analysis of the obtained non-dominated solutions is then performed to decipher important relationships which are useful to understand the problem. Later, the obtained relationships are used to prepare guidelines for practitioners. At the last, the obtained non-dominated solutions are validated with the experimental results from the literature. In the following sections, the multi-objective formulations are presented which are developed chronologically by incorporating realistic details and information in terms of objective, constraints and decision variables.

3.2 Bi-Objective Optimization Formulation

The first formulation is developed by using two objectives and one constraint. The first objective is to minimize the cutting force on a blade of a bulldozer and the second objective is maximizing the blade capacity (Barakat and Sharma 2017). Both the objectives are developed using decision variables for operating conditions, such as cutting depth (D), blade cutting angle (α), bulldozer velocity (v), and for dimensions of blade, such as blade width (B), blade height (H), blade curvature radius (R) and blade curvature angle (θ). A constraint is designed on the remaining power of bulldozer engine during the soil cutting operation. The bi-objective optimization formulation is given as

$$\begin{array}{lll} \text{Minimize} & F, & \text{(Cutting force)}, \\ \text{Maximize} & V, & \text{(Blade capacity)}, \\ \text{subject to} & P_R \geq 0, & \text{(Remaining power)}, \\ & 0.01 \leq D \leq 0.5, & \text{(Decision variables)}, \\ & 0.785 \leq \alpha \leq 1.309, & \\ & 0.278 \leq v \leq 1.389, & \\ & 3 \leq B \leq 5, & \\ & 1 \leq H \leq 2.5, & \\ & 0.9 \leq R \leq 1.5, & \\ & 1.047 \leq \theta \leq 1.309. & \end{array} \tag{3.1}$$

The lower and upper limits of decision variables are developed from the guidelines given in (Caterpiller 1996).

3.2.1 Details of Formulation

Objective Function-1: Cutting Force The first objective is minimizing the cutting force on a blade of a bulldozer. It means that resistance generated by this cutting force also gets minimized. Thus, the power required from a bulldozer to overcome this resistance also gets minimized. Overall, less power requirement signifies less fuel consumption thereby making the soil cutting operation economical.

Two force models are adopted in this thesis for determining the cutting force by considering a soil failure zone in front of a blade and by adopting the passive earth pressure theory. Both the models consider different resistance forces due to friction, cohesion and adhesion between a blade and soil. The first force model adopted in this thesis is proposed by Qinsen and Shuren (1994) which is developed for wide blades. The another force model adopted is proposed by McKyes (1985) which is developed for the narrow blades. The details of both the force models can be found in Appendix A in which the cutting force is determined when a blade is fully loaded with soil. It signifies that a blade experiences maximum cutting force during soil cutting.

Objective Function-2: Blade Capacity The second objective is maximizing the blade capacity. This objective function signifies that a larger volume of soil can be cut by a blade under the assumption that a blade is fully loaded with soil when the cutting force is determined. It means that a bigger blade has more capacity than a smaller blade and thus, it can cut more soil. The blade capacity is determined by calculating soil-pile volume in front of a blade when it is fully loaded with soil as shown in Fig. 3.1.

The blade capacity (V) is determined as

$$V = V_1 + V_2 + V_3 + V_4, \tag{3.2}$$

where V_1 is the volume of (fde), V_2 is the volume of (afg), V_3 is the volume of (abdg), and V_4 is the volume of soil inside the arc (ab). These soil-pile volumes are calculated

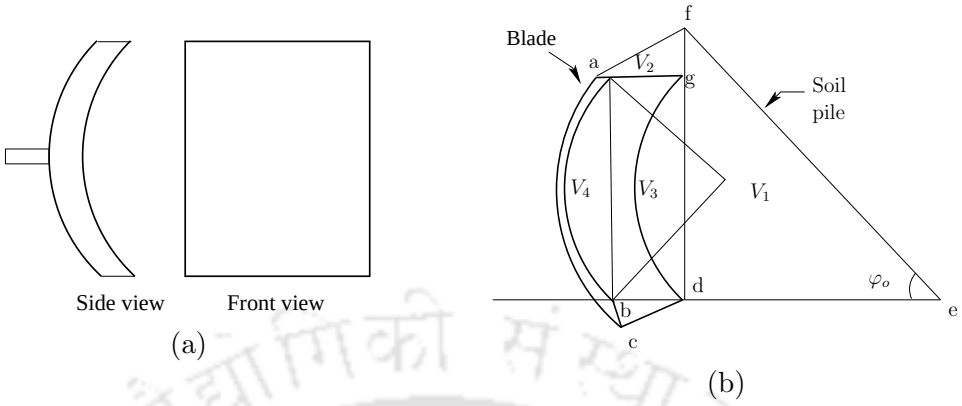

Figure 3.1: (a) Schematic of a bulldozer blade. (b) The blade capacity in terms of soil pile.

geometrically as

$$\begin{aligned} V_1 &= 0.5B(H + 2D\tan\varphi_o)^2\cot\varphi_o, \\ V_2 &= 2BD^2\tan\varphi_o, \\ V_3 &= DHB(\cot\alpha + \cot\beta), \\ V_4 &= 0.5B\theta R^2 - 0.5R^2 sin\theta. \end{aligned} \tag{3.3}$$

Constraint One constraint is developed which is based on the remaining power of a bulldozer engine. This constraint ensures that a bulldozer should able to overcome resistance generated due to the cutting force and weight of a bulldozer. It is given as

$$P_R = 0.85P_{bull} - (F + \mu G_1)v \geq 0, \tag{3.4}$$

where P_{bull} is the flywheel power which is assumed to be rated at 85%, F is the cutting force, μ is the coefficient of friction between a bulldozer and the ground, and G_1 is the weight of a bulldozer.

3.2.2 Optimization Techniques

The proposed bi-objective optimization problem is solved using one of the benchmark EMO techniques, that is, the elitist non-dominated sorting genetic algorithm (NSGA-II). The details of NSGA-II can be found in Appendix B.1. Since NSGA-II is a meta-heuristic algorithm, it is run for 30 times, and each time its starts from different initial population. The performance of NSGA-II is analyzed statistically using the

inverse generalized distance (IGD) indicator. The details of IGD indicator are given in Appendix C.1.

The ϵ-constraint method is also used which is capable for solving convex and non-convex multi-objective optimization problems (Haimes et al. 1971). Using the $\epsilon-$ constraint method, the given optimization problem is written as

$$\begin{aligned} \text{Minimize} \quad & F, \\ \text{subject to} \quad & V \geq \epsilon_V \\ & P_R \geq 0, \\ & 0.01 \leq D \leq 0.5, \\ & 0.785 \leq \alpha \leq 1.309, \\ & 0.278 \leq v \leq 1.389, \\ & 3 \leq B \leq 5, \\ & 1 \leq H \leq 2.5, \\ & 0.9 \leq R \leq 1.5, \\ & 1.047 \leq \theta \leq 1.309. \end{aligned} \tag{3.5}$$

Here, ϵ_V is the upper bound on V. For solving the above problem, *fmincon* solver of Matlab 2016b® is used in which sequential quadratic programming (SQP) technique is chosen. In this thesis, *fmincon* starts from the solution obtained from NSGA-II, instead of any random solution so that it can converge quickly.

It can be observed that both the optimization techniques solve the bi-objective optimization problem in a different manner. On one hand, the ϵ-constraint method converts the bi-objective optimization problem into a single-objective optimization problem by considering another objective as constraint. NSGA-II, however, simultaneously optimizes both the objectives. Any numerical optimization technique can be used with the ϵ-constraint method to generate the PO solution. At this stage, NSGA-II can generate a set of non-dominated solutions in one run. It means that the problem stated in Eq. (3.5) has to be solved with different values of ϵ_V to generate multiple non-dominated solutions. Here, the challenge is to generate a well-diverse set of non-dominated solutions, which gets influenced by different ϵ_V because uniform values of it cannot ensure diversity (Shukla and Deb 2007). In NSGA-II, the non-dominated sorting and crowding distance operators are used to emphasis convergence and diversity of the PO solutions.

3.2.3 Results and Discussion

For solving the proposed bi-objective optimization problem, a few parameters of NSGA-II are kept fixed which are presented in Table 3.1. For *fmincon* solver, the SQP terminates as per the default values set in MATLAB, for example, maximum iterations are set at 1000 and termination tolerance on the first-order optimality is set at $1.0e^{-6}$.

Table 3.1: Constant parameters for NSGA-II.

Population (N)	Generation (T)	Crossover probability
100	200	0.9
Crossover operator index	Mutation probability	Mutation operator index
15	0.333	20

For the bi-objective optimization problem, a mid-stiffness clay soil is considered and its physical parameters are given in Table 3.2 (Jack and Liu 1985). SI units are considered for all parameters, except for C_o, C and A_d values which are given in (N/m^2) and value of angle is given in degrees. Two parameters of a bulldozer equipment are also used in this study, that are, the flywheel power which is rated at $P_{bull} = 227.438$ kN.m/sec, the total weight of a bulldozer equipment is $G_1 = 328.613$ kN, and the friction factor between the ground and bulldozer crawler is $\mu = 0.4$ (Caterpiller 1996).

Table 3.2: A mid-stiffness clay soil parameters.

γ_o	γ	C_o	C	δ	A_d	β	φ_o	φ
640.74	1601.85	1019.715	2039.43	21.6	0	23°	30°	27°

3.2.3.1 Statistical Performance Analysis of EMO Technique

Two force models are adopted for determining F, and these models are coupled with NSGA-II independently. Model-1 is referred when the cutting force model by Qinsen and Shuren (1994) is used, and model-2 is referred when the cutting force model by McKyes (1985) is used. The statistical values of IGD[1] indicator from 30 runs are presented in Table 3.3. The smaller IGD indicator values suggest that NSGA-II is consistent in generating a good set of the approximate PO solutions.

[1]The details of generating the reference non-dominated solutions set for calculating IGD are given in Appendix C.1.

Table 3.3: IGD indicator values of NSGA-II for both force models.

Value	Model-1	Model-2
Best	0.0263	0.0283
Median	0.0274	0.0284
Worst	0.0274	0.0284

3.2.3.2 Obtained Non-Dominated Solutions

The obtained non-dominated solutions from both the models are shown together in Fig. 3.2. A linear trend between the two objectives can be seen from the figure, despite the fact that the cutting force and volume capacity objective functions involve nonlinear

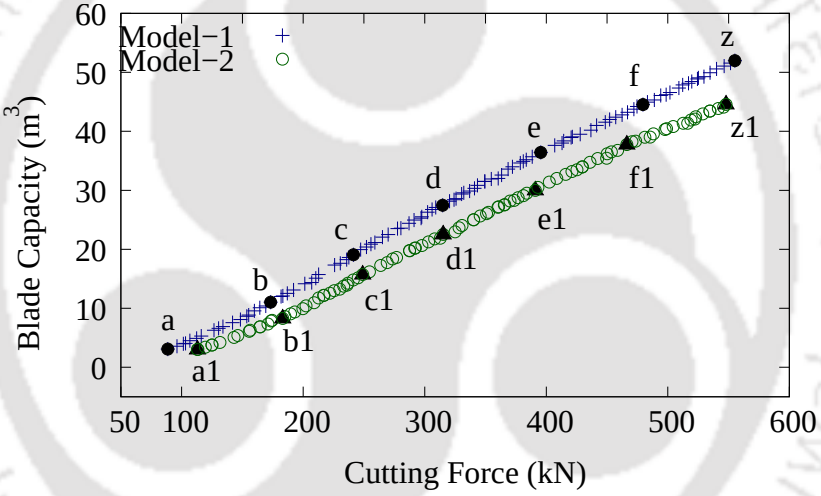

Figure 3.2: The obtained non-dominated solutions from NSGA-II for both the models.

equations. The extreme solutions 'a' from model-1 and '$a1$' from model-2 correspond to the minimum force but with a smaller blade capacity. Other extreme solutions 'z' and '$z1$' correspond to the maximum blade capacity with an expense of larger cutting force. From Tables 3.4 and 3.5, it can be seen from the column of NSGA-II solutions that the extreme solution 'a' shows less cutting force than solution '$a1$'. This contradicts the finding of King et al. (2011) in which the model of McKyes (1985) predicted results closer to the experimental cutting force and the model of Qinsen and Shuren (1994) over predicted the cutting force. It is noted that King et al. (2011) did not consider the assumption of Qinsen and Shuren (1994) wherein the cutting force is determined when a blade is fully loaded with soil. The surcharge pressure given in Appendix Eq. (A.25) for the model of (McKyes 1985) is included so that maximum cutting force is

calculated under the assumption of a fully loaded blade with soil. Solutions 'a' and '$a1$' show equivalent values of volume capacity from Tables 3.4 and 3.5.

Table 3.4: The solutions obtained from NSGA-II and $\epsilon-$constraint method considering model-1 are presented.

Solutions	NSGA-II solutions (F, V)	$\epsilon-$ constraint solutions (F, ϵ_V)
a	(88.593, 3.098)	(86.890, 3.098)
d	(173.200, 11.034)	(172.634, 11.034)
b	(241.376, 19.080)	(239.839, 19.080)
c	(314.716, 27.473)	(312.066, 27.473)
e	(395.493, 36.437)	(394.852, 36.437)
f	(479.602, 44.531)	(477.155, 44.531)
z	(555.221, 51.987)	(554.235, 51.987)

Table 3.5: The solutions obtained from NSGA-II and $\epsilon-$constraint method considering model-2 are presented.

Solutions	NSGA-II solutions (F, V)	$\epsilon-$ constraint solutions (F, ϵ_V)
$a1$	(112.988, 3.017)	(112.142, 3.017)
$d1$	(183.107, 8.276)	(177.794, 8.276)
$b1$	(248.998, 15.726)	(248.689, 15.726)
$c1$	(315.180, 22.529)	(314.203, 22.529)
$e1$	(391.008, 29.994)	(387.966, 29.994)
$f1$	(466.262, 37.750)	(465.008, 37.750)
$z1$	(547.973, 44.558)	(547.421, 44.558)

The extreme solutions 'z' and '$z1$' in Fig. 3.2 show equivalent cutting forces but different volume capacities. The equivalent cutting force value is observed due to the constraint given in Eq. (3.1). Different values of decision variables are observed for the models which constitute different volume capacities for solutions 'z' and '$z1$' as shown in Tables 3.4 and 3.5. The other non-dominated solutions show similar trade-off between the two objectives.

The same bi-objective optimization problem is solved using the $\epsilon-$ constraint method as stated in Eq. (3.5). The starting solutions for *fmincon* solver are 'a', 'b', 'c', 'd', 'e', 'f' and 'z' obtained from NSGA-II which are also shown in Fig. 3.2. The value of ϵ_V in Eq. (3.5) for these starting solutions are shown in the column of $\epsilon-$constraint solutions in Table 3.4. A marginal difference can be seen in the cutting force values

from the table. This analysis offers two folds of advantages. First, the $\epsilon-$constraint method is able to generate the approximate PO solutions in less iterations when starting from a good solution that is evident from (Sharma et al. 2007, Kumar et al. 2007). Second, closeness of NSGA-II and the $\epsilon-$constraint method solutions suggest that NSGA-II solutions might have converged to the true PO front. Here, NSGA-II evolved many non-dominated solutions in one run. However, the $\epsilon-$constraint method has to run many times at different starting points to generate a diverse set of non-dominated solutions.

The same analysis of the $\epsilon-$ constraint method is performed on the bi-objective optimization problem by considering model-2. The results of NSGA-II and the $\epsilon-$constraint method are presented in Table 3.5. Similar observation can be seen as discussed in the last paragraph.

Perturbation Analysis of Obtained Solutions The perturbation analysis is now performed for a few non-dominated solutions obtained from NSGA-II using model-1. In this analysis, one variable is perturbed at a time and the change in the cutting force value (ΔF) is observed. The perturbation is allowed within 1% of the variable range. If any decision variable of the obtained non-dominated solution is evolved at its lower bound, the forward difference technique is used to determine ΔF. In case any decision variable is evolved at its upper bound, the backward difference technique is used. Otherwise, the center difference technique is used.

Table 3.6 presents ΔF value by perturbing one variable at a time. Except for α, ΔF value is positive, which means that the cutting force increases with perturbation. It can be seen from the table that maximum ΔF can be seen with perturbing D. From solution 'a' to 'z', a larger change in ΔF values can be seen. Next is H, that shows increasing trend of ΔF values. The same observation can be seen with B decision variable. The variables θ and R show almost equivalent change in ΔF values for these solutions. These observations suggest that D, H and B are the sensitive parameters in the same hierarchy for the given problem, which have to be chosen carefully. The variables θ and R are also sensitive to the problem, but change in ΔF remains similar for all solutions. The negative values of ΔF by perturbing α suggest that the cutting force can further reduce. However, α is not very sensitive for the given problem as

Table 3.6: The change in the cutting force (ΔF) is presented for the perturbation analysis of decision variables of the obtained non-dominated solutions generated using the model-1.

Solutions	D	α	B	H	R	θ
a	295.189	-0.008	29.501	74.564	21.731	18.691
b	308.093	-0.008	57.358	95.786	18.571	15.865
c	343.044	-0.214	79.145	108.079	18.139	15.651
d	396.653	-3.938	100.430	117.748	19.084	16.339
e	444.946	-14.219	126.339	123.971	19.633	16.658
f	522.635	-17.789	130.319	147.634	20.029	19.877
z	596.712	-19.003	130.533	171.563	26.779	22.981

Table 3.7: The change in the cutting force (ΔF) is presented for the perturbation analysis of decision variables of the obtained non-dominated solutions generated using the model-2.

Solutions	D	α	B	H	R	θ
$a1$	286.961	39.199	37.629	82.908	41.710	35.695
$b1$	321.606	53.701	51.679	92.245	42.524	36.926
$c1$	342.891	68.819	63.018	99.515	43.023	35.766
$d1$	435.214	137.888	114.664	130.003	42.316	36.461
$e1$	325.362	59.589	54.883	94.399	42.531	35.758
$f1$	415.824	128.174	97.189	120.659	42.599	36.340
$z1$	463.585	193.049	151.129	145.312	41.487	35.905

change in ΔF value is very marginal for all solutions.

Same perturbation analysis is performed for the obtained non-dominated solutions from model-2. Table 3.7 presents ΔF values that are positive for all decision variables. It means that the cutting force increases with perturbation of decision variables. In this analysis also, large change in ΔF is observed by perturbing D followed by H, α and B. Here, a new observation can be seen that α is sensitive for model-2. The variables θ and R show the same trend as observed with model-1.

The perturbation analysis brings out the observation that the selection of appropriate blade is also important along with cutting depth for optimal cutting. Moreover, the analysis also suggests that the obtained solutions from NSGA-II may either be true or very close to the true PO front of the given problem.

3.2.3.3 Post-Optimal Analysis

The post-optimal analysis of the obtained non-dominated solutions from NSGA-II is now performed. The analysis is presented to find new and innovative design principles or relationships that can be used for deeper understanding of the problem as demonstrated for many engineering optimization problems in (Deb and Srinivasan 2006, Sharma 2010, Baishya et al. 2014). Moreover, some guidelines can also be made for the practitioners that can help them for choosing the optimal input parameter values. It is always interesting to reveal the common design principles that are responsible for generating approximate solutions. Also, some dissimilar relationships can be extracted that are responsible for trade-off among the approximate PO solutions.

Relationships Between Objective Function and Decision Variables Firstly, the relationships between objective function and various decision variables are presented. The relationships of the cutting force and the blade width values of the approximate PO solutions are shown in Figs. 3.3 and 3.4. Many solutions are evolved at the lower bound of the blade width in both models that are aligned vertically. For these solutions, the cutting force increases when the blade width is at its lower value. The solutions 'a' and '$a1$' in the figures are the extreme solutions corresponding to the minimum cutting force that are same as shown in Fig. 3.2. The transition points 'w' and '$w1$' in both the figures are also observed. After these points the cutting force increases with increase in the blade width. A linear trend can be seen from the transition points to the extreme points 'z' and '$z1$'.

Figs. 3.5 and 3.6 show the relationships between the cutting force and the blade height for both models. Same extreme points (a, z) and ($a1$, $z1$) can be seen in the figures. Another set of transition points, that are, 'h' and '$h1$' can also be observed. Between (a, h) and ($a1$, $h1$), the cutting force increases with increase in the blade height values. At the transition point, the blade height reaches to its upper bound value. It can be seen that many non-dominated solutions are evolved at the upper bound of the blade height decision variable, which are aligned vertically from (h, z) for model-1 and ($h1$, $z1$) for model-2.

Figs. 3.7 and 3.8 present the relationships between the cutting force and the cutting

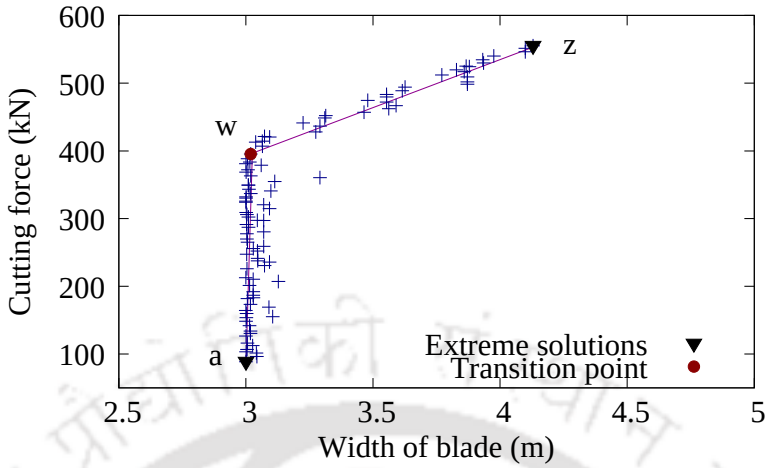

Figure 3.3: Relationship between the cutting force and the blade width obtained using model-1

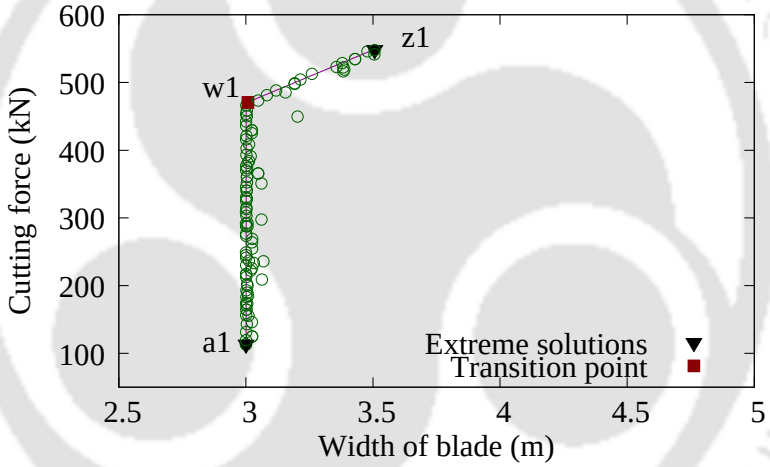

Figure 3.4: Relationship between the cutting force and the blade width obtained using model-2

depth for both models. In the figures the extreme solutions are same as discussed earlier. It can be observed that many solutions are evolved at the lower and upper bounds of the cutting depth where the cutting force increases. The rest of the solutions show a linear trend between the bounds. Here, the first transition points in both models are 'h' and '$h1$' that are same as presented in Figs. 3.5 and 3.6. Also, the other transition points in both the models are 'w' and '$w1$' that are same as shown earlier in Figs. 3.3 and 3.4.

The relationship between the cutting force and the cutting angle is presented in Figs. 3.9 and 3.10. In both the figures, the solutions are evolved at the lower bound of the cutting angle. This relationship is useful, which suggests that the cutting angle

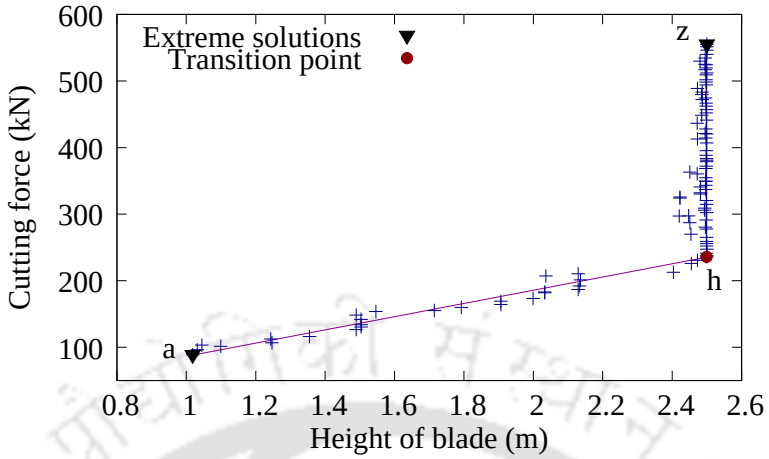

Figure 3.5: Relationship between the cutting force and the blade height obtained using model-1

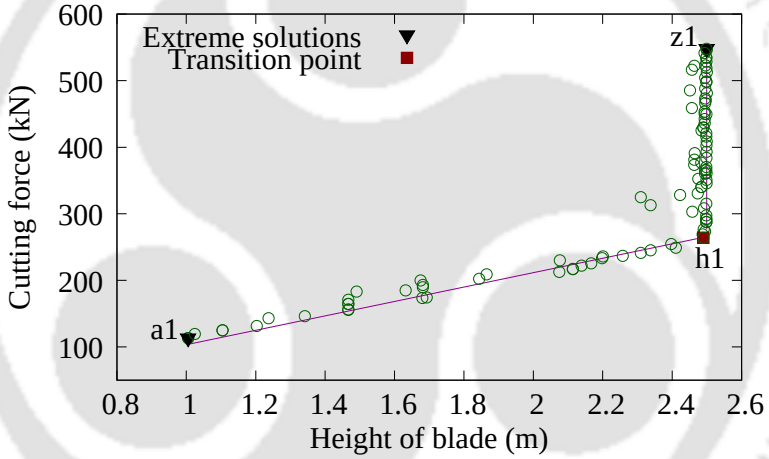

Figure 3.6: Relationship between the cutting force and the blade height obtained using model-2

should be chosen at its lower bound for the optimal soil cutting. Similar relationship can be seen in Figs. 3.11 and 3.12 in which the non-dominated solutions are evolved at the lower bound of the curvature angle.

The non-dominated solutions also show similar relationship for the curvature radius with the cutting force as shown in Figs. 3.13 and 3.14. In this case, the solutions are evolved closer to the lower bound of the decision variable. It can be observed that the cutting angle, curvature radius and curvature angle decision variables are evolved at their respective lower bounds that decipher a common relationship of these variables with the objective function. These commonality is useful, which suggests that these variables should be chosen at their lower bounds to make the soil cutting operation

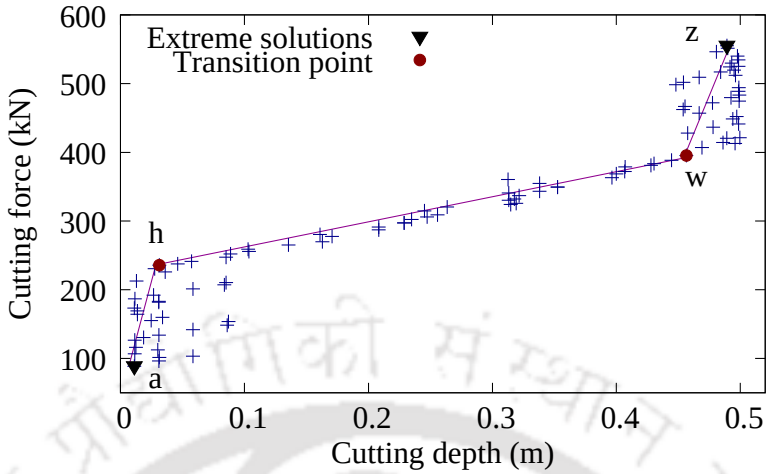

Figure 3.7: The post-optimal relationship between the cutting force and the cutting depth obtained using model-1

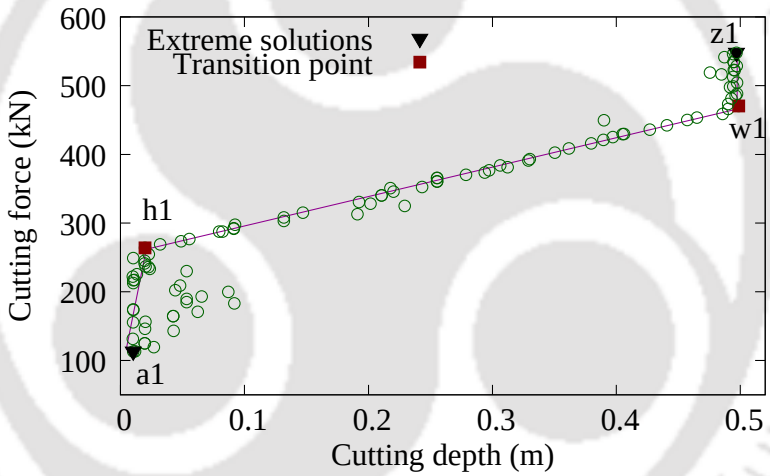

Figure 3.8: The post-optimal relationship between the cutting depth and the cutting depth obtained using model-2

optimal for the given bi-objective optimization.

Relationships Among Decision Variables Now, the relationships among the decision variables are presented. Figs. 3.15 and 3.16 show that many solutions are aligned closer to the lower bound of the cutting depth starting from the extreme solution 'a' in model-1 and solution '$a1$' in model-2. Thereafter, the transitions points 'h' and '$h1$' are observed. Between (a, h) and ($a1$, $h1$), the blade height increases, but the cutting depth remains at its lower bound value. After the transition point in both figures, rest of the solutions are aligned at the upper bound of the blade height, and the cutting depth variable keeps on increasing to its upper bound. Here, the blade height and

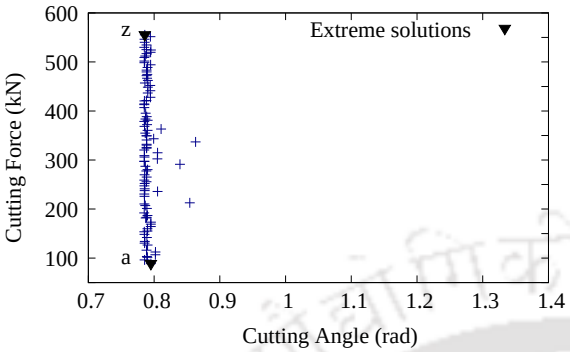

Figure 3.9: The post-optimal relationship between the cutting force and the cutting angle of a blade obtained using model-1

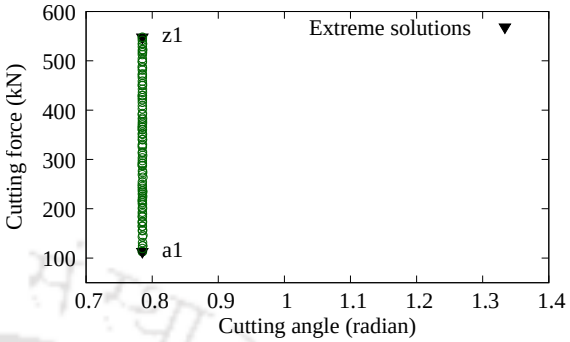

Figure 3.10: The post-optimal relationship between the cutting force and the cutting angle of a blade obtained using model-2

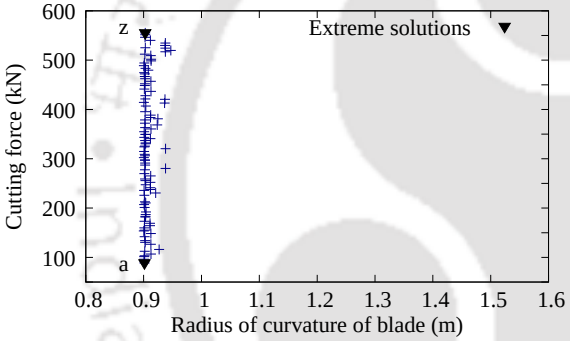

Figure 3.11: The post-optimal relationship between the cutting force and the curvature radius of a blade obtained using model-1

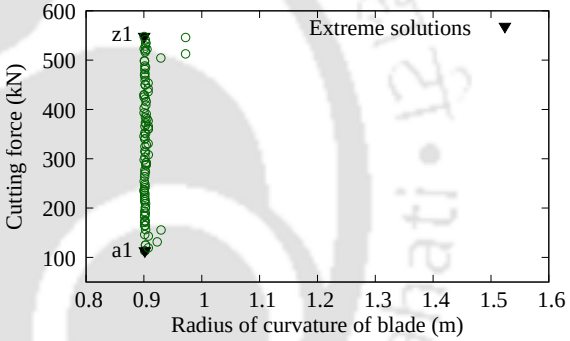

Figure 3.12: The post-optimal relationship between the cutting force and the curvature radius of a blade obtained using model-2

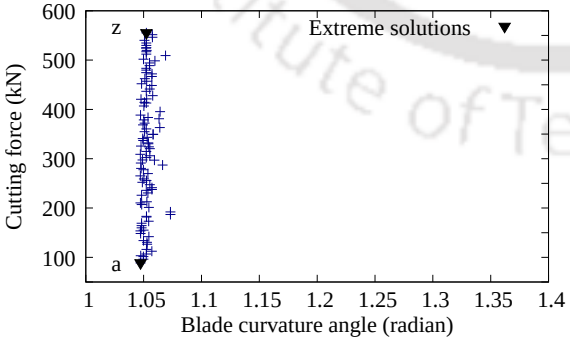

Figure 3.13: The post-optimal relationship between the cutting force and the curvature angle of a blade obtained using model-1

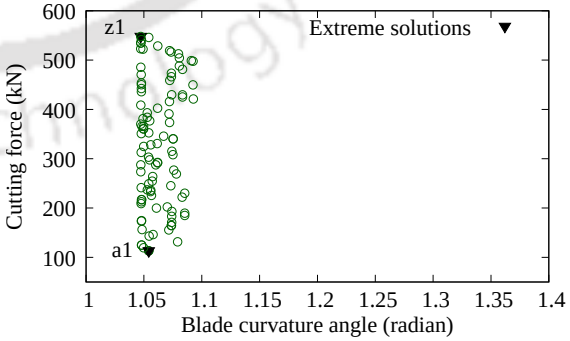

Figure 3.14: The post-optimal relationship between the cutting force and the curvature angle of a blade obtained using model-2

cutting depth of the transition points 'w'and '$w1$'are evolved closer to the extreme solutions 'z' and '$z1$'.

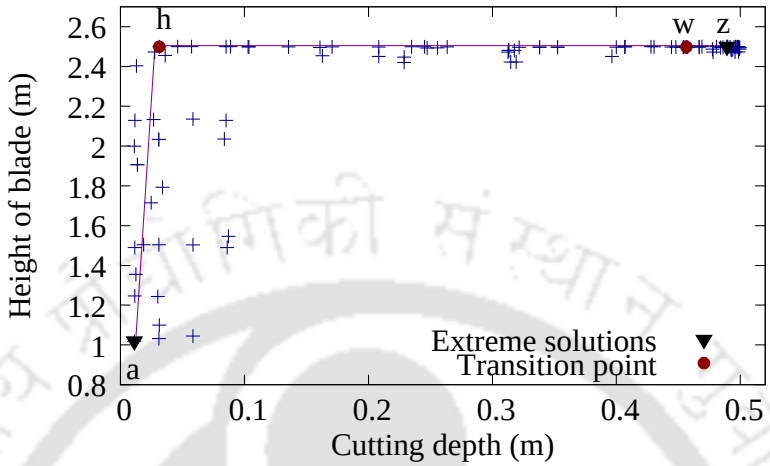

Figure 3.15: The post-optimal relationship between the cutting depth and the blade height obtained using model-1

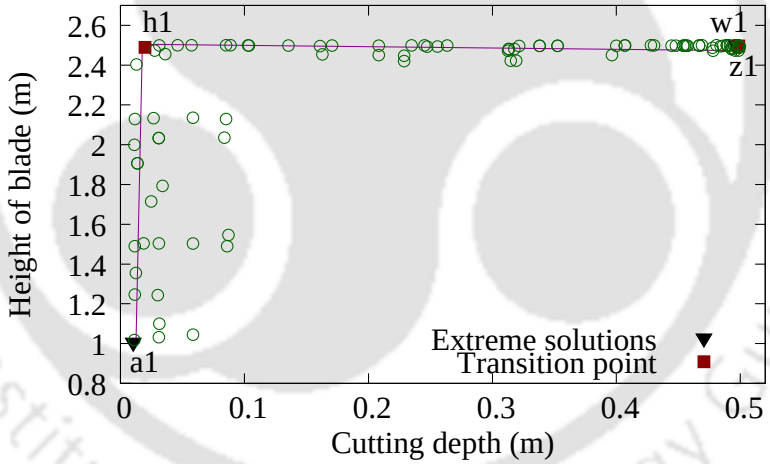

Figure 3.16: The post-optimal relationship between the cutting depth and the blade height obtained using model-2

When a trend between the cutting depth and the blade width is observed, many solutions are aligned at the lower bound of the blade width as shown in Figs. 3.17 and 3.18. In this case, the extreme solution 'a' and the transition solution 'h' of model-1 is evolved closer to each other. Similar observation can be seen with model-2. From the extreme solutions 'a' and '$a1$' to the transition solutions 'w' and '$w1$', increase in the cutting depth values can be seen till it reaches to its upper bound. After the transition points in both the figures, increase in the blade width values is observed till 'z' and '$z1$' in both figures.

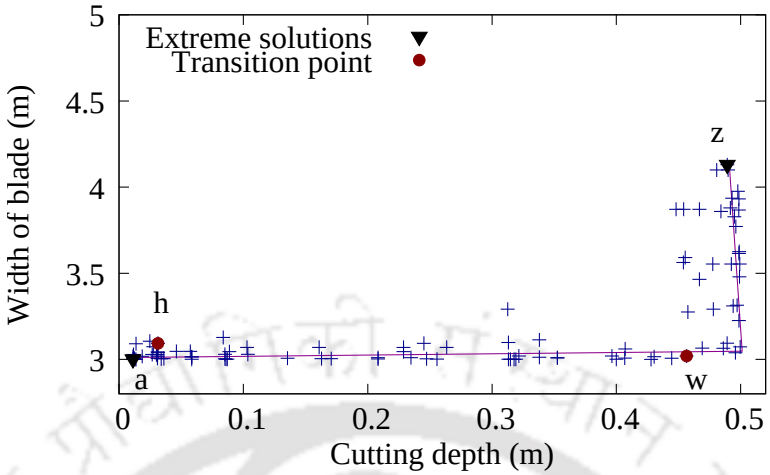

Figure 3.17: The post-optimal relationship between the cutting depth and the blade width obtained using model-1

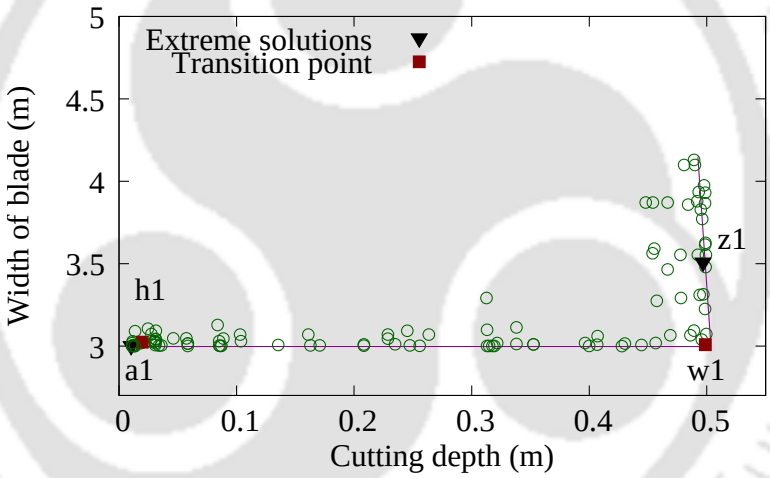

Figure 3.18: The post-optimal relationship between the cutting depth and the blade width obtained using model-2

From these figures it can be observed that trade-off among the approximate PO solutions exists due to change in these variables. First the blade height value increases from the extreme solutions 'a' in model-1 and '$a1$' in model-2 till the transition points 'h'and '$h1$'. In the zone of 'a' to 'h' in model-1 and '$a1$' to '$h1$' in model-2, the solutions are evolved at the lower bounds of the cutting depth and the blade width. From the transition points 'h' and '$h1$' to another transition points 'w' and '$w1$', the cutting depth variable keeps on increasing till it reaches to its upper bound. At the transition points 'w' and '$w1$', the solutions are evolved at the upper bounds of the height of blade and the cutting depth. In the last zone made by the transition points 'w' and '$w1$' to the extreme solutions 'z' and '$z1$', the blade width value starts increasing and reaches

to its maximum allowed value. It is noted that maximum allowed value of blade width is smaller than its upper bound because after this value the constraint is violated.

3.2.3.4 Guidelines for Practitioners

The relationships shown among the objective function and decision variables can be used for making guidelines in which a blade should be selected based on its height over width. For example, a blade with a smaller height and width can be chosen for minimum cutting force that should operate at a lower cutting depth. Bigger blades can be used for the maximum blade capacity with a higher cutting depth. In practice, the extreme solutions are not opted always, but some aspiration of practitioner or decision maker is required to choose an appropriate blade size. For example, some desired blade capacity for the operation can help us to know the cutting force from Fig. 3.2 that can be related to fuel consumption. If solution '*b*' is chosen from Fig. 3.2, then it can provide the optimal dimensions for the blade from Figs. 3.3 and 3.5. In practice, a set of blades with their fixed dimensions is available. Here, a blade from the available set of blades can be chosen that has its height closer to the optimal value of the height of solution '*b*'. Thereafter, an emphasis should be given to the blade width because both objectives depend on it. Once the blade has been chosen, the optimal cutting depth can be found out from Fig. 3.15. This signifies that a decision can be made in priori or on sight from the plots of the post-optimal analysis. On the other hand, the cutting angle, curvature radius and curvature angle parameters can be kept at their lower bounds while designing a blade for bulldozer.

Critical Observation It can be observed from the results of the post-optimal analysis that the maximizing blade capacity leads to a higher time for cutting soil when a big size blade is used at a relatively lower cutting depth. Moreover, the bi-objective optimization problem of soil cutting operation stated in Eq. (3.1) lacks realistic objectives and problem specific constraints that can be adopted by the practitioners or decision makers. Therefore, a modified bi-objective optimization problem for soil cutting operation is proposed in the following section.

3.3 Modified Bi-Objective Optimization Formulation

The soil cutting operation is modeled using two objectives and three constraints. The modified bi-objective formulation is given in Eq. (3.6). It can be seen that the power and time are minimized simultaneously, and more problem-specific constraints are developed to make the optimization problem realistic.

$$\begin{array}{lll} \text{Minimize} & P, & \text{(Power)}, \\ \text{Minimize} & T, & \text{(Time)}, \\ \text{subject to} & P_R \geq 0, & \text{(Remaining power)}, \\ & F \leq F_{max}, & \text{(Blade failure)}, \\ & P_d \geq P_{d_{min}}, & \text{(Production rate)}, \\ & 0.01 \leq D \leq 0.5, & \text{(Decision variables)}, \\ & 0.785 \leq \alpha \leq 1.309, & \\ & 0.278 \leq v \leq 1.389, & \\ & 3 \leq B \leq 5, & \\ & 1 \leq H \leq 2.5, & \\ & 0.9 \leq R \leq 1.5, & \\ & 1.047 \leq \theta \leq 1.309. & \end{array} \tag{3.6}$$

3.3.1 Details of Formulation

Objective Function-1: Power Requirement The first objective function is minimizing the power required from a bulldozer to overcome the cutting force which is given as

$$P = F \times v. \tag{3.7}$$

Here, F is the soil cutting force which was described in Section 3.2.1. The details for the cutting force models adopted in this thesis are given in Appendix A. The minimum power requirement can be viewed as less fuel consumption by a bulldozer during the soil cutting that can make the operation economical. Moreover, a larger amount of remaining power of a bulldozer will be available for performing the soil cutting at a higher cutting depth and velocity.

Objective Function-2: Time Required to Cut Soil The second objective function is designed to minimize the time required to cut soil that can fill the blade completely in one pass. It means that the soil cutting operation can be finished quickly thereby signifying higher productivity of the operation. The second objective function is given as

$$T = \frac{L}{v}. \tag{3.8}$$

Here, L is calculated as

$$L = \frac{V}{B \times D}. \tag{3.9}$$

Here, V is the blade capacity of a bulldozer blade which was shown in Fig. 3.1 and determined using Eqs. (3.2) and (3.3).

Constraints Three problem-specific constraints are designed for the modified bi-objective optimization problem. The first constraint is developed for the remaining power of bulldozer engine which is given as

$$P_R = 0.85P_{bull} - F \times v \geq 0, \tag{3.10}$$

The second constraint is developed for preventing blade failure during the soil cutting operation. The blade failure will occur if the cutting force is more than the maximum allowed force that a blade can withstand. The maximum allowed cutting force generated during the soil cutting operation is assumed to be F_{max} = 300kN (Caterpiller 1996). The second constraint is given as

$$F \leq F_{max}. \tag{3.11}$$

The third constraint is designed on the production rate of the soil cutting operation. The production rate is defined as the maximum volume of soil cut by a bulldozer blade per pass per unit time that is given as

$$P_d = \frac{V}{T}. \tag{3.12}$$

The third constraint is developed such that the production rate should be greater than

$P_{d_{min}}$ that is given as

$$P_d \geq P_{d_{min}}. \tag{3.13}$$

A small value of $P_{d_{min}} = 0.008$ cubic meter per second is chosen from the results of Section 3.2.3 so that a wide range of the approximate PO solutions can be generated.

3.3.2 Optimization Techniques

The formulation given in Eq. (3.6) has non-linear equations, therefore it is solved using five benchmark EMO techniques, that are, elitist non-dominated sorting genetic algorithm (NSGA-II), strength Pareto evolutionary algorithm-2 (SPEA2), Pareto archived evolution strategy (PAES), speed-constrained multi-objective particle swarm optimization (SMPSO) and generalized differential evolution algorithm (GDE3) and one numerical optimization technique using the $\epsilon-$ constraint method. The details of EMO techniques are given in Appendix B. The $\epsilon-$ constraint method is used to modify the multi-objective optimization problem into the single-objective optimization by converting objective on the time into an additional constraint. The optimization problem using the $\epsilon-$ constraint method is given as

$$\begin{array}{ll} \text{Minimize} & P, \\ \text{subject to} & T \leq \epsilon_T \\ & P_R \geq 0, \\ & F \leq F_{max}, \\ & P_d \geq P_{d_{min}}, \\ & 0.01 \leq D \leq 0.5, \\ & 0.785 \leq \alpha \leq 1.309, \\ & 0.278 \leq \upsilon \leq 1.389, \\ & 3 \leq B \leq 5, \\ & 1 \leq H \leq 2.5, \\ & 0.9 \leq R \leq 1.5, \\ & 1.047 \leq \theta \leq 1.309. \end{array} \quad , \tag{3.14}$$

Here, ϵ_T is the lower bound on T. The value of ϵ_T is obtained from the results of five EMO techniques. For solving the above problem, *fmincon* solver of Matlab 2016b® is used in which the SQP technique is chosen.

3.3.3 Results and Discussion

Few parameters of EMO techniques are kept constant for solving the modified bi-objective optimization problem, which are given in Table 3.8. The performance of EMO techniques are observed through IGD and HV indicators and their details are given in Appendix C. A mid-stiffness clay soil (Jack and Liu 1985) is considered and its physical parameters are given in Table 3.2. The flywheel power is rated at P_{bull}= 227.438 kNm/s (Caterpiller 1996).

Table 3.8: Constant parameters for EMO techniques. Here, p_c and p_m are crossover and mutation probabilities; η_c and η_m are distribution indexes of simulated binary crossover and polynomial mutation. CR is the crossover probability and F_{sf} is the scaling factor for GDE3.

EMO techniques	Parameters
NSGA-II	Population size = 100; generation = 100; $p_c = 0.9$; $\eta_c = 20$; p_m =1/no. of variables; $\eta_m = 20$
SPEA2	Population size = 100; archive size = 100; generation = 100; $p_c = 0.9$; $\eta_c = 20$; p_m =1/no. of variables; $\eta_m = 20$
PAES	Archive size = 100; generation = 100; p_m =1/no. of variables; η_m = 20
SMPSO	Population size = 100; archive size = 100; generation = 100; p_m =1/no. of variables; $\eta_m = 20$
GDE3	Population size = 100; generation = 100; CR = 0.5, $F_{sf} = 0.5$

3.3.3.1 Statistical Performance Analysis of EMO techniques

EMO techniques are run for 30 times from different initial population for observing their performances. Table 3.9 presents the statistical values of IGD indicator for five EMO techniques. It can be observed from the table that the mean and standard deviation of IGD values for all EMO techniques are very small. Similar observation can be seen in Table 3.10 in which the statistical hypervolume indicator values are presented. Smaller indicator values suggest better convergence and diversity. These tables suggest equivalent performance of EMO techniques for the modified bi-objective optimization problem.

Table 3.9: Mean and standard deviation of IGD indicator for five EMO techniques.

	NSGAII		SPEA2		PAES	
	Mean	Std. dev.	Mean	Std. dev.	Mean	Std. dev.
Model-1	3.74e-04	1.6e-05	3.94e-04	1.4e-04	2.62e-03	4.0e-03
Model-2	3.88e-04	1.1e-05	1.19e-03	2.5e-03	2.89e-03	4.0e-03
	SMPSO		GDE3			
	Mean	Std. dev.	Mean	Std. dev.		
Model-1	3.80e-04	8.2e-05	3.19e-04	6.1e-05		
Model-2	3.76e-04	9.9e-05	3.75e-04	3.9e-05		

Table 3.10: Mean and standard deviation of HV indicator for five EMO techniques.

	NSGAII		SPEA2		PAES	
	Mean	Std. dev.	Mean	Std. dev.	Mean	Std. dev.
Model-1	9.74e-01	5.1e-04	9.75e-01	1.7e-03	9.70e-01	8.0e-03
Model-2	9.74e-01	2.0e-04	9.73e-01	2.5e-03	9.53e-01	8.6e-02
	SMPSO		GDE3			
	Mean	Std. dev.	Mean	Std. dev.		
Model-1	9.74e-01	2.0e-04	9.75e-01	7.3e-05		
Model-2	9.74e-01	2.4e-04	9.74e-01	2.5e-04		

3.3.3.2 Obtained Non-dominated Solutions

The performance of five EMO techniques was found to be equivalent, therefore the results of NSGA-II have been chosen for further study in this section. It is worth to mention that model-1 refers to the bi-objective optimization problem given in Eq. (3.6) by calculating the cutting force given in Eq. (A.20). Model-2 is referred when the same bi-objective optimization problem is solved by using Eq. (A.26) for determining cutting force.

The non-dominated solutions obtained from NSGA-II by considering both the models are shown in Fig. 3.19. A clear trade-off between the posed objectives can be seen from the figure. The extreme solutions '$a1$' from the model-1 and '$a2$' from the model-2 represent the minimum power requirement from a bulldozer for soil cutting. Other extreme solutions '$z1$' from the model-1 and '$z2$' from the model-2 signify the minimum time to cut soil in one pass. The knee region (black color circle and diamond symbols) is also visible from the obtained PO front. The knee region signifies a descent trade-off between the objectives. Outside this region (green and blue colors circle and diamond

symbols) suggests that any gain in one objective infers higher loss in other objective. These outside regions are least preferred by any decision maker or practitioner. It is interesting to note that both models show similar trade-off between two objectives, although both models have been developed on different failure zones.

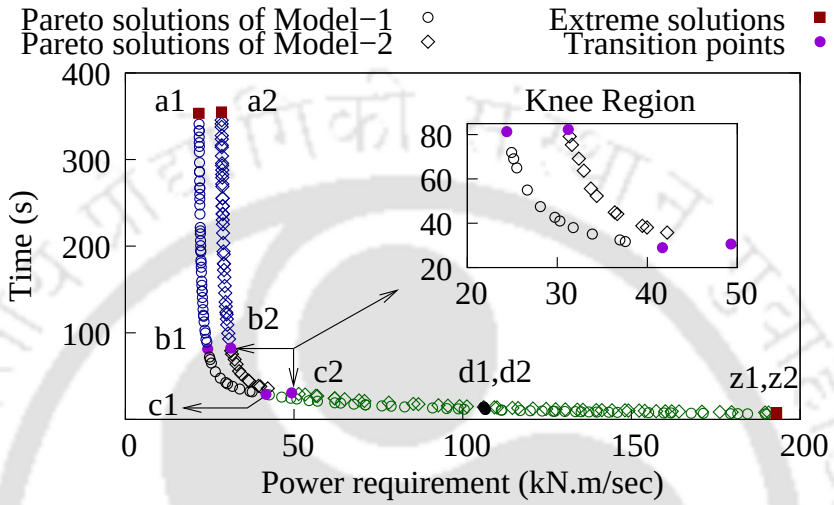

Figure 3.19: The non-dominated solutions from NSGA-II for both the models.

Table 3.11: The solutions obtained from NSGA-II and $\epsilon-$constraint method considering model-1 are presented.

Solutions	NSGA-II solutions (P, T)	$\epsilon-$ constraint solutions (P, ϵ_T)
$a1$	(21.822, 353.381)	(21.818, 353.381)
$b1$	(22.136, 237.011)	(22.132, 237.011)
$c1$	(26.672, 54.990)	(26.666, 54.990)
$d1$	(106.749, 11.546)	(102.929, 11.546)
$z1$	(192.997, 6.286)	(170.798, 6.286)

Table 3.12: The solutions obtained from NSGA-II and $\epsilon-$constraint method considering model-2 are presented.

Solutions	NSGA-II solutions (P, T)	$\epsilon-$ constraint solutions (P, ϵ_T)
$a2$	(28.524,354.894)	(28.512,354.894)
$b2$	(28.854, 237.345)	(28.848, 237.345)
$c2$	(33.719, 55.659)	(33.711, 55.695)
$d2$	(106.222, 14.269)	(105.673, 14.269)
$z2$	(193.024, 7.818)	(183.560, 7.818)

The bi-objective optimization problem is also solved by a numerical optimization

technique using the ϵ-constraint method given in Eq. (3.14). The starting solutions for *fmincon* solver are '$a1$', '$b1$', '$c1$', '$d1$' and '$z1$' obtained from NSGA-II as shown in Fig. 3.19. The value of ϵ_T in Eq. (3.14) for these starting solutions are given in Table 3.11. A marginal improvement in P values of the $\epsilon-$constraint method can be seen with respect to NSGA-II solutions. It can be concluded that NSGA-II is able to generate a set of solutions, which may be closer to the true PO front in just one run.

The same analysis of the ϵ-constraint method is also performed using model-2. The solutions from NSGA-II and the ϵ-constraint method are presented in Table 3.12. Except solution '$z2$', a smaller difference in the power objective value is observed. Since solution '$z2$' lies away from the knee region, the modified solution shows difference in P values.

Perturbation Analysis of Obtained Solutions A perturbation analysis of decision variables, which was presented in Section 3.2.3, is performed to observe change in the power requirement (ΔP) values. Table 3.13 presents ΔP values that are positive for all variables, except α. It means that perturbing a variable increases the power requirement, and thus the power cannot be further minimized. However, the negative values of the power requirement by perturbing α suggest that the power requirement can further be reduced. Another observation can be seen in drastic change of ΔP values for solutions '$c1$', '$d1$' and '$z1$'. Such ΔP change is associated with the solutions lying away from the knee region as it is observed with '$d1$' and '$z1$' solutions. Similar observation cannot be seen with '$a1$' solution even though it is also lying away from the knee region. It is because '$a1$' and '$b1$' solutions are vertically aligned to $P-$objective axis in Fig. 3.19.

The perturbation analysis also brings out sensitivity of decision variables with respect to ΔP value. It can be seen from the same table that v is the most sensitive decision variable as larger ΔP values can be seen from solutions '$a1$' to '$d1$'. Thereafter, D decision variable followed by H, B, R and θ are sensitive to the given problem for the same set of solutions. However for '$z1$', which is lying in the flat region of the PO front, D is more sensitive than v. It also seems that α is not very sensitive for the given problem in Eq. (3.6) as change in ΔP values is very marginal for solutions '$a1$' to '$z1$'.

Table 3.13: The change in ΔP value for perturbation analysis of the non-dominated solutions for model-1.

Solutions	D	α	v	B	H	R	θ
$a1$	58.902	-0.0006	78.481	7.272	15.888	6.251	5.370
$b1$	59.033	-0.0014	79.540	7.369	15.921	6.220	5.344
$c1$	62.571	-0.049	95.957	8.855	16.311	5.827	5.007
$d1$	197.831	-1.078	137.139	33.814	48.422	15.224	13.095
$z1$	347.621	-2.274	138.921	62.528	84.115	26.095	22.495

Table 3.14: The change in ΔP value for perturbation analysis of the non-dominated solutions for model-2.

Solutions	D	α	v	B	H	R	θ
$a2$	61.062	9.922	102.561	9.503	17.842	11.518	9.901
$b2$	61.077	10.186	103.879	79.626	17.854	11.518	9.901
$c2$	61.415	13.668	121.283	11.239	18.017	11.518	9.901
$d2$	160.958	48.950	147.165	35.406	47.444	29.964	25.732
$z2$	279.009	91.112	154.406	64.336	82.390	51.841	44.520

The perturbation analysis is also performed for the non-dominated solutions from model-2. Table 3.14 presents change in the power requirement values. All positive values can be seen from the table, which suggests that the power requirement cannot be reduced further, and NSGA-II evolved solutions that may be closer to the true PO solutions. For model-2, decision variables v, D, H, α, B, R, and θ are sensitive in this hierarchical order for solutions '$a2$' to '$d2$'. For solution '$z2$', the hierarchy of sensitivity of decision variables is D, v, α, H, B, R, and θ.

3.3.3.3 Post-Optimal Analysis

The post-optimal analysis of the non-dominated solutions from NSAG-II is presented. As mentioned earlier in Section 3.2.3.3, the aim behind this analysis to decipher important relationships among the approximate PO solutions.

Post-Optimal Analysis of Solutions Obtained using Model-1 The common principles are those, which are being followed by all non-dominated solutions. Figs. 3.20−3.24 show that the optimal values of B, H, R, α and θ decision variables for all non-dominated solutions are evolved at their bounds. These are not the intuitive

relationships when the power and time objectives are minimized simultaneously, and thus it makes the design principle for the given optimization problem.

The dissimilar relationships among the approximate PO solutions are now presented that are responsible for trade-off between the two objectives. Fig. 3.25 shows trend of D decision variable and Fig. 3.26 shows trend of v with respect to both the objectives. It can be seen that solutions with different values of D and v are responsible for trade-off between the two objectives. It is important to understand that such trends of D and v are not intuitive. For deeper understanding, a closer relationship between these two variables is shown in Fig. 3.27. The solution lying in between '$a1$'-'$b1$' are evolved with fixed v at its lower bound, but with marginal increase in D values. For the solutions lying in between '$b1$'-'$c1$' (the knee region), D has been increasing till its upper bound, but without change in v value. The solutions lying in between '$c1$'-'$z1$' are evolved with increasing v values till it reaches to its upper bound. For the same set of solutions D value is fixed at its upper bound. This suggests an intuitive observation that a bulldozer with the minimum power requirement objective has to be run at a lower cutting depth and velocity. However, the soil cutting has to be done in minimum time by adopting larger cutting depth and velocity. From these results, it can be concluded that trends observed in D and v are responsible for trade-off among the non-dominated solutions.

Post-Optimal Analysis of Solutions Obtained using Model-2 The post-optimal analysis of the non-dominated solutions from model-2 is presented. The common design principles can be seen from Figs. 3.28−3.32 in which the same set of decision variables, as discussed in the last section, is evolved at their lowest bounds. Again, such design principles are not intuitive when both the objectives are minimized simultaneously.

The dissimilar relationships are shown in Figs. 3.33−3.34 that are responsible for trade-off among the approximate PO solutions. The pattern is same as discussed in the last section. The relationship between D and v is shown in Fig. 3.35 in which the solutions lying between '$a2$'−'$b2$' are evolved with fixed v. Thereafter, the solutions between '$b2$'−'$c2$' are evolved with increasing value of D that reaches to its upper bound without increase in v value. The last set of solutions lying in between '$c2$'−'$z2$' is evolved with increasing value of v till it reaches to its upper bound with fixed D.

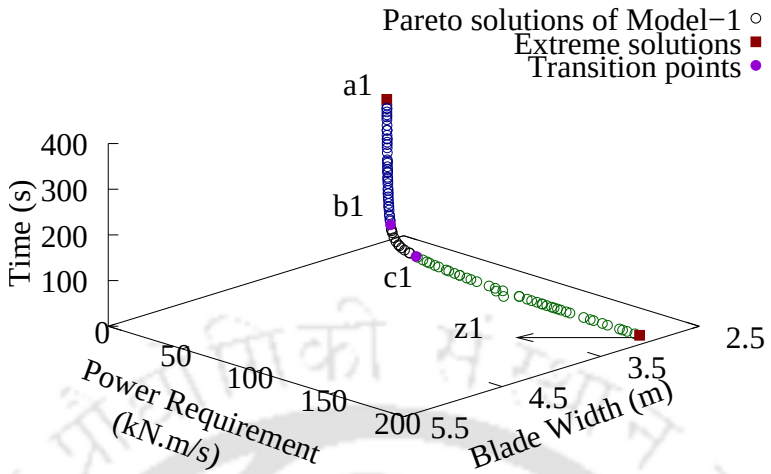

Figure 3.20: The post-optimal relationship of the blade width with the objectives using model-1 is presented.

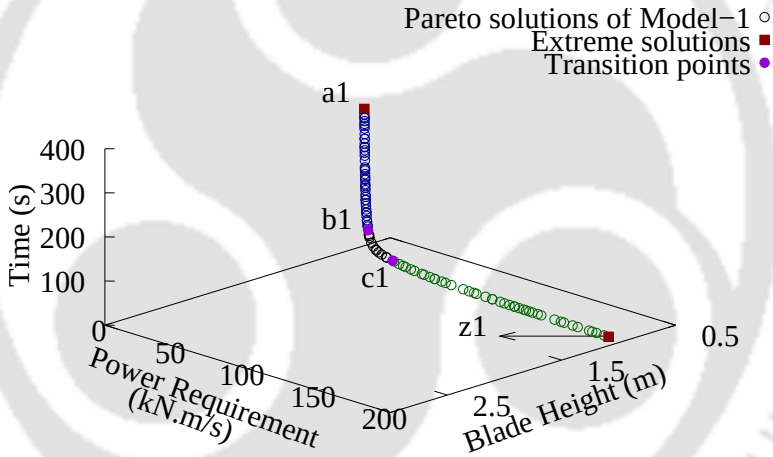

Figure 3.21: The post-optimal relationship of the blade height with the objectives using model-1 is presented.

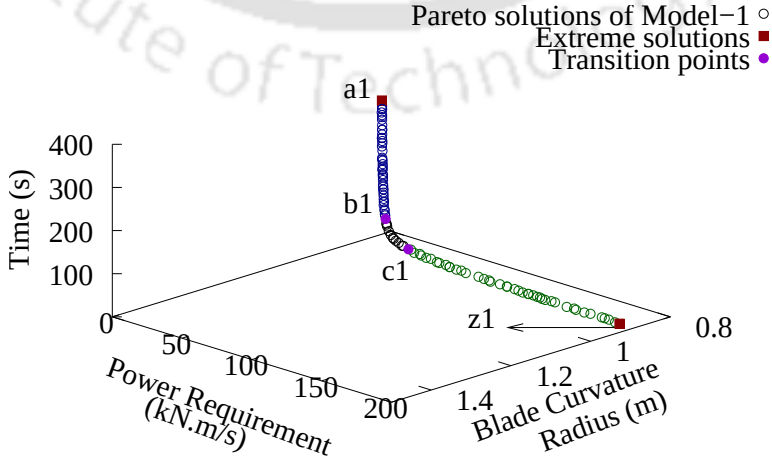

Figure 3.22: The post-optimal relationship of the curvature radius with the objectives using model-1 is presented.

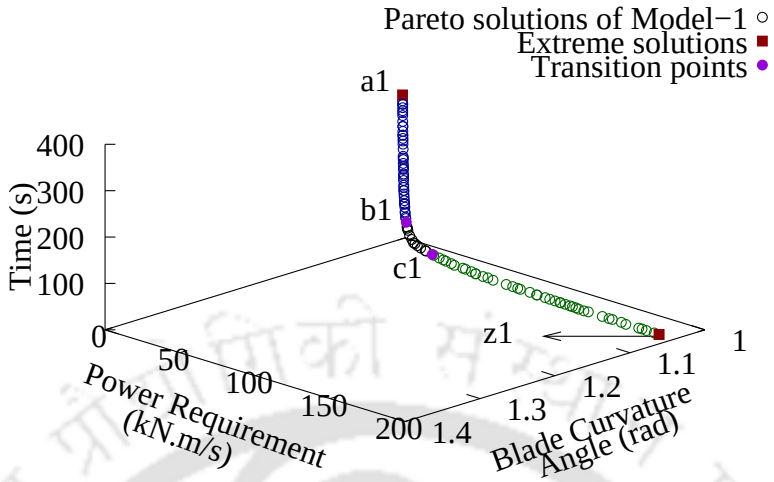

Figure 3.23: The post-optimal relationship of the blade curvature angle with the objectives using model-1 is presented.

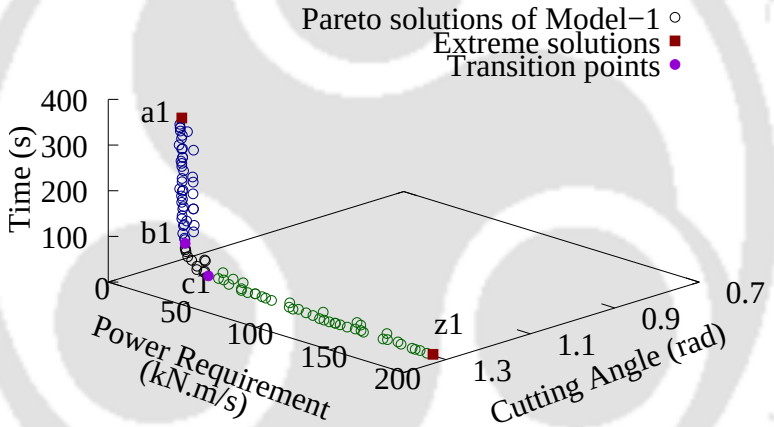

Figure 3.24: The post-optimal relationship of the cutting angle with the objectives using model-1 is presented.

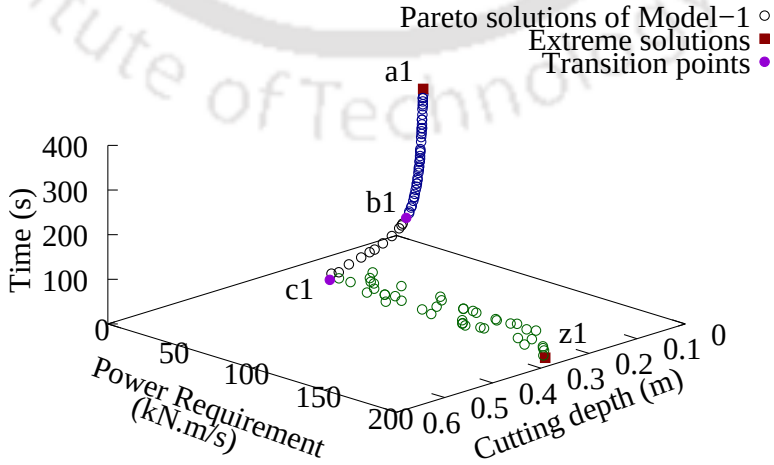

Figure 3.25: The post-optimal relationship of the cutting depth with the objectives using model-1 is presented.

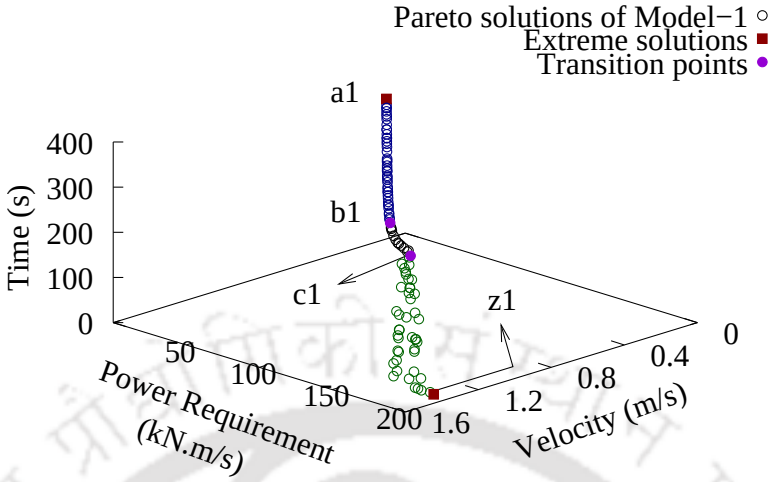

Figure 3.26: The post-optimal relationship of the velocity with the objectives using model-1 is presented.

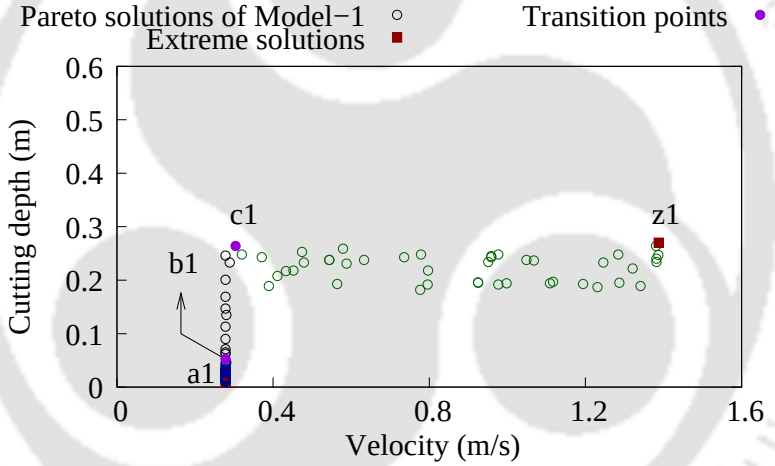

Figure 3.27: The post-optimal relationship of the cutting depth and velocity using model-1 is presented.

3.3.3.4 Guidelines for Practitioners

The aim of presenting the post-optimal analysis of the non-dominated solutions is to decipher important design principles and relationships. It is found that four decision variables, that are, B, H, R and θ should be set at their lower limit for generating the non-dominated solutions. Since the blade dimensions are evolved at their lower bounds, an interesting observation can be made that a small size blade can achieve the proposed objectives of minimizing the power and time simultaneously. This guideline is useful when a decision has to be made for optimal soil cutting.

The knee region shown in Fig. 3.19 is always preferable for choosing an optimal set

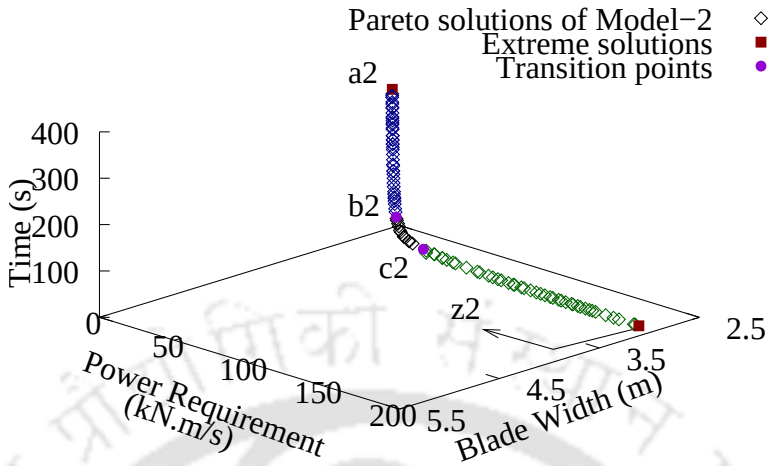

Figure 3.28: The post-optimal relationship of the blade width with the objectives using model-2 is presented.

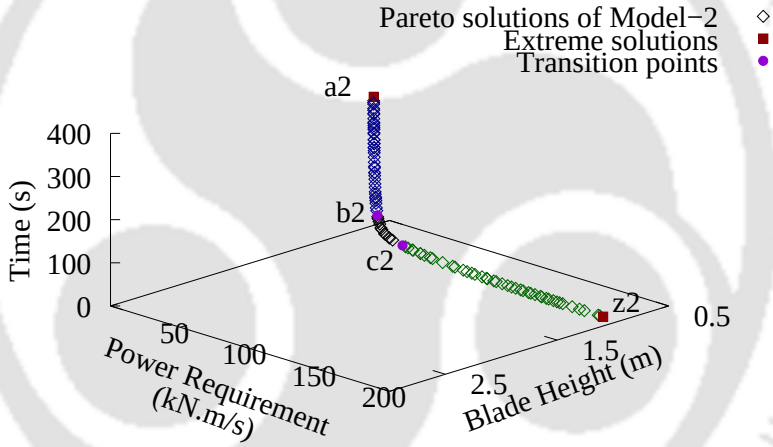

Figure 3.29: The post-optimal relationship of the blade height with the objectives using model-2 is presented.

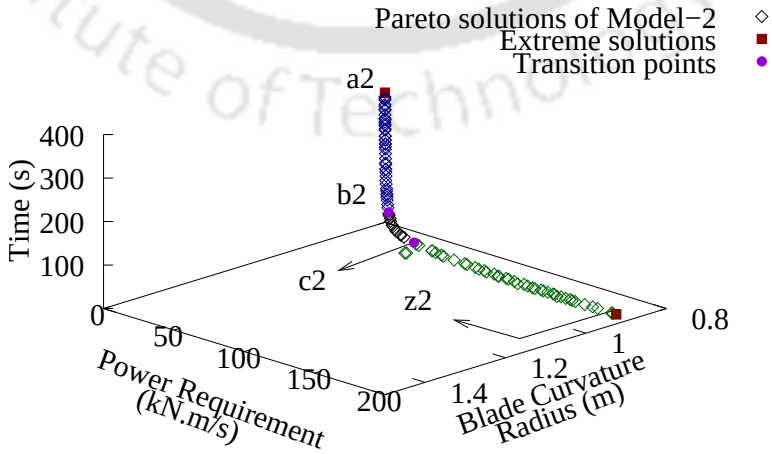

Figure 3.30: The post-optimal relationship of the radius of curvature with the objectives using model-2 is presented.

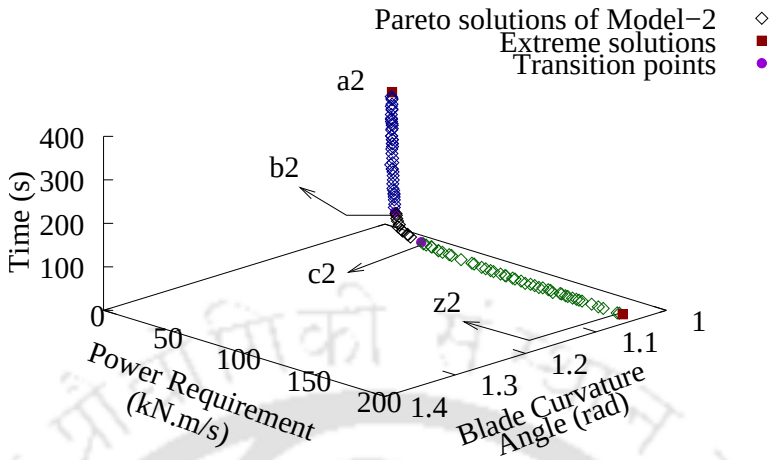

Figure 3.31: The post-optimal relationship of the curvature angle with the objectives using model-2 is presented.

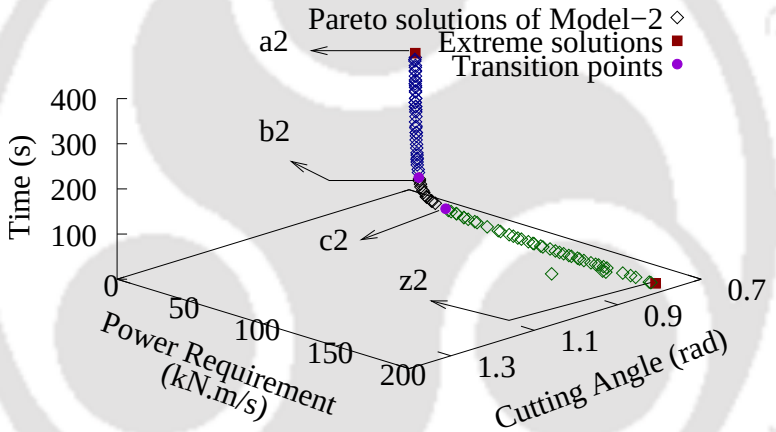

Figure 3.32: The post-optimal relationship of the cutting angle with the objectives using model-2 is presented.

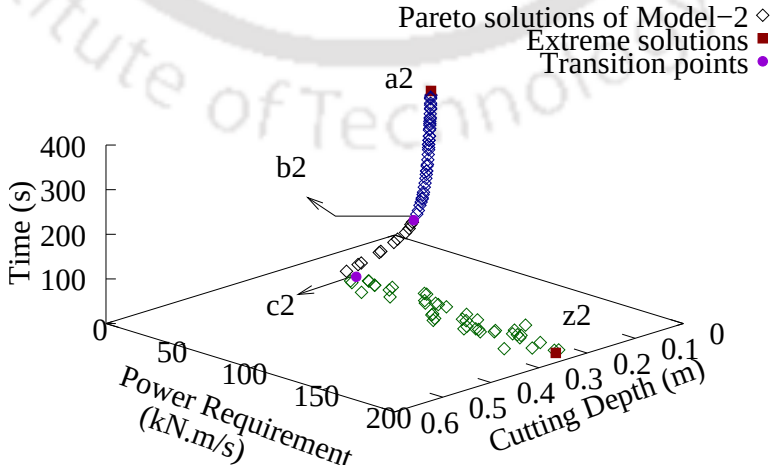

Figure 3.33: The post-optimal relationship of the cutting depth with the objectives using model-2 is presented.

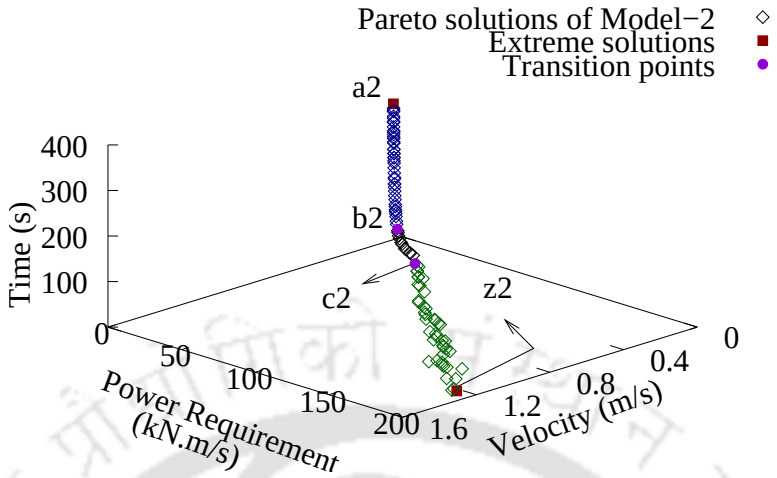

Figure 3.34: The post-optimal relationship of the velocity with the objectives using model-2 is presented.

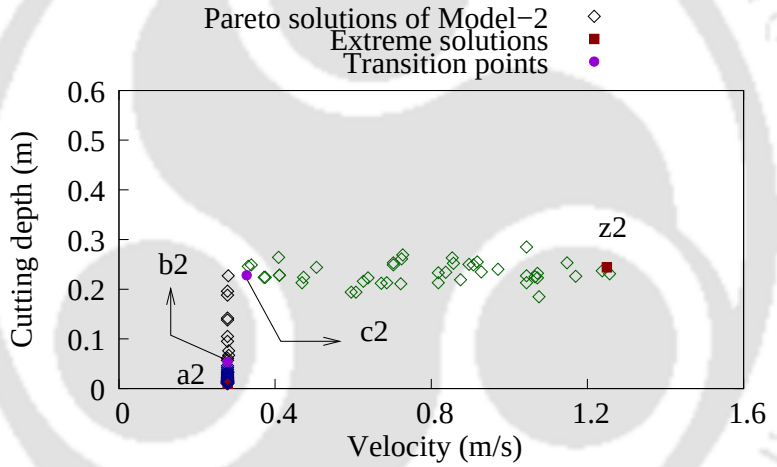

Figure 3.35: The post-optimal relationship of the cutting depth and velocity with the objectives using model-2 is presented.

of input decision variables. Since B, H, R, θ and α should be chosen at their bounds, the optimal values can be chosen from Figs. 3.20−3.23. The values of cutting depth and velocity can be chosen from Fig. 3.36, which is redrawn for the solutions lying in the knee region. In this figure, solutions corresponding to lower power objective value are evolved at the lower cutting depth and velocity, and vice-versa for lower time objective value.

Generally, the power requirement is not known earlier. However, a fair idea of time to cut soil can help the practitioner to choose the optimal solution from Fig. 3.19. Corresponding to the chosen solution, value of the power requirement can help the practitioner to analysis the solution because the power requirement can affect the fuel

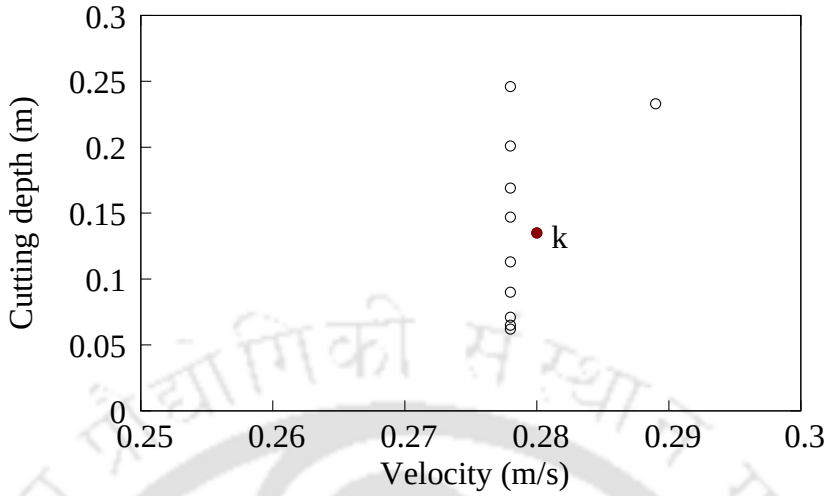

Figure 3.36: The non-dominated solutions lying in the knee region of Fig. 3.19.

consumption that can be understood as the economy of the operation. The set of non-dominated solutions can provide a useful comparison among them for appropriate decision making. For example, solution 'k' should be chosen over solution '$b1$' or '$c1$' as it is lying in the knee region. If the practitioner chooses any solution (say 'k') from Fig. 3.19 that is evolved in the knee region, then the power requirement is 29.743 kNm/s and the time required to cut soil is 42.6 s. Fig. 3.36 shows that the cutting depth of solution 'k' should be chosen at 13.5 cm and the velocity of a bulldozer should be kept at 0.28 m/s. Rest of the input decision variable can be chosen based on the decision principles described in the last paragraph. All the figures referred in this section can be used for on-site decision making for choosing an optimal set of input parameters for the proposed set of objectives. Similar guidelines can be made by using model-2 as both models showed similar trends and relationships.

Critical Observation The post-optimal results showed that the blade dimensions are evolved at their lower bounds. It means that a smaller size blade can minimize P and T simultaneously. Since the productivity was defined to minimize T to cut soil in one pass, the proposed objective cannot maximize the productivity of overall operation in which the soil cutting task can be finished quickly by using a large blade and gets operated at higher D and v. To introduce variation in the blade dimensions among the non-dominated solutions, a multi-objective formulation is proposed in the following section.

3.4 Multi-Objective Optimization Formulation

The proposed multi-objective formulation is given in Eq. (3.15).

$$
\begin{array}{lll}
\text{Minimize} & P, & \text{(Power requirement)},\\
\text{Minimize} & N, & \text{(Number of passes)},\\
\text{Minimize} & T, & \text{(Time)},\\
\text{subject to} & P_R \geq 0, & \text{(Remaining power)},\\
& F \leq F_{max}, & \text{(Blade failure)},\\
& P_d \geq P_{dmin}, & \text{(Production rate)},\\
& 0.01 \leq D \leq 0.5, & \text{(Decision variables)},\\
& 0.785 \leq \alpha \leq 1.309, & \\
& 0.278 \leq v \leq 1.389, & \\
& 3 \leq B \leq 5, & \\
& 1 \leq H \leq 2.5, & \\
& 0.9 \leq R \leq 1.5, & \\
& 1.047 \leq \theta \leq 1.309. &
\end{array}
\tag{3.15}
$$

It can be seen that one additional objective function on the number of passes is included in the formulation. Here, the second and third objectives signify productivity. The second objective signifies overall productivity for the operation by finishing it in less number of passes. It can happen when a large size blade is used at a higher cutting depth and velocity thereby increasing power requirement from the bulldozer. The third objective signifies local perspective of productivity of the operation by filling a blade in less time. It conflicts the overall productivity of the operation when a small size blade is used that will be filled quickly but will require more number of passes to finish the operation. Also, the third objective conflicts with the power requirement objective when a small blade is used at a higher depth of cut and velocity for reducing time for filling a blade with soil.

The objectives on P and T have already been described in Section 3.3. Here, L is determined as

$$L = V_{max}/B \times D. \tag{3.16}$$

The number of passes (N) is determined as

$$N = V_{max}/V, \tag{3.17}$$

where V_{max} is the fixed volume of soil to be cut, and V is the blade capacity that is calculated in Eq. (3.2). The constraints and their limits are same as described in Section 3.3.

3.4.1 Optimization Techniques

For solving the multi-objective optimization problem, five EMO techniques and the $\epsilon-$constraint method are used. The details of five EMO techniques can be found in Appendix B. The $\epsilon-$constraint method is used in which the objectives on N ans T are converted into the constraints. The single-objective optimization formulation is given as

$$\begin{aligned} \text{Minimize} \quad & P, \\ \text{subject to} \quad & N \leq \epsilon_N \\ & T \leq \epsilon_T \\ & P_R \geq 0, \\ & F \leq F_{max}, \\ & P_d \geq P_{dmin}, \\ & 0.01 \leq D \leq 0.5, \\ & 0.785 \leq \alpha \leq 1.309, \\ & 0.278 \leq v \leq 1.389, \\ & 3 \leq B \leq 5, \\ & 1 \leq H \leq 2.5, \\ & 0.9 \leq R \leq 1.5, \\ & 1.047 \leq \theta \leq 1.309, \end{aligned} \tag{3.18}$$

where ϵ_N and ϵ_T are the lower bounds on N and T.

3.4.2 Results and Discussion

The parameters for five EMO techniques are kept same for 30 runs which are presented in Table 3.15. The IGD and HV indicators are used for observing performance of these EMO techniques. The mid-stiffness clay soil is used and its parameters are presented in Table 3.2. The fixed volume of soil to be cut is set to $V_{max} = 200$ m^3.

Table 3.15: The constant parameters for EMO techniques are presented. Here, p_c and p_m are the crossover and mutation probabilities, η_c and η_m are the distribution indexes of simulated binary crossover and polynomial mutation. CR is the crossover probability and F_{sf} is the scaling factor for GDE3.

EMO techniques	Parameters
NSGA-II	Population size =500; generation = 500; $p_c = 0.9$; $\eta_c = 20$; p_m =1/no. of variables; $\eta_m = 20$
SPEA2	Population size = 500; archive size = 500; generation = 100; $p_c = 0.9$; $\eta_c = 20$; p_m =1/no. of variables; $\eta_m = 20$
PAES	Archive size = 500; generation = 500; p_m =1/no. of variables; η_m = 20
SMPSO	Population size = 500; archive size =500; generation = 100; p_m =1/no. of variables; $\eta_m = 20$
GDE3	Population size = 500; generation = 500; CR = 0.5, $F_{sf} = 0.5$

3.4.2.1 Statistical Performance Analysis of EMO techniques

The mean and standard deviation of IGD and HV indicators for 30 runs of EMO techniques are presented in Tables 3.16 and 3.17. Except for PAES, all EMO techniques show equivalent performance based on the mean values of indicators. Moreover, the standard deviation is quite small that suggests similar outcome of the non-dominated solutions from the EMO techniques.

3.4.2.2 Obtained Non-dominated Solutions

All EMO techniques showed equivalent performance on IGD and HV indicators, therefore the solutions obtained from NSGA-II are considered in this section. The non-dominated solutions generated using model-1 are shown in Fig. 3.37. For discussion, these solutions are categorized into three groups. The first group of the non-dominated solutions is referred as the surface solutions (blue color symbols) in which most of the solutions are generated at lower P values. The second group of solutions (black color filled symbols) is referred as the knee-solutions that show a decent trade-off among the objectives. The third region is referred as the extension solutions in which the solutions do not show much trade-off between T and N, but objective P increases to higher value. Three extreme solutions are also shown in Fig. 3.37 in which solution '$a1$' represents minimum P, solution '$z1$' represents minimum T, and solution '$e1$' represents minimum N.

Table 3.16: Mean and standard deviation of IGD indicator for five EMO techniques.

	NSGAII		SPEA2		PAES	
	Mean	Std. dev.	Mean	Std. dev.	Mean	Std. dev.
Model-1	7.26e-04	6.0e-05	7.53e-04	5.0e-05	4.65e-03	6.7e-04
Model-2	7.50e-04	3.6e-05	7.55e-04	4.5e-05	5.02e-03	1.5e-03
	SMPSO		GDE3			
	Mean	Std. dev.	Mean	Std. dev.		
Model-1	8.12e-04	6.2e-05	8.63e-04	5.2e-05		
Model-2	7.94e-04	4.3e-05	8.84e-04	3.4e-05		

Table 3.17: Mean and standard deviation of HV indicator for five EMO techniques.

	NSGAII		SPEA2		PAES	
Model-1	5.11e-01	2.1e-02	4.87e-01	2.2e-02	2.68e-01	7.5e-02
Model-2	4.86e-01	2.1e-02	4.69e-01	3.0e-02	2.38e-01	6.5e-02
	SMPSO		GDE3			
	Mean	Std. dev.	Mean	Std. dev.		
Model-1	5.76e-01	9.1e-02	5.17e-01	2.3e-02		
Model-2	5.69e-01	1.1e-01	5.16e-01	2.6e-02		

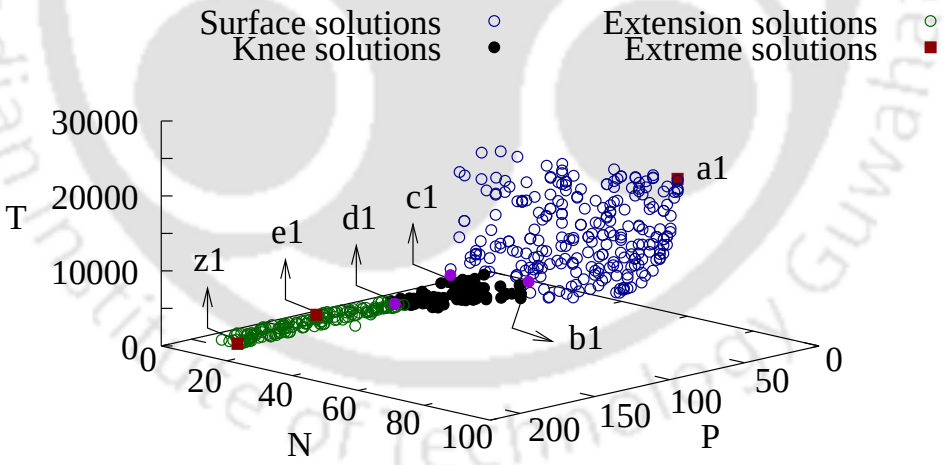

Figure 3.37: The approximate PO solutions from NSGA-II using model-1 are presented. The solutions are categorized into three groups. Different colors are used for distinguishing the solutions lying in three groups. The unit of P and T are kN.m/s and s, respectively.

The scatter plots for three objectives are shown in Fig. 3.38 for model-1 solutions. Since different colors for the symbols are used, three groups of the approximate PO solutions can be distinguished. The surface solutions are generated with lower P values. The same solutions show trade-off between N and T (refer Fig. 3.38c) in which these

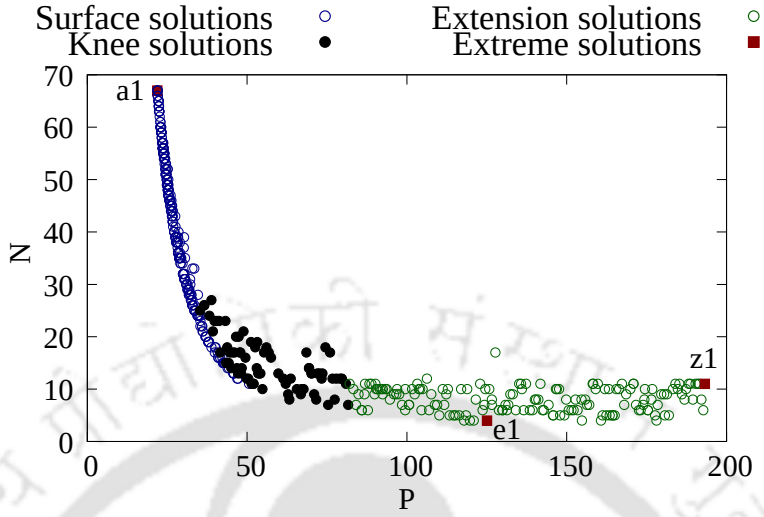

(a) P vs N

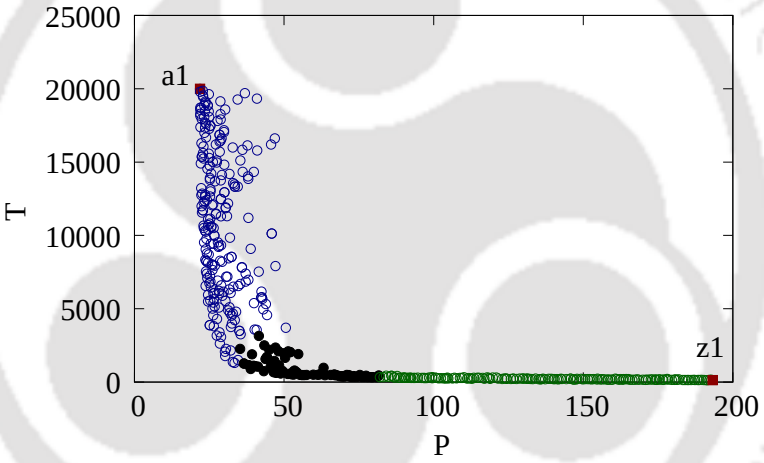

(b) P vs T

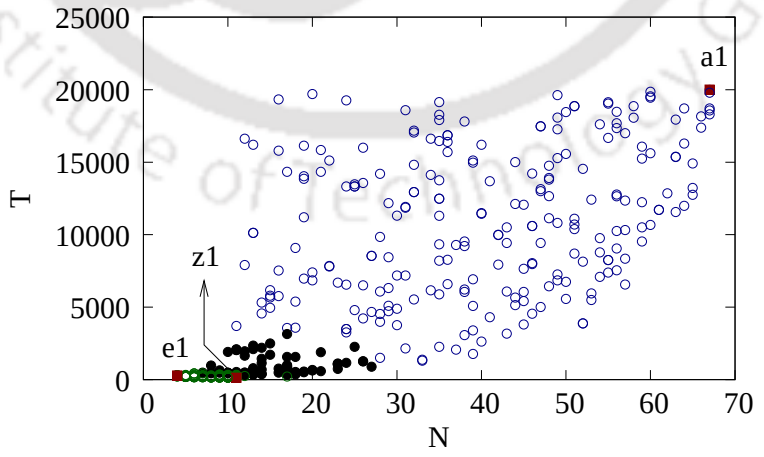

(c) N vs T

Figure 3.38: The scatter plots for three objectives are presented in which the relationships among the objectives are shown for three groups of the approximate PO solutions using model-1.

solutions are generated over a wide range of N and T objectives. The second group is made of the knee-solutions, which is always important for a practitioner or decision maker. It is because the solutions show a decent trade-off among the posed objectives in this region. The extension solutions are generated with lower N and T values (refer Figs. 3.38a and 3.38b). However, higher P values can be observed.

The approximate PO solutions obtained using model-2 are shown in Fig. 3.39. The solutions again can be categorized into three groups. The surface solutions have lower P values and wider ranges of T and N. The knee-solutions show a decent trade-off among the objectives. The extension solutions are evolved with larger P values but with less N and T ranges. In the figure, solution '$a2$' represents minimum P value, solution '$e2$' represents minimum N value, and solution '$z2$' represents minimum T value. The scatter plots are also shown in Fig. 3.40 for model-2 in which same observation can be made as observed with model-1 solutions.

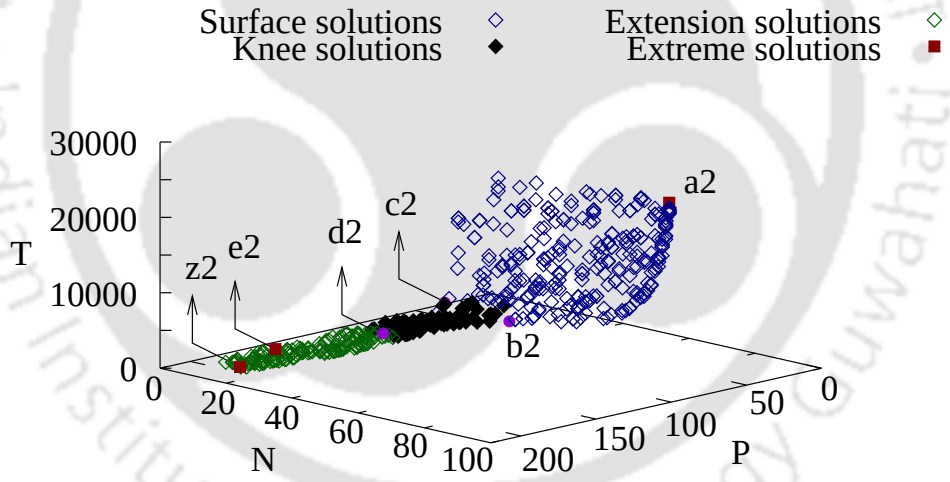

Figure 3.39: The approximate PO solutions from NSGA-II using model-2 are presented. The solutions are categorized into three groups. Different colors are used for distinguishing the solutions lying in three groups.

The non-dominated solutions are also generated using the $\epsilon-$constraint method. The starting solutions for *fmincon* solver are marked in Fig. 3.37 for which values of ϵ_N and ϵ_T are set from NSGA-II solutions. Table 3.18 presents NSGA-II solutions and the improved solutions using the $\epsilon-$constraint method. It can be observed that P values have marginally improved from its original values.

For model-2, the starting solutions for the *fmincon* solver are marked in Fig. 3.39. The solutions obtained from NSGA-II and $\epsilon-$constraint method are presented in Table

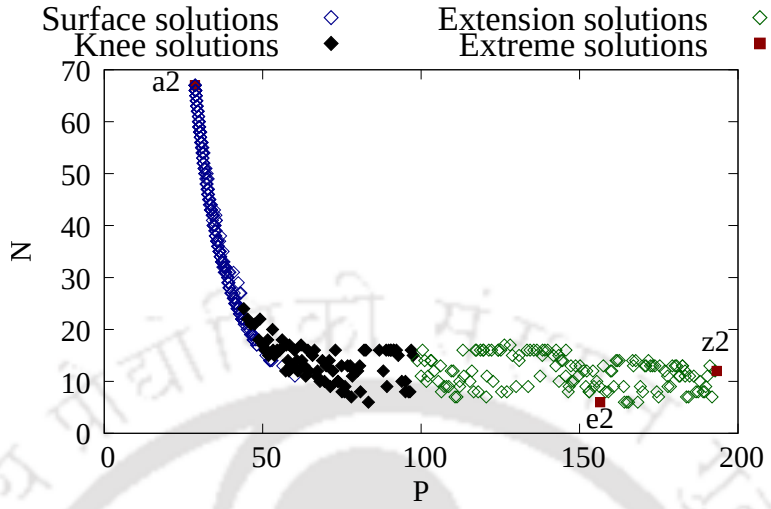

(a) P vs N

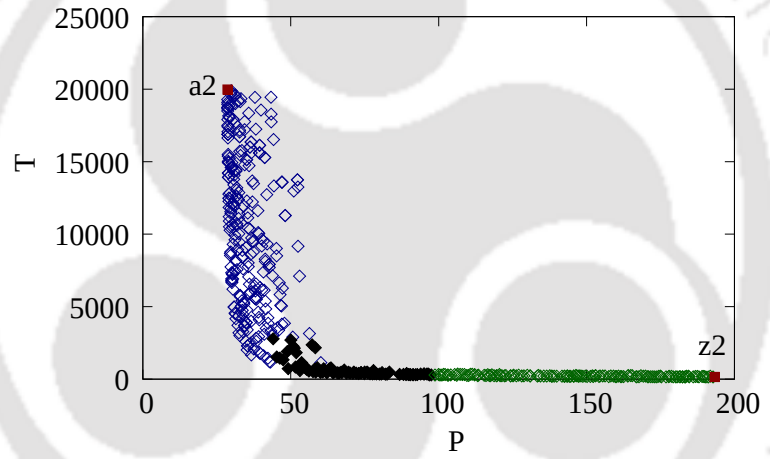

(b) P vs T

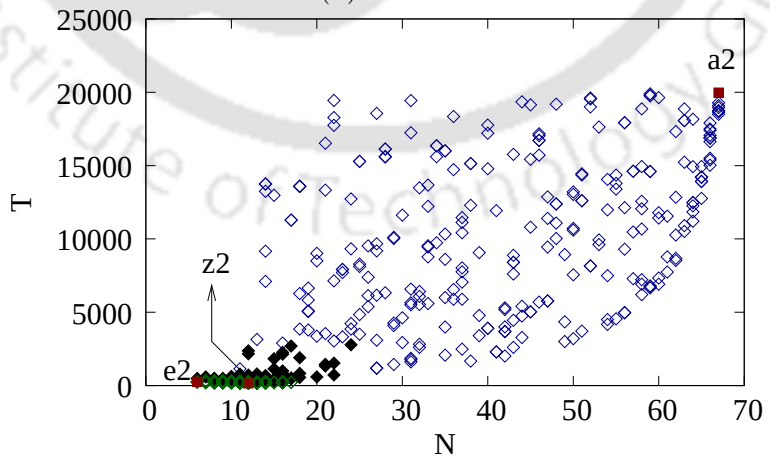

(c) N vs T

Figure 3.40: The scatter plots for three objectives are presented in which the relationships among the objectives are shown for three groups of the approximate PO solutions using model-2.

Table 3.18: The solutions obtained from NSGA-II and $\epsilon-$constraint method considering model-1 are presented.

Solutions	NSGA-II (P, N, T)	$\epsilon-$ constraint $(P, \epsilon_N, \epsilon_T)$
$a1$	(21.936, 67, 19999.920)	(21.935, 67, 19999.920)
$b1$	(33.623, 27, 2849.314)	(33.232, 27, 2849.314)
$c1$	(50.859, 11, 2907.186)	(49.605, 11, 2907.186)
$d1$	(83.584, 9, 362.356)	(80.299, 9, 362.356)
$z1$	(193.231, 11, 134.563)	(192.767, 11, 134.563)

Table 3.19: The solutions obtained from NSGA-II and $\epsilon-$constraint method considering model-2 are presented.

Solutions	NSGA-II (P, N, T)	$\epsilon-$ constraint $(P, \epsilon_N, \epsilon_T)$
$a2$	(28.635, 67, 19968.430)	(28.635, 67, 19968.430)
$b2$	(44.686, 26 881.653)	(44.654, 26, 881.653)
$c2$	(57.017, 12, 2536.945)	(56.378, 12, 2536.945)
$d2$	(97.844, 12, 295.281)	(95.735, 12, 295.281)
$z2$	(193.280, 12, 146.261)	(193.276, 12, 146.261)

3.19. Again, marginal difference can be seen in P values among the solutions obtained from both techniques.

3.4.2.3 Post-Optimal Analysis

The post-optimal analysis of the non-dominated solutions from NSGA-II is now performed to decipher important relationships.

Post-Optimal Analysis for Model-1 The non-dominated solutions using model-1 are shown in Fig. 3.41 in which some decision variables are responsible for trade-off among the solutions, and others decipher the commonality principle for generating the approximate PO solutions. It can be seen from $D - R$ and $D - \theta$ plots (refer Figs. 3.41a and 3.41b) that for all obtained solutions θ and R decision variables are evolved at their lowest bounds. This suggests a commonality principle that a solution can be the approximate PO solution when θ and R are fixed at their lowest values.

Other decision variables are responsible for trade-off among the solutions. The

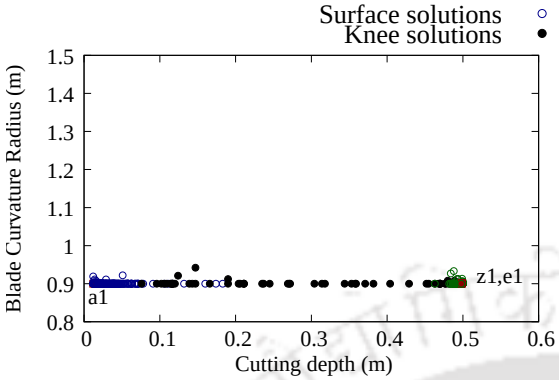

(a) $D - R$ plot

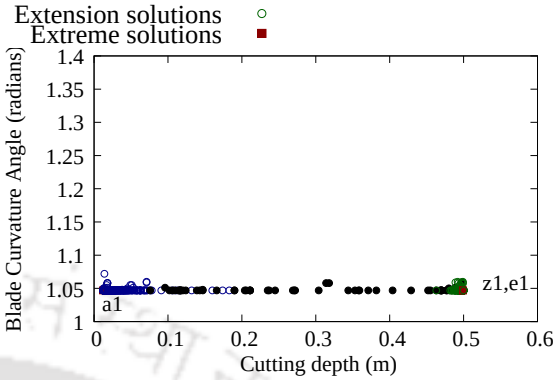

(b) $D - \theta$ plot

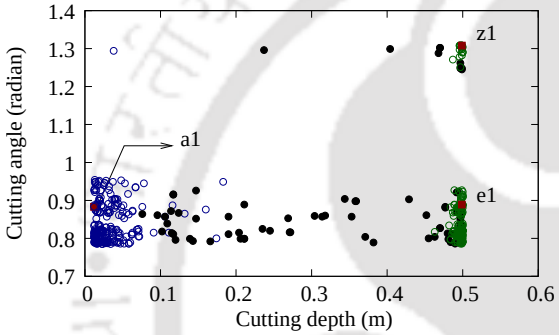

(c) $D - \alpha$ plot

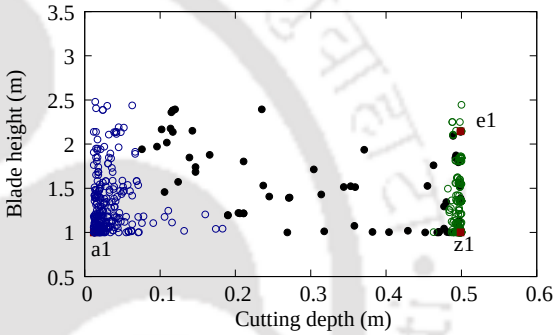

(d) $D - H$ plot

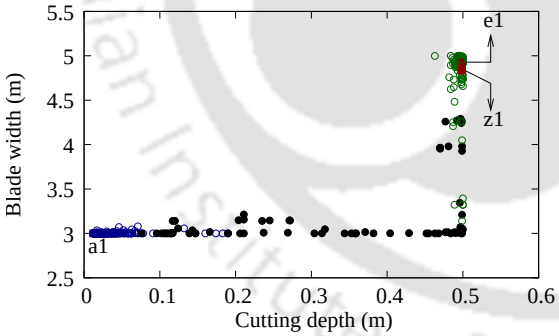

(e) $D - B$ plot

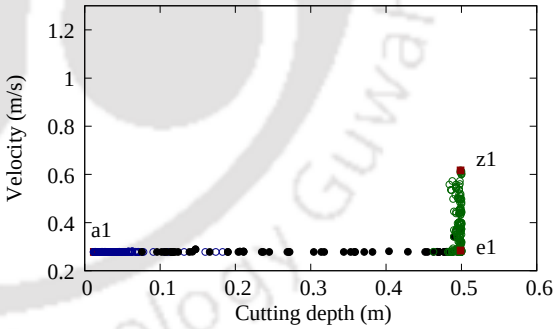

(f) $D - v$ plot

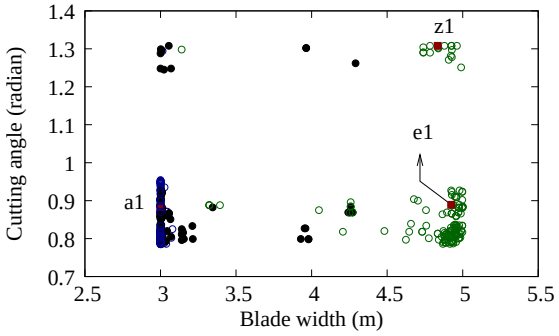

(g) $B - \alpha$ plot

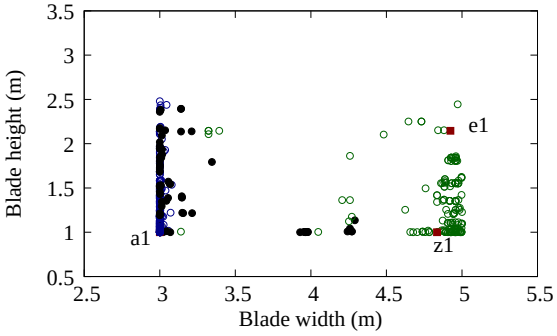

(h) $B - H$ plot

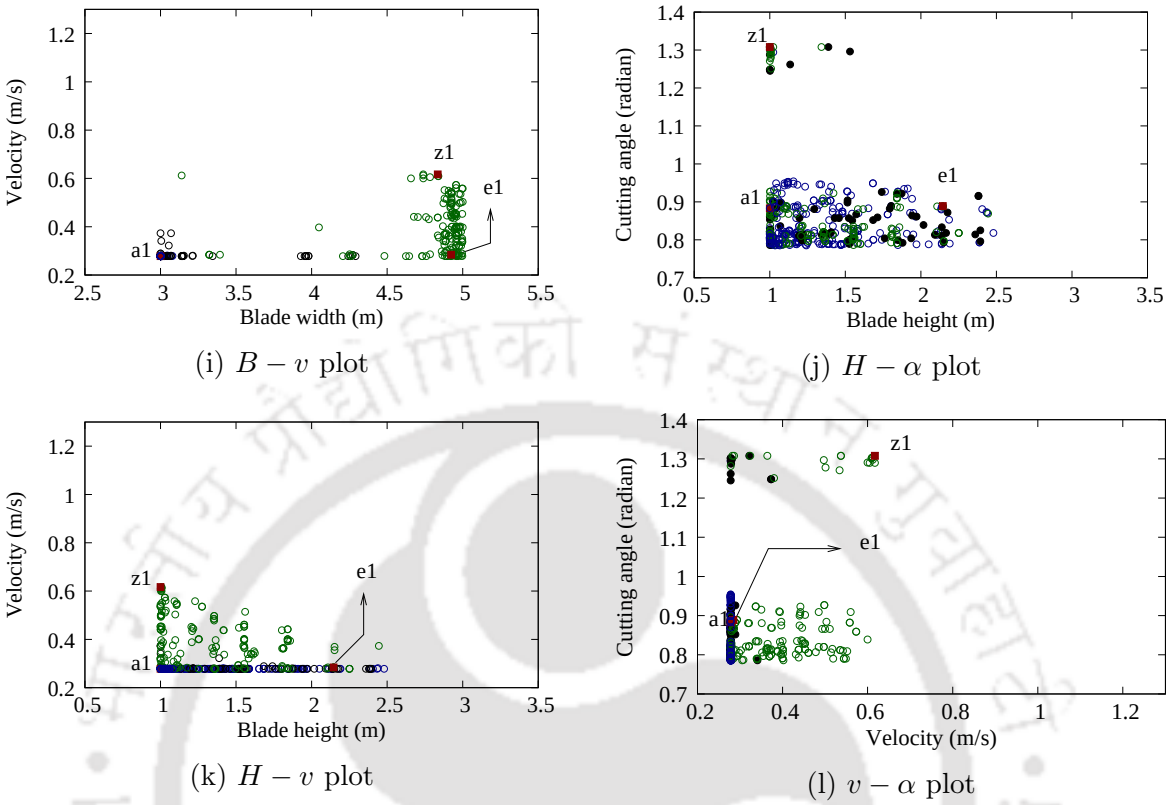

(i) $B - v$ plot (j) $H - \alpha$ plot

(k) $H - v$ plot (l) $v - \alpha$ plot

Figure 3.41: The scatter plots for all decision variables of the approximate PO solutions using model-1 are presented.

surface solutions are evolved with lowest B and v as shown in Fig. 3.41i. The range of D for these solutions is small that lies between $(0.01, 0.183)$ as shown in Fig. 3.41c. Similarly, the range of α lies in between $(0.78, 0.95)$. A wide range of H can be seen from Fig. 3.41d for the surface solutions which vary from 1 to 2.48m. It can be observed that the dimension of the blade changes only for different H values, and other decision variables for blade dimension are evolved at their bounds. Since these solutions are evolved with lower values of D, it can be justified that these solutions are corresponding to lower P values as observed in Fig. 3.37. For the same set of solutions, a wide range of T and N is also observed. It is because when a small size blade, meaning H is small, is used with lower D, it can get filled with soil quickly. However, this blade can take many passes to cut the fixed volume of soil. Contrary to this, a larger size blade with higher H is used, it can take more time to get filled with soil. However, the operation can be completed in less number of passes.

For the knee-solutions, a wide range of D from 0.07 to 0.5m can be seen in Fig.

3.41j. The range of α is also widened from 0.78 to 1.3. The dimensions for a blade are also varied which can be observed from the ranges of H and B (refer Fig. 3.41h). It means that different blades dimensions are evolved which are operated at different D and α values. Since D is varying from its lower limit to upper limit, different size blade show trade-off among all objectives. For example, a smaller blade at lower D takes more time to get filled as compared to larger D. In this case, N remains the same but with larger D, the soil cutting operation can be finished early but requires more power from a bulldozer. Any bigger blade with larger D can finish the operation relatively early against the lower D. However, the bigger blade takes less N but higher P values to finish the soil cutting operation. All observations are in line with the knee-solutions of Fig. 3.37 which showed a decent trade-off among the objectives.

For extension solutions, the decision variables B, H, v, and α are varying from their lower to upper limits. Moreover, D remains at its upper bound of 0.5m. This observation suggests that a wide range of blades are evolved for these solutions that have been used at higher D and all ranges of v and α. This is the reason that higher P values are observed in Fig. 3.37 with less time and number of passes.

Post-Optimal Analysis for Model-2 The post-optimal analysis is presented for the approximate PO solutions obtained using model-2. It can be seen from Figs. 3.42a-3.42c that three variables (R, θ, α) are evolved at their lower bounds which makes a commonality principle for generating the approximate PO solutions. The other decision variables are evolved over their bounds that are responsible for trade-off among the approximate PO solutions. For the surface solutions, similar ranges of D and H are observed as found in Section 3.4.2.3. With the similar discussion on different blade sizes with lower D values, the solutions are evolved at lower P values. However, these solutions show a wide range of N and T because dimension H of the blade is varying as shown in Fig. 3.42d.

For the knee-solutions, the wide ranges of D, B, H, and v can be observed which are responsible for a decent trade-off among these solutions as shown in Fig. 3.39. Similar observation of Section 3.4.2.3 can be made when different sizes of blades are evolved at different operating conditions.

The extension solutions are generated with the similar wide ranges of B, H, and

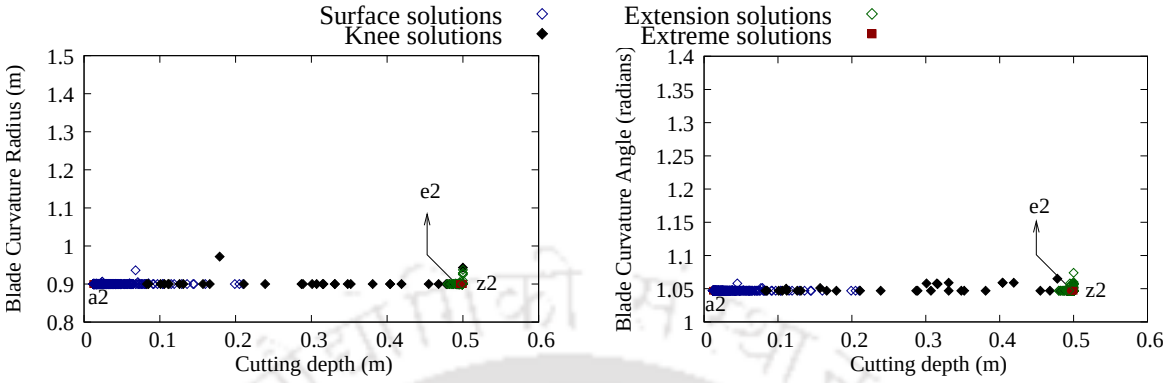

(a) $D - R$ plot

(b) $D - \theta$ plot

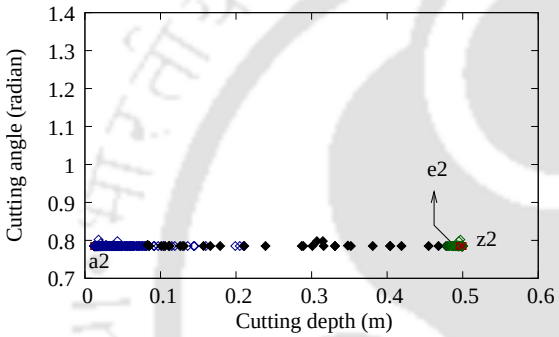

(c) $D - \alpha$ plot

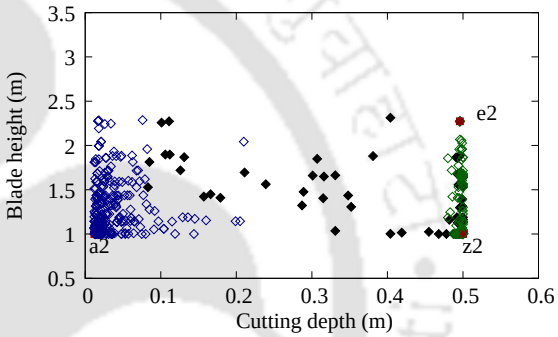

(d) $D - H$ plot

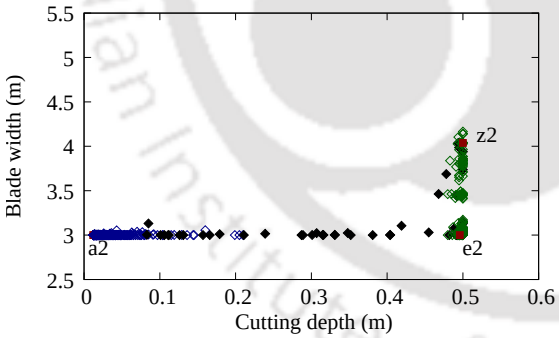

(e) $D - B$ plot

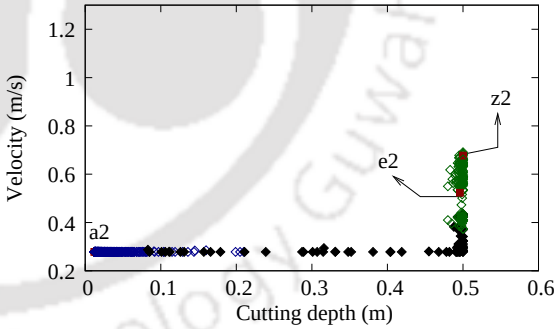

(f) $D - v$ plot

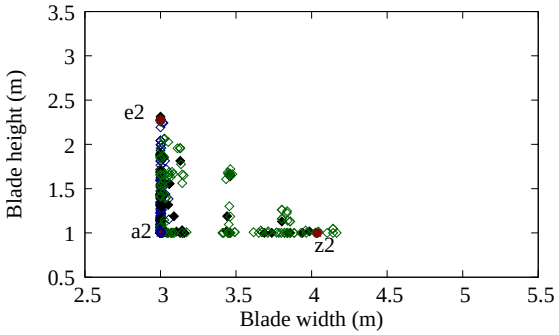

(g) $B - H$ plot

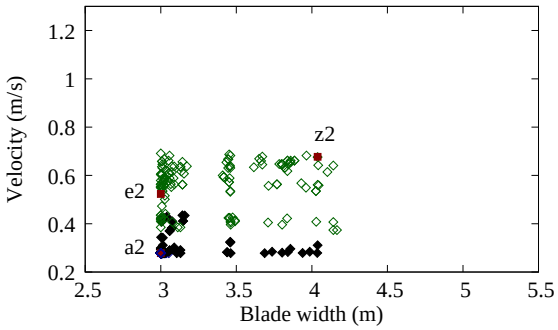

(h) $B - v$ plot

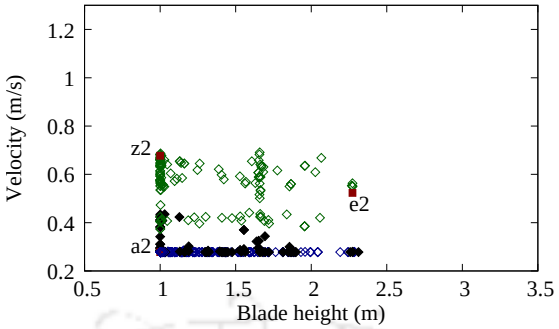

(i) $H - v$ plot

Figure 3.42: The scatter plots for all decision variables of the approximate PO solutions using model-2 are presented.

v as observed with the knee-solutions. However, D is evolved at its upper bound. It means that all blades are operated at higher value of D which can reduce N and T but requires large P value. This is also evident from Fig. 3.39 in which all extension solutions are evolved at higher P values.

3.4.2.4 Guidelines for Practitioners

The non-dominated solutions and their post-optimal analysis offer a platform to make guidelines for the practitioner. From Fig. 3.37, it clear that the practitioner has three wide choices for selecting an optimal solution in practice. For example, lower P value solution can be chosen from the surface solutions. On the other hand, the extension solutions offer lower N and T values. The knee-solutions offer a decent trade-off among the objectives for selection.

In case the group of the surface solutions is chosen by the practitioner, one non-dominated solution has to be chosen from many solutions having trade-off between N and T. As it can be seen from Fig. 3.38c, solution '$a1$' corresponds to minimum P but with very large N and T. If any solution with lower T value is chosen, then approximately $N = 30$ passes are required to finish the soil cutting operation. It is because this solution is evolved with a lower value of H and D (refer Fig. 3.41d). Meaning, a small size is blade is used for soil cutting at lower D. If a solution with lower N is chosen, then approximately 3700s are required to fill the blade with soil. It means that a bigger size blade is used at lower D to finish the soil cutting task.

The next group, which can be chosen by the practitioner, is the extension solutions.

These solutions are corresponding to lower N and T objective values but with higher P values. It is because medium to bigger size blades are used at higher D and v for soil cutting, which can be seen from Fig. 3.41f. The solutions '$e1$' and '$z1$' belong this group. The range of T is from 146s to 250s, and the range of N is 6 to 13 for both solutions. Solution '$z1$' corresponds to minimum T, but P is relatively high as compared to solution '$e1$'. It is because the bigger size blade with larger D and v is evolved for solution '$z1$' against medium size blade at the same operating condition for solution '$e1$'. So, the practitioner can choose '$e1$' over '$z1$'. However, a solution with lowest P from the group of the extension solutions can be chosen since the ranges of T and N are small.

The group of the knee-solutions is always preferable to the practitioner. It is because all solutions under this group show a decent trade-off among all objectives. The solutions are evolved with smaller to bigger size blades that are operated from lower to higher D values and moderate v range. The P values are not high, and the operation can finish in a decent range of N and T. In this group, the soil cutting operation can be finished early if the bigger size blade is used at higher D but at an expense of higher P values. Otherwise, a smaller blade with lower D and moderate v can be used.

From the above discussion, it is clear that once a partitioner chooses the appropriate group of solutions, then one non-dominated solution can be chosen. This study offers many choices to the practitioner for a relative comparison and also for, final selection of an appropriate solution, which otherwise is difficult to find with the single-objective optimization. In practice, a set of bulldozer blades is available for performing the soil cutting. An appropriate blade and the operating condition can be found using the plots shown in Sections 3.4.2.2 and 3.4.2.3. For example, a suitable blade can be chosen from the evolved dimensions of the blade of the non-dominated solution. The blade is then used with the evolved optimal operating conditions so that the desired objective function values can be achieved.

3.5 Experimental Validation of Solutions

In the literature both the adopted force models were compared with the experimental data to determine accuracy of the cutting force at various cutting depths. These models

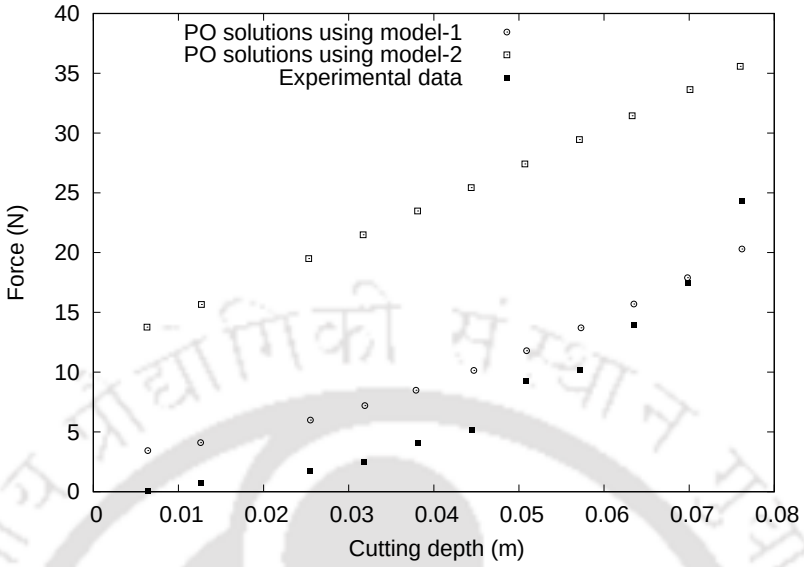

Figure 3.43: Validation of the PO obtained using model-1 and model-2

were tested for different types of soil, blades and operating conditions in their respective studies. In King et al. (2011) both models were compared on two types of soil and same set of bulldozer and its blade. For validating the multi-objective optimization formulation given in 3.15, NSGA-II is run for the given set of parameters for soil, blade and bulldozer given by King et al. (2011), which are presented in Table 3.2. NSGA-II parameters are kept same as presented in Table 3.20. F_{max} is chosen as 0.05 kN.

Table 3.20: The parameters for experimental validation of solutions are presented.

γ_o (kg/m^3)	γ (kg/m^3)	C_o (N/m^2)	C (N/m^2)	δ
700	1000	700	1400	17
A_d (N/m^2)	β	φ_o	φ	B (m)
39	35°	30°	30°	0.0127
H (m)	R (m)	θ	α	v (m/s)
D+0.1	10000	0.001°	89°	0.0033

It can be seen from Fig. 3.43 that the cutting force of the non-dominated solutions of the model-1 shows a closer agreement with the experimental data of King et al. (2011). The model-2 predicts little higher cutting force values for different cutting depths. This observation for model-2 contradicts finding of King et al. (2011) it is because surcharge pressure in Eq. (A.25) due to soil pile is included in the cutting force equation.

3.6 Closure

The chapter presented three multi-objective formulations, which were developed chronologically by identifying their usefulness and scope for further improvement. Since the aim was to incorporate economic and productive aspects of a bulldozer and its blade in soil cutting, various objectives, constraints, and decision variables were designed that can help users and practitioners to adopt the optimal input parameters for the operation. Therefore in each attempt, the optimization problem was made realistic with inclusion of problem-specific objectives and constraints.

The approximate PO solutions were then presented and further analysis was done to conclude that the non-dominated solutions generated by EMO techniques might be close to the true PO front. Moreover, the studies were supported by the post-optimal analysis that helped to decipher important relationships, which were later used for making guidelines for users and practitioners. It is found that three-objective formulation can be adopted in practice in which the approximate PO solutions were generated with different blade dimensions and operating conditions. The formulation has been validated through the experimental data from the literature so that it can be used by the users and practitioners.

Chapter 4

Hybrid Evolutionary Multi-Objective Procedure

The formulations proposed in the last chapter were solved using the existing five EMO techniques. These EMO techniques can be made faster by coupling them with the local search. Such algorithms are being referred as memetic or hybrid EMO techniques. In this work, we refer them as hybrid EMO techniques.

4.1 Background

The main challenge with the hybrid EMO techniques is the implementation of local search. It is because a multi-objective optimization problem has to be converted into a single-objective optimization problem. There exist various methods for converting multi-objective optimization problems wherein every method has its own characteristics and limitations (Deb 2001). For example, the simplest and most commonly used method is the weighted-sum method in which the weights are assigned to each objective to make a composite objective function for the single-objective optimization. However, the main limitation is that the method cannot be used for non-convex optimization problems. Moreover, appropriate weights for the objectives need to be fixed to the obtain PO solution in a desired region, which is not known a priori. The normalization is also required for which a range of each objective should be known to the user. The method also faces difficulty when a multi-objective optimization problem

has minimization and maximization types of objectives.

Another method is the $\epsilon-$constraint method that can be used for convex and non-convex optimization problems by keeping one objective as primary and make other objectives as constraints. If the primary objective is minimization, the $\epsilon-$ constraint method can generate the PO solution by altering the upper bounds of constraints formed from other objectives as reported by Miettinen (1998). Another important method is the weighted-metric method in which Tchebyecheff function, augmented scalarizing function to name a few, can be used for converting the optimization problem. This method can also be used for convex and non-convex optimization methods, and the PO solution can be generated with respect to the reference point. The major limitations of this method are to fix the reference point and normalization of each objective function.

Another challenge for implementing the local search is the rules for updating or selecting a newly created solution from the local search against its parent solution (Murata et al. 2002, Jaszkiewicz 2002, Sharma et al. 2011, 2014, 2008, Sharma and Deb 2014, Sharma et al. 2007, Kumar et al. 2007, Sindhya et al. 2013). In multi-dimensional objective space, a new solution is generally evolved non-dominated with respect to its parent solution. If this new solution is compared with its parent solution only, the decision is localized. Since solving any multi-objective problem is itself multi-objective in nature wherein convergence and diversity have to be maintained, the localized updating rule may not retain good solution in the population. If a new solution is compared with all current solutions of a population, the global selection rules can be designed but by performing larger computations.

The frequency of executing the local search is another challenge in which two issues can be addressed. The first issue is when to execute the local search with EMO technique? The second issue is related to the number of solutions on which the local search can be executed. In case of the first issue, the local search can be executed at different stages, such as at the beginning on the initial population, during the generation, after finishing the number of generations, or combination of two or more stages (Ishibuchi et al. 2003, Ishibuchi and Narukawa 2004, Murata et al. 2002, Jaszkiewicz 2002, Sharma et al. 2011, 2014, 2008, Sharma and Deb 2014, Sharma et al. 2007, Kumar et al. 2007, Sindhya et al. 2013). If the local search is executed frequently, it will increase the

computational effort of a hybrid EMO technique. On the other hand, lower frequency of the local search may not be effective for faster convergence. Therefore, a heuristic rule has to be designed to execute the local search for different stages of hybrid EMO technique.

The second issue is related to the number of the solutions selected from the current population of a hybrid EMO for executing the local search (Ishibuchi and Narukawa 2004, Sindhya et al. 2013). In case many solutions are chosen for the local search, the computation requirement for a hybrid EMO technique will be very high. If a very few solutions are selected, then the local search may not be effective to support faster convergence to the PO solution.

The choice of a solution for executing the local search is also another challenge because more often performance of the local search depends on the starting solution. Since EMO techniques are population-based techniques, it provides multiple choices to start the local search. Generally, the current non-dominated solutions in any generation can be chosen for the local search (Murata et al. 2002, Jaszkiewicz 2002), or the offspring after crossover and mutation (Bosman 2012). Since the number of such solutions can be high, the hybrid EMO techniques require many function evaluations. The selection of appropriate non-dominated solution can be made heuristic when any solution can be selected with some probability (Ishibuchi et al. 2003, Ishibuchi and Narukawa 2004). If the probability is high, many solutions will be selected for the local search. In case of low probability, the local search will be executed on a few solutions.

It is important to note that challenges and issues discussed above have a direct influence on exploration and exploitation of search space by the local search (Ishibuchi et al. 2003). The efficient strategies have to be designed for making a balance between exploration and exploitation. However, these strategies are more often problem dependent, therefore a single strategy may not be possible.

The termination criterion for the local search can be the last challenge as the local search is allowed to perform many computations till it can generate improved solutions, or some number of iterations can be fixed. Again, this issue is problem dependent.

From the above discussion, it can be realized that there are many challenges and

issues with the hybrid EMO techniques for implementing the local search. In this chapter, we try to address the following issues

1. `Frequency`: When to execute the local search?
2. `Number`: How many solutions are selected for performing the local search?
3. `Choice`: What are those solutions which are selected for the local search?

In the following section, some relevant papers are surveyed that implemented the local search for multi-objective optimization.

4.2 Survey of Hybrid EMO Techniques

One of the earliest implementations of the local search with EMO technique was reported in (Ishibuchi and Murata 1996) wherein the weighted-sum method was used for solving a flowshop scheduling problem for maximizing the fitness. The algorithm was referred as multi-objective genetic local search algorithm (MOGLS). Every solution generated after crossover and mutation was selected for the local search by assigning different weights. Since the hybrid EMO technique was used for a combinatorial optimization problem, the local search was performed by examining $k-$neighborhood solutions of the current population. Later, the algorithm was modified in (Ishibuchi et al. 2003) by performing the local search on the selected good solutions by using the tournament selection of size five. The solutions were then chosen with some probability for reducing the number of computations. For the local search, a direction similar to the steepest descent direction was used for each initial solution. Further, another hybrid algorithm (S-MOGLS) was proposed in (Ishibuchi and Narukawa 2004) wherein the Pareto ranking and weighted-sum method were used for implementing the local search. A set of good solutions was selected through tournament selection and with some probability, the local search was executed on the selected solutions. In another attempt, the cellular multi-objective genetic algorithm (C-MOGLS) was developed in (Murata et al. 2002) wherein the weighted-sum method was used and the local search was applied to all non-dominated solutions in every generation. Another new genetic local search algorithm proposed in (Jaszkiewicz 2002) wherein the local search was

hybridized with recombination operators. All offspring solutions were chosen for the local search. A random utility function was used for the single-objective optimization.

Apart from the combinatorial optimization problem, the local search has been used for structural topology optimization (Sharma et al. 2011, 2014, 2008, Sharma and Deb 2014). The weight-sum method was used and the local search was applied to a few non-dominated solutions. A clustering algorithm was used to make a fixed number of clusters from the current non-dominated solutions. A representative non-dominated solution was then chosen from each cluster. The weights were assigned to each selected solution based on its position in the current non-dominated front. The exhaustive local search was applied to each solution by perturbing its neighborhood. The new solutions were added to the population after deleting the bad solutions in terms of Pareto rank and crowding distance operator.

Pareto-archived evolutionary strategy (PAES) has also been coupled with the local search in (Knowles and Corne 2000) for solving multi-objective 0/1 knapsack problems. All solutions of the current population were chosen in every generation for the local search by performing mutation using (1+1)-ES. For updating the population, the Pareto ranking and the grid-type partitioning were used. The algorithm was referred as M-PAES.

For continuous multi-objective optimization problems, the local search was performed using the $\epsilon-$constraint method (Sharma et al. 2007, Kumar et al. 2007) in which all non-dominated solutions were selected. The sequential quadratic programming (SQP) technique was used for the single-objective optimization. Apart from the primary objective, other objectives were made constraints and their upper bounds were set on the objective values of the current non-dominated solutions. The local search was executed in every iteration and the solutions from the local search were mixed with the current population and the best solutions were chosen for the next generation for NSGA-II. The hybrid EMO technique was terminated based on the fixed number of function evaluations.

Based on gradient information, combined objective repeated line search was used as the local search in (Bosman 2012). This local search was coupled with the EMO technique in which the local search was executed on the non-dominated solutions in every generation.

The local search has been explored for determining the Nadir point (Deb et al. 2009, 2010). The local search was executed for every worst solution in each objective by using the augmented achievement scalarizing function. The reference point was chosen same as the current solution. The SQP technique was used as a local optimizer which was initiated adaptively by using the normalized-distance metric.

A standalone hill climbing sidestep was proposed and coupled with EMO techniques in (Lara et al. 2010). The new solution was found by performing line search along the desired direction. The sidestep was performed when the new solution was closer to the (local) PO solution. After performing genetic operators, the local search was executed on every solution.

Using augmented achievement scalarizing function, the local search was performed in (Sindhya et al. 2008, 2009, 2013). In (Sindhya et al. 2008), the offspring population was selected for performing the local search with some adaptive probability rule in every generation of NSGA-II. The selected solutions were replaced by the solutions generated using the SQP technique for the local search. The non-dominated sorting was then performed on the combined population of parent and offspring solutions. The hybrid NSGA-II was modified later in (Sindhya et al. 2009) by replacing the crowding-distance operator with $k-$means clustering algorithm. Moreover, the probability of selecting offspring for the local search was determined by some saw-tooth function. Later, a hybrid framework for EMO techniques was proposed in (Sindhya et al. 2013) wherein the solutions were projected onto the hyperplane and $k-$clusters were made. Randomly one cluster was picked and a solution was chosen for local search with some probability. The new solution was then added to the current population, and the Pareto ranking and crowding distance were re-evaluated for the modified population. Only one solution was selected in every generation, however, the local search was applied to all solutions after completing the maximum allowed number of generations. A novel diversity mechanism was incorporated in which the non-dominated sorting was applied to the clusters independently, and the next generation population was filled by copying solutions from each cluster one by one based on their non-dominated ranks.

In (Ke et al. 2014), the Pareto local search (PLS) was coupled with multi-objective evolutionary algorithm based on decomposition (MOEA/D) (Zhang and Li 2007). In MOEA/D, a multi-objective optimization problem was decomposed into a number of

scalar sub-problems and then, EA was applied to these sub-problems in a collaborative manner. For each sub-problem, a set of neighborhood sub-problems was identified that was used for restricted mating and solution update. In PLS, three sets of populations were maintained that included the current solutions from every sub-problem, the population which underwent through PLS, and the external population storing non-dominated solutions. Inside the loop, PLS was applied to update other two population sets. Then, every solution of the sub-problem in the current population was perturbed and then the local search was applied. The new solution was then used to update all three population sets. The local search was applied using the weighted-sum approach.

In (Chen et al. 2015), the local search has been included by perturbing the decision vector variable-wise similar to the Gaussian mutation by using two randomly selected solutions from the population. The new population was created when the perturbed solution was better than the parent solution. The local search solutions and the parent solutions were combined and the rank was assigned using the non-dominated sorting. For the last front solutions that to be selected for the next generation population, the farthest-candidate solution method was adopted in which the unselected solution which was farthest from the selected solutions was chosen first.

From this literature survey, it can be observed that the earlier studies addressed many challenges and issues that were discussed earlier. Many studies execute the local search in every generation regardless of the fact that the local search is really needed to improve the solutions. Only very handful studies have used some adaptive rule for executing the local search. It is also observed that many of the studies selected solutions based on some probability rule so that a number of solutions can be reduced for the local search. Otherwise, all the solutions generated after crossover and mutation or all non-dominated solutions have been chosen for the local search. Except for a few studies in which solutions have been selected from the clusters of non-dominated solutions, the choice for selecting a solution has been done using heuristic rule. In this thesis, the challenges signifying `frequency`, `number` and `choice` are addressed and a novel approach is suggested based on decomposing the objective space into a set of reference points. In the following section, the proposed approach for the hybrid EMO technique is discussed.

4.3 Approaches for Local Search Challenges

Three important challenges in implementing the local search for continuous multi-objective optimization problems are addressed in this thesis. As defined earlier, `frequency` challenge referrers to guide the hybrid EMO technique for executing the local search at a regular interval of time or adaptively. `Number` challenge refers to devise a mechanism for selecting a number solutions for performing the local search. `Choice` challenge refers to selecting a set of appropriate solutions for the local search. In the following subsections, these challenges are discussed in detail followed by their implementations with NSGA-II.

4.3.1 `Number` and `Choice` for Local Search

The idea of decomposing the objective space into a fixed number of reference points is motivated from (Deb and Jain 2014). A unit hyperplane is generated in the first quadrant, and a set of reference points are generated using (Das and Dennis 1998) approach. In this approach, for any reference point lying on a unit hyperplane satisfies the following condition

$$\sum_{i=1}^{m} f_i = 1, \tag{4.1}$$

where m is the number of objective functions, and f_i is the $i-$the objective function value lying between $[0, 1]$. The steps/divisions are then decided for $m-1$ objectives which lie between $[0, 1]$. The objective function value of f_m is calculated using the above equation. A pictorial representation for 3-objective spaces is shown in Fig. 4.1. The reference points generated in the 2-objective and 3-objective cases are shown in Fig. 4.2. For simplicity, the reference lines are shown for a 2-objective case that are drawn from the origin and the reference points. Similarly, the reference lines can be drawn for 3-objective and higher dimensional objective space.

An approach for `number` and `choice` of solutions is proposed based the objective space decomposition using the reference points. First the non-dominated solutions of the current population of NSGA-II is normalized by using

$$f_i' = \frac{f_i - f_i^{min}}{f_i^{max} - f_i^{min}}, \tag{4.2}$$

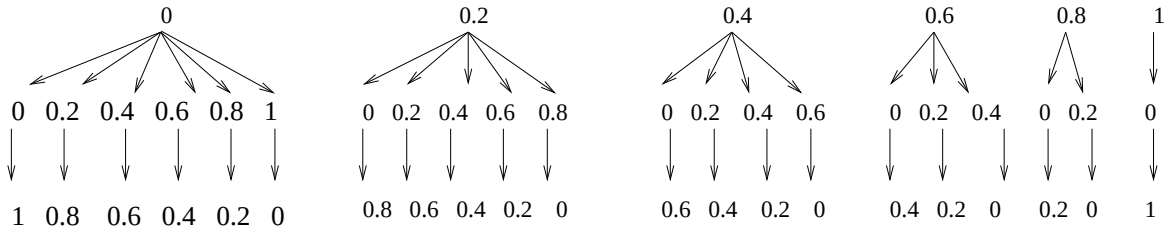

Figure 4.1: The steps/divisions for generating reference points on a unit hyperplane for 3-objective case.

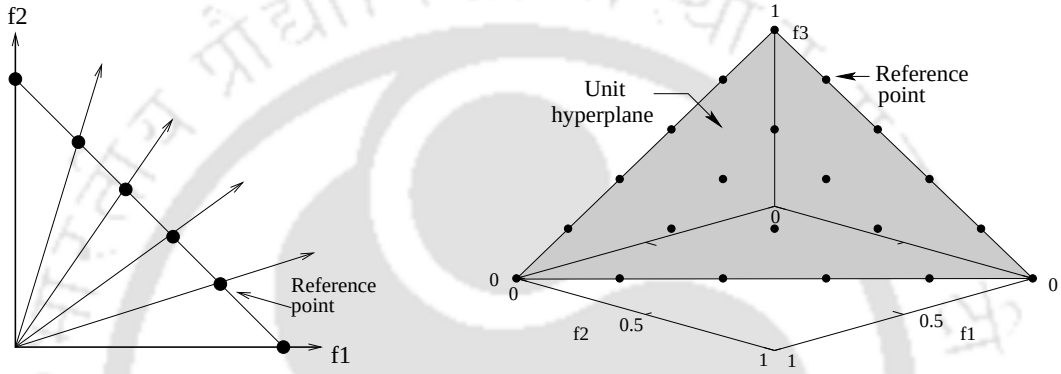

Figure 4.2: The reference points generated on the unit hyperplane for 2-objective and 3-objective cases are shown.

where f_i is $i-$th objective value of a solution. f_i^{min} and f_i^{max} are the minimum and maximum objective function values of $i-$th objective that are determined from the current set of non-dominated solutions. f_i' is the normalized $i-$th objective value which lies in between $[0, 1]$. The non-dominated solutions which are closest to each reference line are selected for the local search. For 2-objective, a hypothetical case is shown in Fig. 4.3 in which the non-dominated solution closest to each reference line is selected for executing the local search.

It can be observed from Fig. 4.3 that the number of selecting the solutions for the local search depends on the number of reference points generated on the hyperplane. As given by (Das and Dennis 1998), the number of the reference points is determined as

$$K = C_p^{m+p-1}, \tag{4.3}$$

where p is the number of division/steps for each axis that has to be fixed by the user. We set $p = 2^n$.

The approach for `choice` and `number` of non-dominated solutions offers the follow-

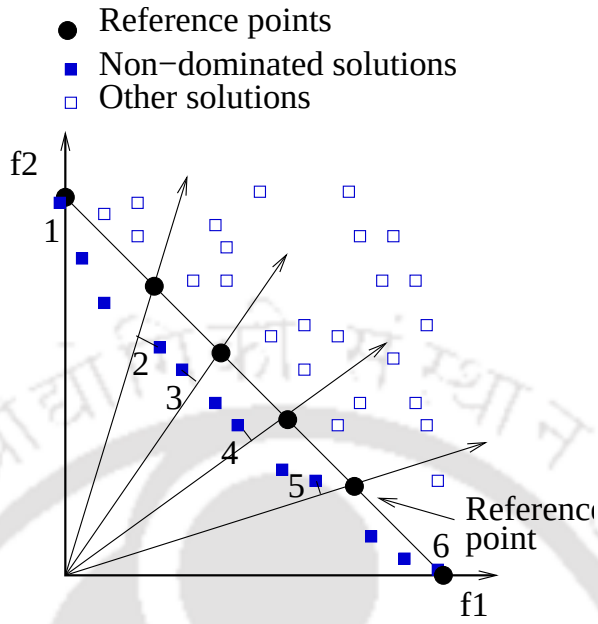

Figure 4.3: The non-dominated solution closest to each reference line is selected for the local search. These solutions are marked from 1 to 6.

ing advantages

- A good diverse set of non-dominated solutions can be selected for addressing the challenge of `choice`. It is justified by the fact that (Das and Dennis 1998) approach always generates a set of structured reference points on a unit hyperplane. The reference lines drawn from these reference points are thus equally distributed in the objective space as can be depicted from Fig. 4.3. Therefore, the non-dominated solutions closest to these lines maintain a good diversity among them.

- Since the starting solutions for the local search are diverse, it expected that the improved solutions can also maintain similar diversity and assist the hybrid EMO technique for faster convergence.

4.3.2 `Frequency` of the Local Search

This challenge is addressed by adaptively deciding the local search execution in every generation that is based on IGD values. The IGD value for each generation is stored

and the statistical values of IGD over past q generations are used as

$$\frac{IGD_{max} - IGD_{min}}{q} \leq \delta, \tag{4.4}$$

where IGD_{min} and IGD_{max} are the minimum and maximum IGD values over past q generations. δ is the user-defined value. When the condition gets satisfied in any generation, the local search is executed on the chosen non-dominated solutions.

4.4 Hybrid EMO Technique

For the hybrid EMO technique, NSGA-II is used as a global optimizer and SQP technique as a local optimizer. The description of NSGA-II is given in Appendix B.1. SQP is used through *fmincon* solver of MATLAB. The bi-objective optimization problem given in Eq. (3.6) in chapter 3 is chosen for testing the optimization technique. The $\epsilon-$constraint method is used for converting the given bi-objective optimization problem into the single-objective optimization problem given in Eq. (3.14) in chapter 3 in which objective on the power is considered as the primary objective.

The hybrid EMO technique on NSGA-II framework is given in Algo. 1. Since NSGA-II details are given in Appendix B.1, only the local search implementation is discussed. It can be seen that all steps of NSGA-II are given in the algorithm, except steps 3 and 14. In step 3, the reference points are generated on the unit hyperplane as explained earlier. These reference points are used later in the local search. In step 14, the local search is executed on the selected non-dominated solutions. The details of the local search implementation are presented in Algo. 2. The adaptive local search is executed when the condition given in step 4 is met. If it is met, the population is normalized by first determining the Ideal and Nadir points from the current non-dominated solutions. Then, the closest non-dominated solution for every line is selected. For these solutions, *fmincon* solver of MATLAB is used and the single-objective optimization problem formulated using the $\epsilon-$constraint is solved. The new solutions then replace their parent solutions in P_{t+1}.

Algorithm 1 Hybrid EMO technique on NSGA-II framework.

Input: Population size (N), maximum generations (T), crossover probability, mutation probability, generation counter (t=0)
Output: Pareto-optimal solutions (P_{t+1})
Generate the reference points on a unit hyperplane;
Initialize random population P_t;
Evaluate P_t;
Assign rank using non-dominated sorting operator and diversity using crowding distance operator to P_t;
while Generation counter $t < T$ **do**
    P'_t := Selection(P_t) using crowded tournament selection operator;
    Q_t := Variation(P'_t) using simulated binary crossover operator and polynomial mutation operator;
    Evaluate Q_t;
    Merge population $R_t = (P_t \cup Q_t)$;
    Assign rank using non-dominated sorting operator and diversity using crowding distance operator to R_t;
    P'_{t+1} := Choose best N solutions from R_t based on rank and crowding distance;
    P_{t+1} := Execute local search using Algo. 2 on the non-dominated solutions of P'_{t+1};
    $t := t + 1$;
end while

Algorithm 2 Local search implementation

Input: Non-dominated solutions of P'_{t+1}, t
Output: Solutions after the local search
Calculate IGD of current generation;
if (IGD$_{max}$−IGD$_{min}$/$q \leq \delta$) for past q generations **then**
    Normalize the population by using the Ideal and Nadir points of the current non-dominated solutions;
    Select the closest non-dominated solution to every reference line;
    Execute local search by using the SQP technique on the single-objective optimization problem formulated using the $\epsilon-$constraint method;
    Replace the selected solutions with the solutions generated after the local search;
end if

4.5 Results and Discussion

4.5.1 Test Cases

The local search implemented in Algo. 2 is used for performing the local search for every generation. Multiple test cases are considered here and their details are as follows:

Case 1: The local search is executed on the initial population after step 6 of Algo. 1 only. In this case, step 14 is commented that does not allow local search in this step.

Case 2: The local search is executed at a regular interval of generations. In this case, step 4 of Algo. 2 is modified as $if(t\%10 == 0)$. It means that the local search is executed after every 10 generations.

Case 3: The local search is executed as proposed in Section 4.4. It means that the local search is executed adaptively based on IGD values of past q generations.

Case 4: It is a combination of cases 1 and 3 in which the local search is executed after step 6 of Algo. 1 and also in step 14 adaptively.

The results of these cases are compared along with the results of NSGA-II.

4.5.2 Parameters

The NSGA-II parameters are presented in Table 4.1. The population size is kept small, but generation number is kept large so that convergence of the algorithm can be observed. For *fmincon* solver, the SQP technique is used which terminates as per the default values set in MATLAB, for example, maximum iterations are set at 1000 and termination tolerance on the first-order optimality is set at $1.0e^{-6}$.

The IGD indicator is used for observing convergence plots. It is noted that a reference set of the PO solutions are generated from the study presented in Section 3.3 in which 30 runs of NSGA-II are taken, and the non-dominated solutions of all runs are combined. Thereafter, only the non-dominated solutions from the combined runs were copied in the reference set of the PO solutions. A total of 1380 reference PO solutions is used for calculating IGD value in this chapter.

Table 4.1: Constant parameters for NSGA-II.

Parameters for NSGA-II	
Population (N)	Generation (T)
40	100
Crossover probability	Crossover operator index
0.9	15
Mutation probability	Mutation operator index
0.033	20

Table 4.2: Number of selected solution for local search.

n	Number of divisions (P)	Number of reference points (K)
0	1	2
1	3	4
2	7	8
3	15	16
4	31	32

In the proposed approach, value of p in Eq. (4.3) is set and the number of reference points is determined. Table 4.2 presents the values for the given problem. Here, the motive is to assess the effect of `number` of non-dominated solutions on which the local search is executed. The maximum number of the reference points is set based on the population size. Value of δ is set to 10^{-3} for adaptive local search.

4.5.3 Convergence Plots

Firstly, the convergence of NSGA-II is shown in Fig. 4.4 in which IGD value is calculated in every generation and IGD average is determined over past 10 generations. It can be seen that IGD value keeps on improving till 80 generations, and then it gets stabilized. The same convergence plot of NSGA-II is used later for comparison.

Case 1: The convergence plots of the hybrid EMO technique for case 1 are shown in Figs. 4.5 and 4.6. It can be seen that multiple convergence plots are shown with respect to the number of reference points (RPs). These RPs signify the number of solutions selected for performing the local search. Generation-wise convergence in Fig. 4.5 shows regular and sudden changes in IGD values. For example, the hybrid EMO technique

with 2 RPs shows regular changes in IGD values, whereas with other plots sudden improvement in IGD value can be seen from 10 to 20 generations. The similar but smooth convergence plot for average IGD value over past 10 generations can be seen in Fig. 4.6. This plot also shows regular and sudden changes in average IGD values. Since the changes in IGD values can be captured from both the figures, average IGD convergence plots are shown and discussed in the rest of the section. The IGD value plots in every generation for every case are shown in Appendix D.

In Fig. 4.6, except for 2 RPs, convergence of the hybrid EMO technique for other RPs are evolved similar. The hybrid EMO technique with 2 RPs seems to be converging in 45 generations. Other variants of the hybrid EMO technique are converged at around 40 generations. This observation suggests that the number of reference solutions has a little effect on the convergence. When all variants of the hybrid EMO technique are compared with NSGA-II, a significant improvement can be seen. It concludes that when a good set of solutions generated through the local search is provided to NSGA-II at the beginning, its convergence can be improved.

Case 2: In case 2, the convergence plots of the hybrid EMO technique are shown in Fig. 4.7. In this case, the local search executed at a regular interval of 10 generations seems to be not effective as almost of variants of the hybrid EMO technique converge similar to NSGA-II. The hybrid EMO technique with 2 RPs and 4 RPs seems to be improving in every generation. However, some fluctuations in average IGD can be seen with the convergence plots of 8, 16 and 32 RPs. It means that the local search sometimes cannot help in stabilizing the convergence.

Case 3: Case 3 is an adaptive implementation of the local search based on statistical IGD values over past q generations as shown in step 4 of Algo. 2. Since q is set by the user, five test cases are considered in which q is set to $(5, 10, 15, 20, 25)$. Fig. 4.8 shows average IGD value plot for $q = 5$. It can be seen that the convergence plots for 4 and 16 RPs converge faster than NSGA-II in which the hybrid EMO with 16 RPs converges fastest in 60 generations. Rest of the variants of the hybrid technique deteriorate the convergence. Moreover, many fluctuations in average IGD value over $q = 5$ generations can be seen with all plots. It is because the local search is executed too frequently.

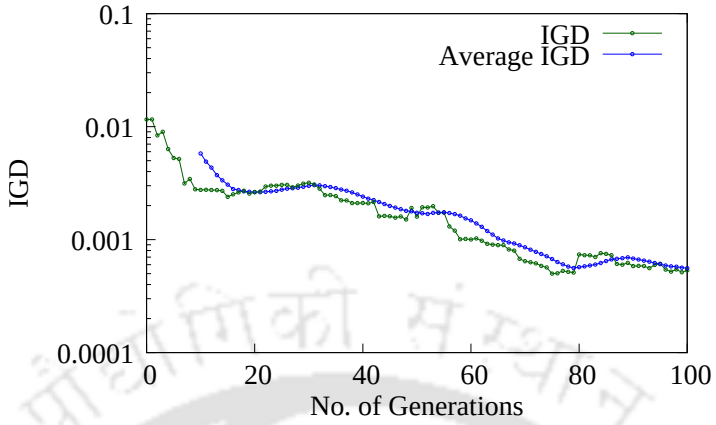

Figure 4.4: Convergence of NSGA-II for modified bi-objective problem proposed in Eq. (3.6).

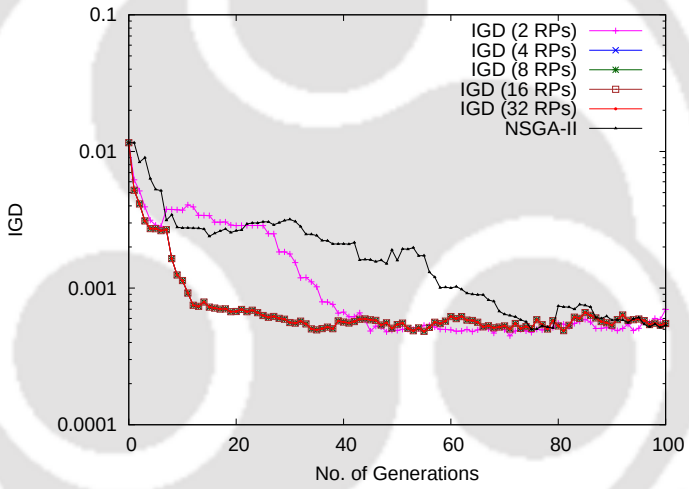

Figure 4.5: IGD convergence plot of case 1 for different reference points (RPs).

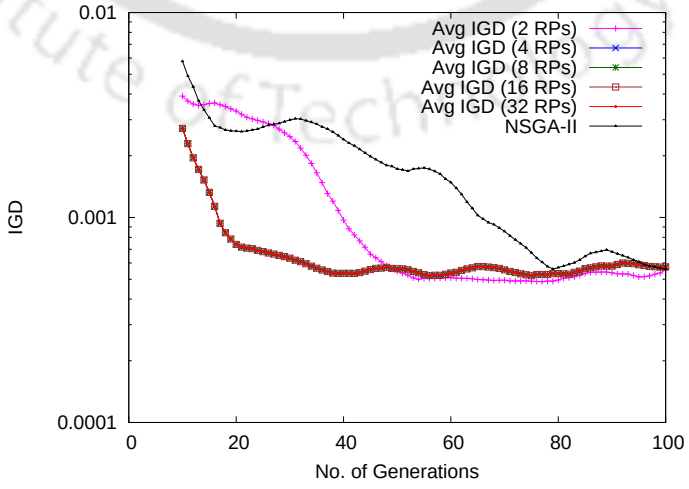

Figure 4.6: Average IGD convergence plot of case 1 for different reference points (RPs).

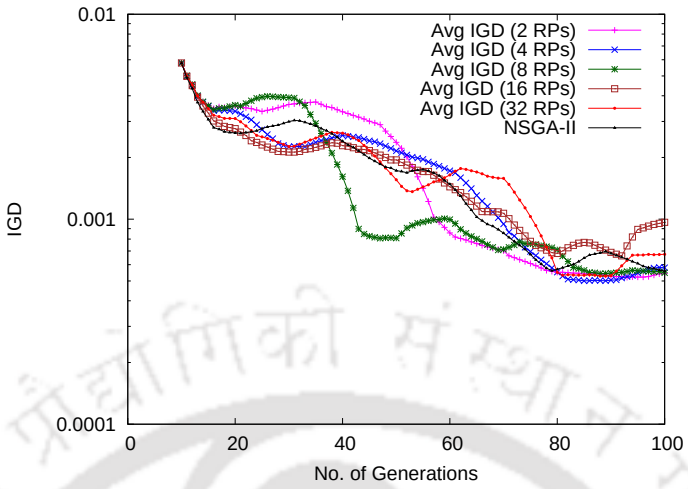

Figure 4.7: Average IGD convergence plot of case 2 for different reference points (RPs).

Fig. 4.9 shows convergence plots when $q = 10$. In this case, 2, 8, and 32 RPs variants of the hybrid EMO technique are found to be better than NSGA-II. Other variants show inferior convergence to NSGA-II. The fluctuations in average IGD values have been reduced as well. The hybrid EMO technique with 8 RPs has converged in almost 60 generations.

Fig. 4.10 shows convergence plots when $q = 15$. In this case, 16 and 32 RPs variants show better convergence than NSGA-II. Except for 8 RPs variant, other variants show inferior convergence to NSGA-II. The hybrid EMO technique with 16 RPs has converged almost in 70 generations.

Fig. 4.11 shows convergence plots when $q = 20$. The hybrid EMO technique with 4, 8 and 32 RPs show better convergence in which variants of 4 and 8 RPs have converged before 60 generations. In case of $q = 25$, variants of 8 and 16 RPs of the hybrid EMO technique are converged faster than NSGA-II. Both the variants are converged in 60 generations. The convergence plots are smoother than previous test cases.

From the convergence plots, it can be concluded that the number of solutions selected for the local search has no straightforward relationship for better convergence of the hybrid EMO technique. It was expected that when a large number of RPs (i.e. 32) variant was used, a better convergence in all case for q can be realized. However, the variant of 16 RPs showed better convergence in 3 cases out 5. The variant of the hybrid EMO technique with 8 RPs showed better convergence for the higher value of

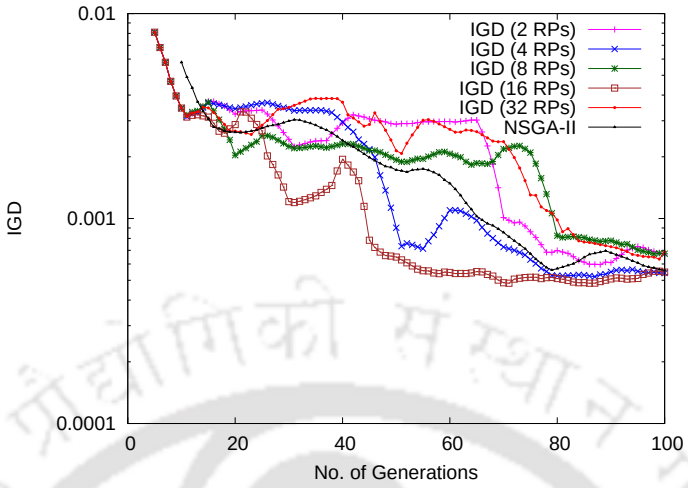

Figure 4.8: Average IGD convergence plot for case 3 by considering $q = 5$.

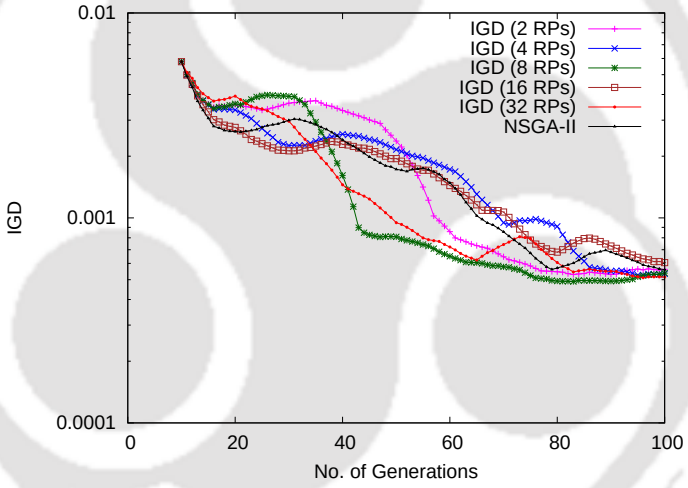

Figure 4.9: Average IGD convergence plot for case 3 by considering $q = 10$.

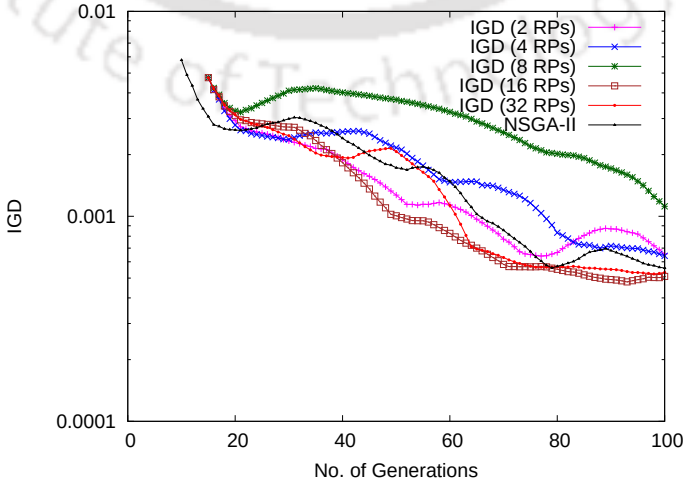

Figure 4.10: Average IGD convergence plot for case 3 by considering $q = 15$.

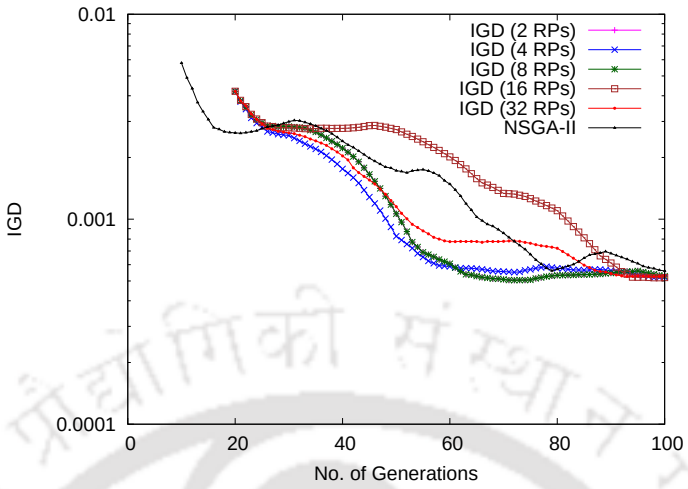

Figure 4.11: Average IGD convergence plot for case 3 by considering $q = 20$.

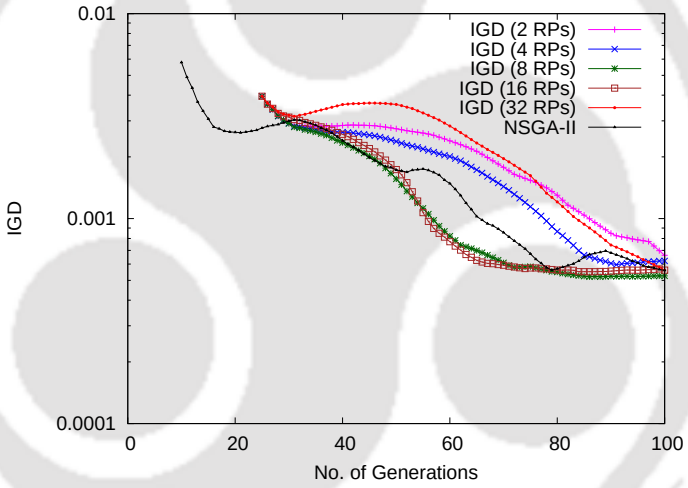

Figure 4.12: Average IGD convergence plot for case 3 by considering $q = 25$.

q, that are, 20 and 25. In both the cases, the hybrid EMO technique was converged in 60 generations.

Case 4: In case 4, the local search is executed at the beginning on the random initial population and also adaptively as described in the last case. Figs. 4.13 to 4.17 are shown for different value of q and RPs. It can be seen that the hybrid EMO technique converges faster than NSGA-II in all case studies of q. Except for a variant of 2 RPs, other variants are well converged in almost 30 generations. Also, the plots of these variants show similar convergence pattern for different numbers of RPs and q. The fluctuation in average IGD values gets smoothened when the size of q gets increased.

It can be concluded here that the local search at the beginning helped the hybrid EMO technique which was further improved by the adaptive approach of local search.

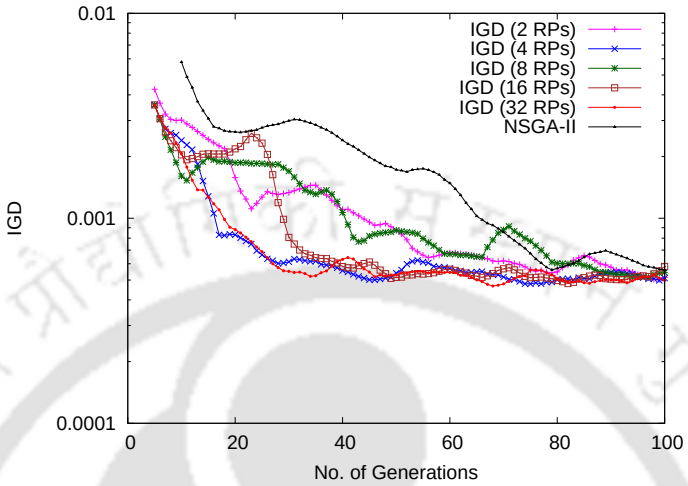

Figure 4.13: Average IGD convergence plot for case 4 by considering $q = 5$.

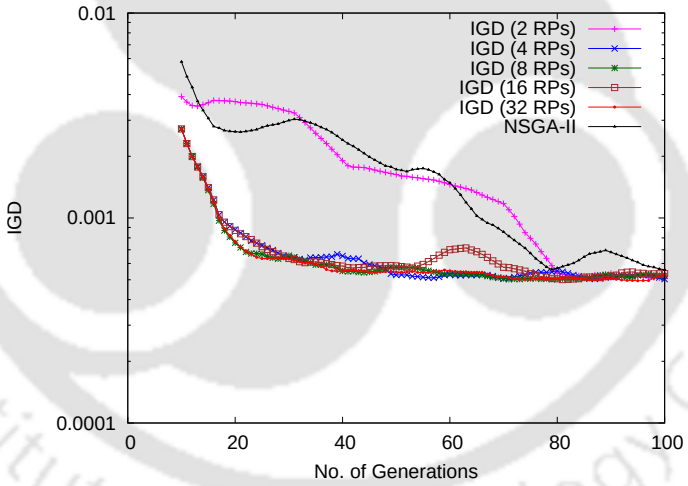

Figure 4.14: Average IGD convergence plot for case 4 by considering $q = 10$.

4.6 Closure

In this chapter, three challenges were addressed that were based on `choice` and `number` of non-dominated solutions for the local search and `frequency` of the local search in every generation. The local search was executed by using the $\epsilon-$constraint method for solving the single-objective optimization. *fmincon* solver of MATLAB was chosen that used SQP technique. The local search was implemented on NSGA-II framework for

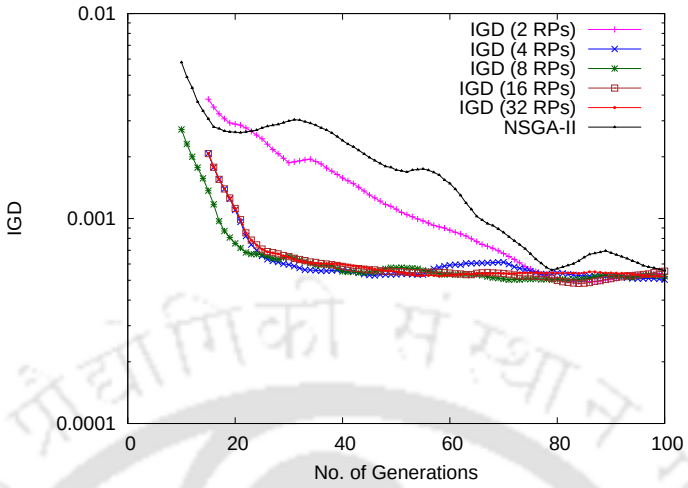

Figure 4.15: Average IGD convergence plot for case 4 by considering $q = 15$.

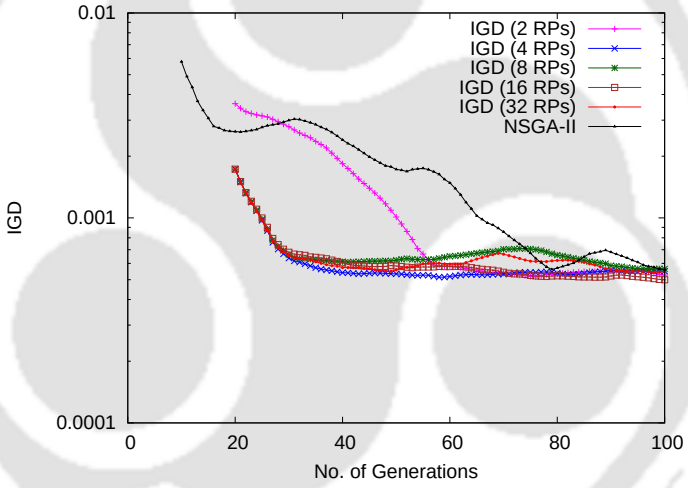

Figure 4.16: Average IGD convergence plot for case 4 by considering $q = 20$.

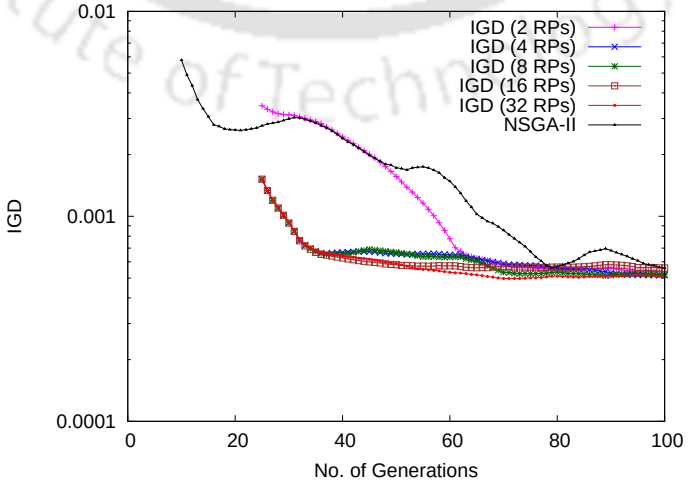

Figure 4.17: Average IGD convergence plot for case 4 by considering $q = 25$.

testing on the modified bi-objective problem given in (Eq. 3.6).

It was found that case 1 and case 4 of the hybrid EMO technique improved the convergence of NSGA-II framework. Except for the small number of RPs, the convergence was independent of the number of RPs. Also, the convergence was independent of q as well. The results of case 4 also suggested that the hybrid EMO technique was converged almost in 30 generations against 70 generations of NSGA-II. It means that the hybrid EMO was twice faster than NSGA-II generations. In case 1, the hybrid EMO was converged in 40 generations. Other cases showed the dependency of convergence on a number of RPs and also q. Overall, it suggests that convergence of the hybrid EMO depends on the stated challenges unless it is implemented in a very efficient manner with the existing EMO technique.

Chapter 5

Conclusions and Future Work

5.1 Conclusions

In this thesis, the soil cutting operation was formulated as an optimization problem so that the operation can be made economical and productive simultaneously. The multi-objective optimization formulations were thus developed in the chronological order in which the formulation was made realistic and practical for usage in every attempt. The nature of PO solutions was presented and their closeness to the true PO solutions was validated using the classical optimization method for multi-objective optimization. The PO solutions were further validated using the experimental data from the literature. Various relationships among the objectives and constraints were presented and guidelines were prepared for the practitioners. In the last phase of the thesis, an attempt has been made to address three challenges of implementing the local search with the EMO technique for better convergence.

Following conclusion are drawn from this study

- The three-objective optimization formulation emerges as the most realistic and practical for usage among other proposed formulations. It was observed that the PO solutions were generated with different operating conditions that were operated on different sizes of the blade.

- Validation of the obtained PO solutions with the experimental results suggests that the three-objective optimization formulation can be used in practice by the

practitioner.

- The nature of the obtained PO fronts suggests that the posed objectives are conflicting in nature and can quantify the economy and productivity of the soil cutting operation.

- The cutting force model of Qinsen and Shuren (1994) generated the solutions closer to the experimental results. Therefore, it can be preferred over the model of McKyes (1985). Moreover, both models generated the PO solutions of a similar trend, even though they were developed using different soil failure zones.

- The decision variables on the operating conditions are the most sensitive for the proposed objectives followed by the decision variables on dimensions for a blade. From the results of all formulations, it can be concluded that the blade curvature angle and blade curvature radius should be kept at their lower bound for generating the PO solutions.

- The post-optimal analysis suggests various non-intuitive and useful commonality and dissimilar relationships that are useful for the deeper understanding of the problem. It is important to note that such relationships cannot be found using the single-objective optimization.

- The guidelines presented in this thesis can help the user or the practitioner to compare solutions and then choose an appropriate solution in practice. The relationships generated by using the post-optimal analysis can be used for identifying the optimal input parameters for the soil cutting.

- An approach for implementing the local search on the initial population and adaptively using IGD indicator can improve the performance of NSGA-II framework.

- The approach for the local search is sensitive to all challenges addressed in this thesis. An effective implementation, as observed in two cases, can make the local search independent of the posed challenges.

- Frequent local search may not assist in stabilizing the convergence.

5.2 Future Work

- A survey can be done for adapting the three-objective optimization formulation in practice with the practitioners.
- The complete soil excavation task by bulldozer can be modeled in future that starts from cutting soil to dumping it at a designated place.
- Heterogeneous fleet of bulldozers working for soil cutting can be included with the optimization formulation.
- The local search approach can be tested on continuous multi-objective optimization problems and other engineering optimization problems.

Appendices

Appendix

A Cutting Force Models

A.1 Qinsen and Shuren (1994) Model for Wide Blade

The model presented by Qinsen and Shuren (1994) is referred as model-1 in this thesis. This model is adopted because it showed a close agreement with the experimental cutting force for a wide blade of a bulldozer. Also, the model considers that a blade is fully loaded with soil as shown in Fig. A.1. Following are the forces acting on soil as depicted in the figure. The details are as follows.

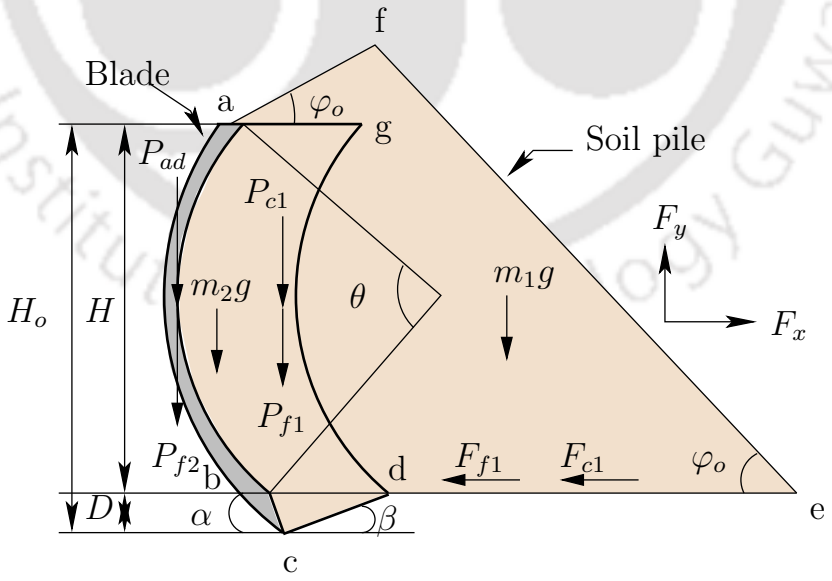

Figure A.1: Forces acting in front of a blade for model-1.

1. The forces generated by the soil pile (fgde) moving on the ground

(a) Weight of the soil pile on the ground is given as

$$m_1 g = (1/2)\gamma_o B(H + 2D\tan\varphi_o)^2 \cot\varphi_o, \tag{A.1}$$

where γ_o is the density of cut soil, and φ_o is the angle of accumulation of cut soil.

(b) Frictional force between the soil pile and the ground is given as

$$F_{f1} = m_1 g \tan\varphi, \tag{A.2}$$

where φ is the angle of internal friction.

(c) Cohesion force between the soil pile and the ground is given as

$$F_{c1} = C_o B(H + 2D\tan\varphi_o)\cot\varphi_o, \tag{A.3}$$

where C_o is the cohesion of cut soil. The magnitude of this force depends on the blade dimensions, cutting depth and the accumulation angle of soil pile in front of the blade.

2. The forces generated by the cut soil (abdgf) sliding up between the blade and the soil pile (fgde)

(a) Frictional force between the cut soil and soil pile is given as

$$P_{f1} = (F_{f1} + F_{c1})\tan\varphi. \tag{A.4}$$

(b) Cohesion force between the cut soil and soil pile is given as

$$P_{c1} = C_o BR\theta. \tag{A.5}$$

This force is affected by the cohesion factor of cut soil and the blade dimensions.

(c) Adhesion force between the cut soil and blade is given as

$$P_{ad} = A_d BR\theta, \tag{A.6}$$

where A_d is the adhesion factor of soil-metal.

(d) Frictional force between the cut soil and blade is given as

$$P_{f_2} = (F_{f1} + F_{c1}) \tan \delta, \tag{A.7}$$

where δ is the angle of soil-metal friction.

(e) Weight of the cut soil sliding up on the surface of blade is given as

$$m_2 g = 2\gamma_o BHD. \tag{A.8}$$

Other forces are acting on the soil wedge at the failure zone which are shown in Fig. A.2. Following is the description of the forces.

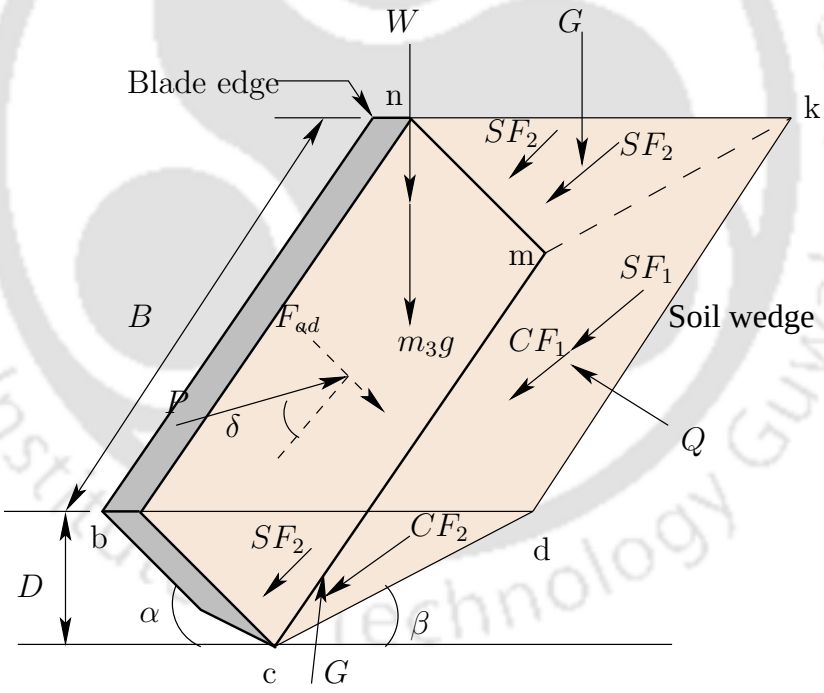

Figure A.2: Forces acting on the soil wedge for model-1.

1. The forces generated on the sides of soil wedge

(a) Force acting normal to the faces (bcd) and (nmk) of the soil wedge is calculated as

$$G = (1/6)\gamma D^3(1 - \sin\varphi)(\cot\alpha + \cot\beta), \tag{A.9}$$

where γ is the density of uncut soil, α is the angle of cutting blade, and β is the angle that the rupture makes with the horizontal.

(b) Frictional force on the sides (bcd) and (nmk) of the soil wedge is calculated as

$$SF_2 = G \tan \varphi, \tag{A.10}$$

where G is the force acting normal to the face (bcd) and (nmk) of soil wedge.

(c) Cohesion force on the sides (bcd) and (nmk) of the soil wedge is calculated as

$$CF_2 = (1/2)CD^2(\cot \alpha + \cot \beta). \tag{A.11}$$

This component is influenced by the cutting depth, cohesion factor of uncut soil, cutting angle and the angle that the failure plane makes with the horizontal.

2. Other forces on the soil wedge

(a) Weight of soil wedge (bcdnmk)

$$m_3 g = (1/2)\gamma BD^2(\cot \alpha + \cot \beta). \tag{A.12}$$

(b) Adhesion force between the soil and cutting edge of the blade is given as

$$F_{ad} = A_d BD/\sin \alpha. \tag{A.13}$$

Thus, the force acting normal to the face (bdkn) of the soil wedge is calculated as

$$W = P_{f1} + P_{f2} + P_{ad} + P_{c1} + m_2 g + m_3 g \tag{A.14}$$

3. Forces on the rupture plane (bdkn)

(a) Cohesion force on the rupture plane is calculated as

$$CF_1 = CBD/\sin \beta, \tag{A.15}$$

where C is the cohesion of uncut soil. The cohesion force on the rupture plane is basically affected by the cutting depth, blade width, uncut soil

cohesion factor and the angle that the rupture plane makes with horizontal.

(b) Frictional force on the rupture plane is calculated as

$$SF_1 = Q \tan \varphi, \tag{A.16}$$

where Q is the normal force acting on the rupture plane.

Thus, the force acting on the cutting edge of the blade is given as

$$P_{ce} = \left(\frac{\begin{array}{c} W \sin(\beta + \varphi) - F_{ad} \cos(\alpha + \beta + \varphi) \\ +2SF_2 \cos \varphi + 2CF_2 \cos \varphi + CF_1 \cos \varphi \end{array}}{\sin(\alpha + \beta + \varphi + \delta)} \right). \tag{A.17}$$

The horizontal component of the resultant force acting on the blade is determined as

$$F_x = P \sin(\alpha + \delta) + F_{f1} + F_{c1}. \tag{A.18}$$

The vertical component of the resultant force acting on the blade is determined as

$$F_y = P \cos(\alpha + \delta) - (P_{f2} + P_{ad}). \tag{A.19}$$

Therefore, the resultant cutting force on the blade is calculated as

$$F = \sqrt{F_x^2 + F_y^2}. \tag{A.20}$$

This force is minimized in the proposed bi-objective optimization formulation.

A.2 McKyes (1985) Model from Fundamental Equation of Earthmoving Mechanics

McKyes (1985) model is referred as model-2 in this thesis. It is the classical soil-tool model which is known as "Fundamental Equation of Earthmoving Mechanics". The resistance force experienced at the blade is given as

$$P = (\gamma g D^2 N_\gamma + CDN_c + qDN_q + A_d DN_{A_d} + \gamma v^2 DN_a)B. \tag{A.21}$$

The symbols used in this model are kept same as in the model-1.

First term in the summation signifies weight of the moving soil wedge as shown in Fig. A.3. The dimensional-less quantity, N_γ, is given as

$$N_\gamma = \frac{\cot\alpha + \cot\beta}{2[\cos(\alpha+\delta) + \sin(\alpha+\delta)\cot(\beta+\varphi)]}. \tag{A.22}$$

Second term in the summation signifies cohesion force between the blade and soil in which N_c is given as

$$N_c = \frac{1 + \cot\beta\cot(\beta+\varphi)}{\cos(\alpha+\delta) + \sin(\alpha+\delta)\cot(\beta+\varphi)}. \tag{A.23}$$

The magnitude of cohesion force relies on the cohesion properties of the soil which is quantified by the cohesion factor (C), cutting depth, cutting angle, frictional angle between soil and blade surface, the angle that the failure plane makes with the horizontal. Third term in (A.21) signifies the surcharge acting vertically on the soil surface. The term N_q is given as

$$N_q = \frac{\cot\alpha + \cot\beta}{\cos(\alpha+\delta) + \sin(\alpha+\delta)\cot(\beta+\varphi)}. \tag{A.24}$$

As stated in Qinsen and Shuren (1994) model, a blade is fully loaded with soil, the surcharge pressure, q, is determined from (A.14) as

$$q = \frac{P_{f1} + P_{f2} + P_{c1} + m_2 g}{2BD}. \tag{A.25}$$

Next two terms in the summation are neglected as the observed adhesion force in fourth term is small and under the static condition, the last term is zero.

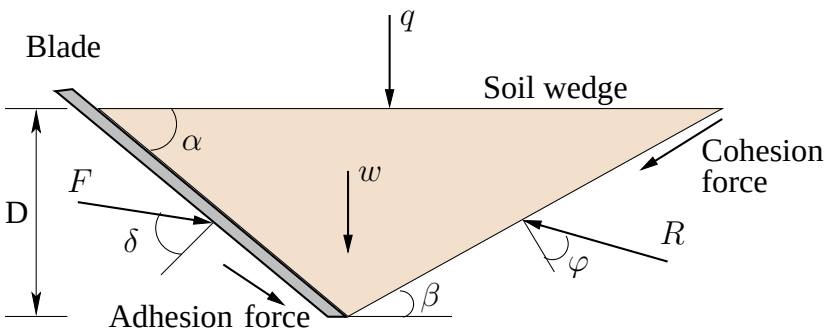

Figure A.3: Forces on the soil wedge considered in model-2.

The resultant cutting force is calculated as

$$F = P\sin(\alpha + \delta) \tag{A.26}$$

B EMO Techniques

A generalized framework is presented in Fig. B.1 on which the existing EMO techniques are discussed in the following subsections. All EMO techniques initialize random population and fitness is assigned to each solution of the population. Following definitions are used for comparing two solutions and defining Pareto-optimal solution.

Definition B.1: Given two solutions $\mathbf{x^{(1)}}, \mathbf{x^{(2)}} \in \Omega$ (feasible search space), $\mathbf{x^{(1)}}$ is said to dominate $\mathbf{x^{(2)}}$, denoted by $\mathbf{x^{(1)}} \prec \mathbf{x^{(2)}}$, iff $f_i(\mathbf{x^{(1)}}) \leq f_i(\mathbf{x^{(2)}})$, for every $i \in \{1, 2, \ldots, m\}$, and $f_j(\mathbf{x^{(1)}}) < f_j(\mathbf{x^{(2)}})$, for at least one objective $j \in \{1, 2, \ldots, m\}$ for minimization of all objective functions.

Definition B.2: A solution $\mathbf{x}^*$ is said to be a non-dominated solution, iff there is no $\mathbf{x}$ in the given population such that $\mathbf{x} \prec \mathbf{x}^*$.

Definition B.3: A solution $\mathbf{x}^{**}$ is said to be the PO solution, iff there is no $\mathbf{x} \in \Omega$ such that $\mathbf{x} \prec \mathbf{x}^{**}$.

Inside the generation loop, good and above average solutions are selected and variation operators like crossover and mutation are applied to generate a new set of solutions. All EMO techniques maintain same size of population before and after selection and variation operators. The fitness is then assigned to each new solution using the dominance principle given in definition 1. Enviornment selection is then performed to select good and above average solutions for the next generation population. The termination condition is then checked, which is the maximum number of generations or iterations. This completes one generation for EMO techniques. Lastly, the obtained PO solutions are reported.

B.1 NSGA-II

The elitist non-dominated sorting genetic algorithm is known as NSGA-II, which is proposed by Deb et al. (2002). After initializing random population, the fitness is assigned by the rank and crowding distance operators. The rank is assigned to each solution using the non-dominated sorting operator in which the non-dominated solutions are grouped as front-1. Similarly other solutions are grouped in different fronts. The crowding distance operator is used to maintain diversity among the same ranked

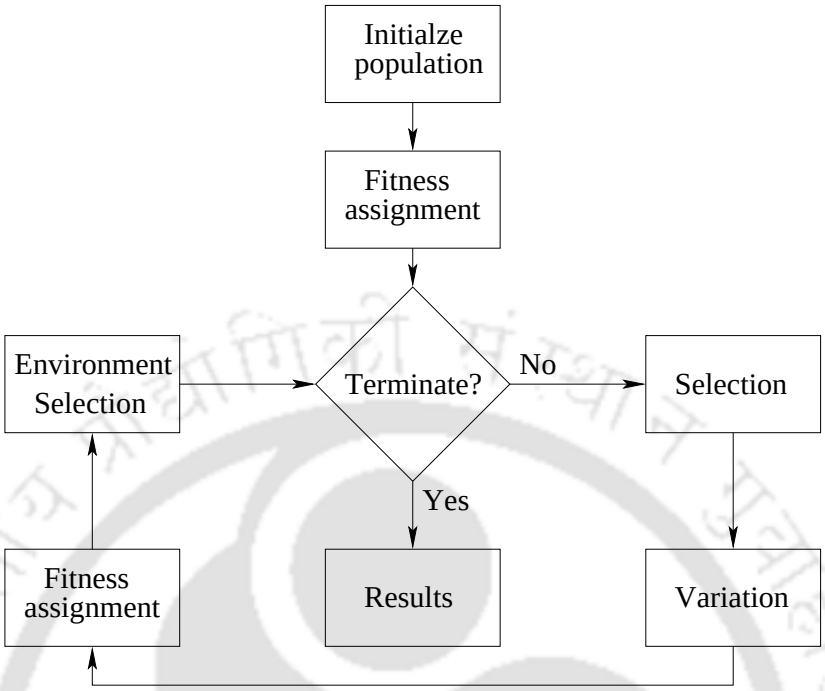

Figure B.1: A generalized framework for EMO techniques.

solutions. In the loop of generation, the crowded binary tournament selection operator is used for creating a mating pool in which two solutions from the population are chosen at random for comparison. Solution with better rank is selected over other. If both solutions have same rank, then solution with larger crowding distance value is selected. In case of tie, any solution is selected randomly. Simulate binary crossover operator is performed on the mating pool and polynomial mutation operator is further applied to the newly created solutions Deb and Agrawal (1995). Environment selection is performed in which a combined population is constructed from the last generation population and newly created population. The best solutions are chosen from the combined population to fill the next generation population. The solutions from front-1 are copied first followed by other fronts. If size of the last front, that to be included in the next generation population, is more than the remaining size of the next generation population, then solutions are copied one-by-one based on the larger crowding distance value. This completes one generation of NSGA-II.

B.2 SPEA2

SPEA2 is known as strength Pareto evolutionary algorithm-2 proposed by Zitzler et al. (2002). It maintains archive of size equal to the population size to keep the non-dominated solutions. The fitness is assigned to each solution by calculating strength value first. For example, strength value of solution i is the number of solutions it dominates in the population. Thereafter, raw fitness for solution i is calculated by summing strength of other solutions, which dominated solutions i. The non-dominated solution is assigned with zero raw fitness value. The density for solution i is calculated using the $k-$th nearest neighbor method. The overall fitness of solution i is the summation of the raw fitness and the density. In the loop of generation, the binary tournament selection operator is used in which two solutions are compared randomly based on the fitness. The one with smaller fitness is selected. The variation operators as defined in NSGA-II are used for creating new population. In environment selection, SPEA-2 assigns fitness to the combined solutions of the newly created population and the archive. Thereafter, the non-dominated solutions and good fitness solutions are selected for updating the archive. The new population is transfered to the next generation population. This completes one generation of SPEA2.

B.3 PAES

Pareto archived evolution strategy (PAES) is another benchmark algorithm, which is proposed by Knowles and Corne (1999). For $(\mu+\lambda)$ variant of PAES, initial population of size μ is generated randomly and fitness is assigned using definition 1 mentioned earlier. The non-dominated solutions and other good solutions are copied to the archive of size μ. In the loop of generation, λ copies are made from the archive using the binary tournament selection operator. These copies are mutated using the polynomial mutation operator described in NSGA-II. The fitness of mutated λ solutions is assigned with respect to the archive using definition 1. The fittest μ solutions are copied to the next generation population from $\mu + \lambda$ solutions. The archive is also updated, if any solution is non-dominated from mutated λ solutions. If the number of non-dominated solutions are more than the size of archive, then the objective space is converted into the fixed-size grids. For each grid in the objective space, the number of non-dominated

solutions are counted. Thereafter, solutions are deleted one-by-one from the grids having higher counts of non-dominated solutions to accommodate less crowded non-dominated solutions in the archive. This completes one generation of PAES.

B.4 SMPSO

SMPSO is known as speed-constrained multi-objective particle swarm optimization, which is proposed by Nebro et al. (2009). In particle swarm optimization (PSO), a solution is called as particle and a population of solutions is called as a swarm. In SMPSO, particles are generated randomly and fitness is assigning using the non-dominated sorting operator described in NSGA-II. The non-dominated solutions are then copied to the archive. In the loop of generation, selection operator is not used as shown in Fig. B.1. However, the position of particle i in the swarm at generation t is updated as $x_i^{(t+1)} = x_i^{(t)} + v_i^{(t+1)}$. Velocity of particle (i) is updated as $v_i^{(t+1)} = wv_i^{(t)} + c_1 r_1 (p_{(i,lb)}^{(t)} - x_i^{(t)}) + c_2 r_2 (p_{gb}^{(t)} - x_i^{(t)})$. Here, w adds to the inertia of the particle, c_1 and c_2 are the acceleration coefficients, r_1 and r_2 are the random numbers $\in [0, 1]$, $p_{(i,lb)}^{(t)}$ is the local best of $i - th$ particle, and $p_{gb}^{(t)}$ is the leader in the swarm, which is determined from the archive. The above particle position update is similar to crossover operator. Thereafter, new position of each particle is mutated using the polynomial mutation operator. The fitness is then assigned to all new particles and their local best positions are updated. The non-dominated solutions of the new particles are then used for updating the archive. If more number of the non-dominated solutions are generated than the size of the archive, the crowding distance operator described in NSGA-II is used to choose less crowded solutions for filling the archive. This completes one generation of SMPSO.

B.5 GDE3

GDE3 is a generalized differential evolution algorithm, which is developed by Kukkonen and Lampinen (2005). The initial population is generated randomly and the fitness is calculated for each solution, which is referred as decision vector, using the non-dominated sorting operator. In the loop of generation, a trail vector for each decision vector i is created by randomly picking four decision vectors from the population.

The creation of trial vector i involves addition of a scaled vector difference of two randomly chosen vectors with third randomly chosen vector from the population with some probability that is called as crossover probability. The scaled vector difference acts like a mutation operation. A new decision vector i is created using old decision vector i and trial vector i. Now, old decision vector i and new decision vector i are compared and one is selected as described in NSGA-II for the next generation population. At this stage, the number of selected solutions can be larger than the population size. Here, NSGA-II's environment selection is performed to select the non-dominated and other good solutions for the next generation population. This completes one generation of GDE3.

C Performance Indicators

Since EMO techniques are stochastic in nature, these algorithms are compared using the statistical indicators that are inverse generalized distance (IGD) indicator and hypervolume (HV) indicator. The details are as follows. It is noted that the PO solutions are constructed by copying the non-dominated solutions from the combined solutions of all 30 runs of EMO techniques. Thereafter, only the non-dominated solutions are copied to make a set of PO solutions for determining IGD value.

C.1 Inverse Generalized Distance (IGD) Indicator

Inverse generalized distance (IGD) is calculated as

$$IGD = \frac{(\sum_{i=1}^{|P^*|} d_i^2)^{1/2}}{|P^*|}, \tag{C.1}$$

where P^* is the set of Pareto-optimal solutions, d_i is the Euclidean distance in the objective space between the solution $i \in P^*$ and the nearest member $k \in P_{t+1}$. The distance is calculated as

$$d_i = \min_{k=1}^{|P_{t+1}|} \sqrt{\sum_{m=1}^{M} \left(\frac{f_m^{(i)} - f_m^{(k)}}{f_m^{max} - f_m^{min}} \right)^2}, \tag{C.2}$$

where m is the number of objectives, f_m^{max} and f_m^{min} are the maximum and minimum of $m-$th objective function values in P^*.

C.2 Hypervolume (HV) Indicator

The hypervolume indicator HV measures the hypervolume of that portion of the objective space that is weakly dominated by an approximate set A. This indicator gives the idea of spread quality and has to be maximized. As recommended in the study Knowles et al. (2006), the difference in values of hypervolume indicator between the approximate set A and the reference set R is calculated in this paper, that is, $HV = HV(R) - HV(A)$. The smaller value suggests good spread Zitzler et al. (2003), Knowles et al. (2006).

D Convergence Plots of Chapter 4

Fig. D.1 presents IGD value in every generation for case 2 in which the local search is executed at a regular interval of 10 generations.

Figs. D.2-D.6 show IGD value in every generation for case 3 in which the local search is executed adaptively.

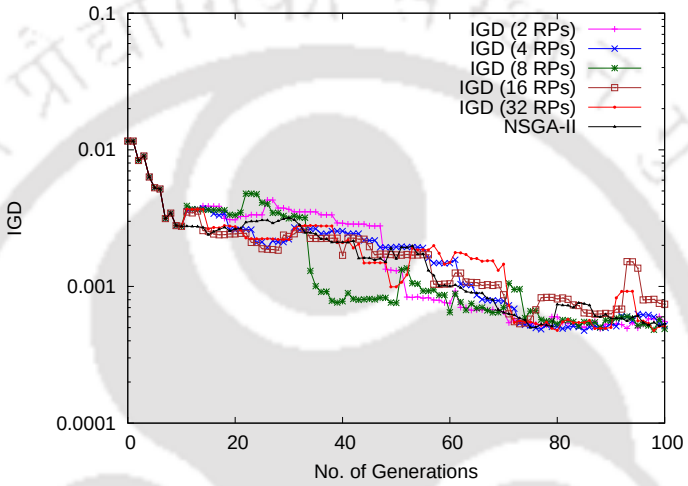

Figure D.1: IGD convergence plot of case 2 for different reference points (RPs).

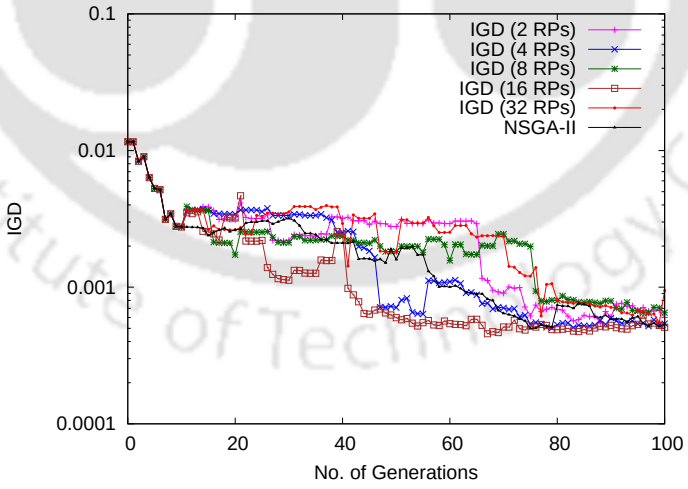

Figure D.2: IGD convergence plot for case 3 by considering $q = 5$.

Figs. D.7-D.11 show IGD value in every generation for case 4 in which the local search is executed at the beginning on the initial population and also, adaptively during the generation.

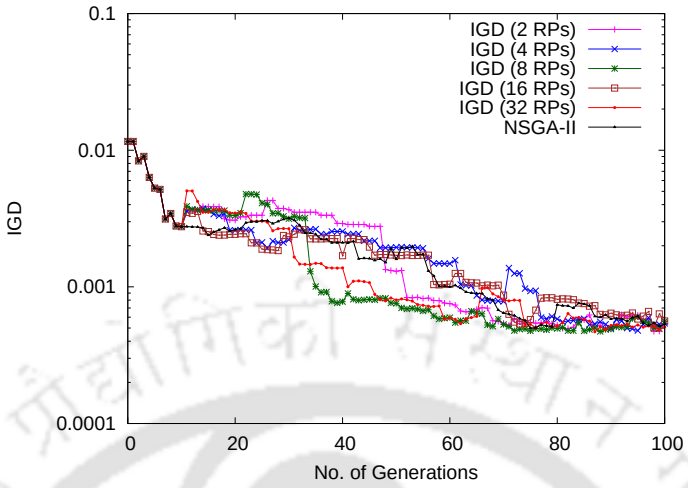

Figure D.3: IGD convergence plot for case 3 by considering $q = 10$.

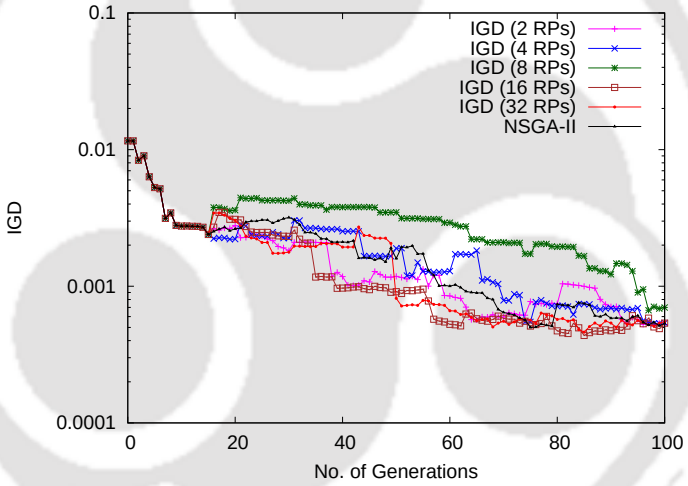

Figure D.4: IGD convergence plot for case 3 by considering $q = 15$.

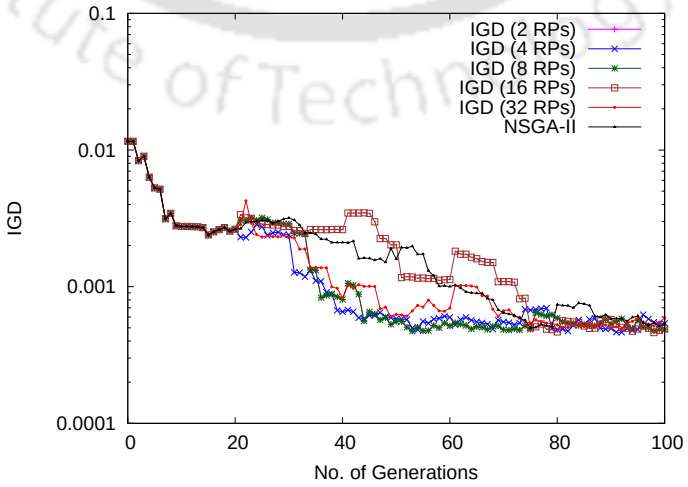

Figure D.5: IGD convergence plot for case 3 by considering $q = 20$.

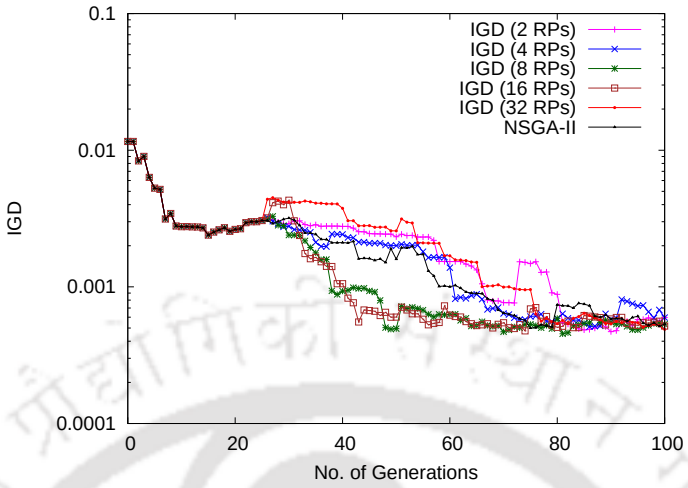

Figure D.6: IGD convergence plot for case 3 by considering $q = 25$.

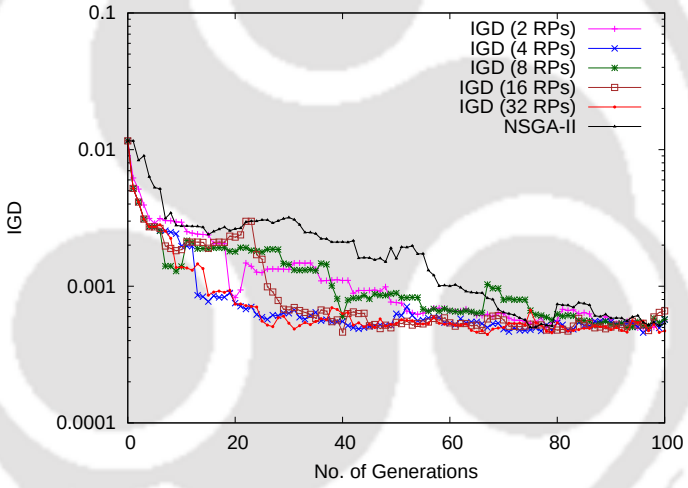

Figure D.7: IGD convergence plot for case 4 by considering $q = 5$.

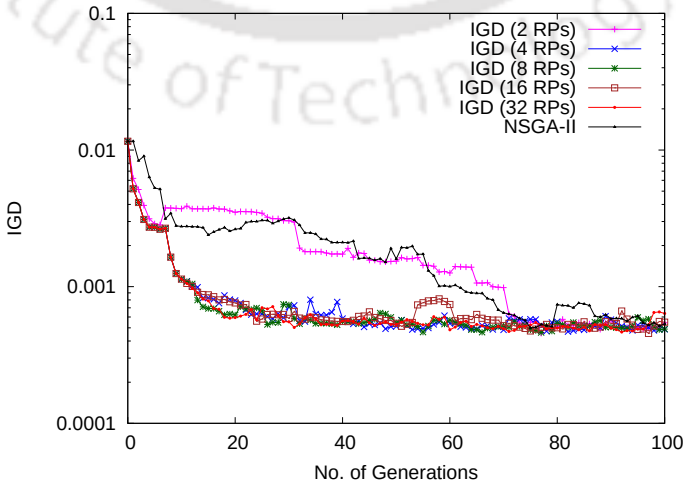

Figure D.8: IGD convergence plot for case 4 by considering $q = 10$.

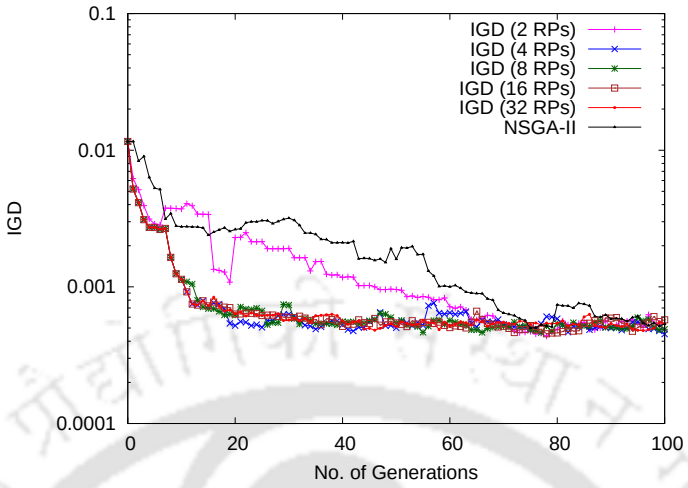

Figure D.9: IGD convergence plot for case 4 by considering $q = 15$.

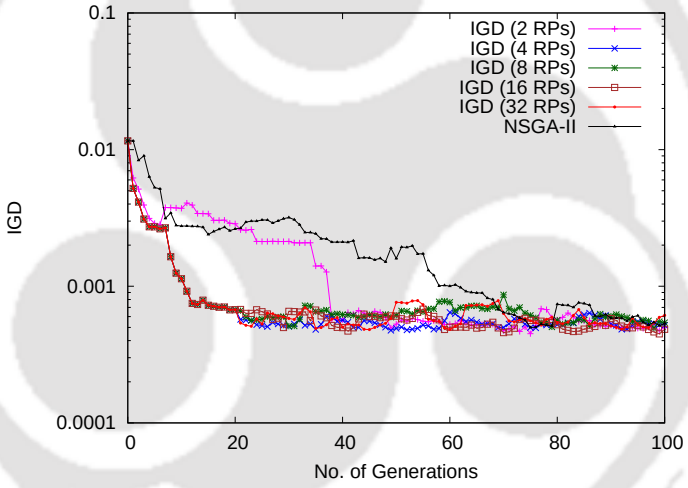

Figure D.10: IGD convergence plot for case 4 by considering $q = 20$.

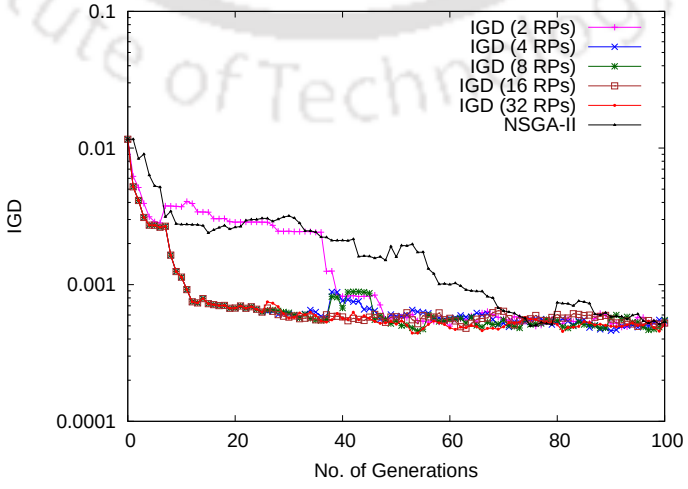

Figure D.11: IGD convergence plot for case 4 by considering $q = 25$.

References

Abo-Elnor, M., Hamilton, R. & Boyle, J. T. (2003), '3D dynamic analysis of soil-tool interaction using the finite element method', *Journal of Terramechanics* **40**(1), 51 – 62.

Abo-Elnor, M., Hamilton, R. & Boyle, J. T. (2004), 'Simulation of soil-blade interaction for sandy soil using advanced 3D finite element analysis', *Soil and Tillage Research* **75**(1), 61 – 73.

Armin, A., Fotouhi, R. & Szyszkowski, W. (2014), 'On the FE modeling of soil-blade interaction in tillage operations', *Finite Elements in Analysis and Design* **92**, 1 – 11.

Bagster, D. F. & Bridgwater, J. (1967), 'The measurement of the force needed to move blades through a bed of cohesionless granules', *Powder Technology* **1**(4), 189 – 198.

Baishya, N. J., Sharma, D. & Dixit, U. S. (2014), 'Optimization of pressure vessel under thermo-elastic condition', *Journal of The Institution of Engineers (India): Series C* **95**(4), 389–400.
URL: *http://dx.doi.org/10.1007/s40032-014-0149-6*

Barakat, N. & Sharma, D. (2017), 'Modelling and bi-objective optimization of soil cutting and pushing process for bulldozer and its blade', *Journal of The Institution of Engineers (India): Series C* .
URL: *https://doi.org/10.1007/s40032-017-0421-7*

Bentaher, H., Ibrahmi, A., Hamza, E., Hbaieb, M., Kantchev, G., Maalej, A. & Arnold, W. (2013), 'Finite element simulation of moldboard-soil interaction', *Soil and Tillage Research* **134**, 11 – 16.

Bosman, P. A. N. (2012), 'On gradients and hybrid evolutionary algorithms for real-valued multiobjective optimization', *IEEE Transactions on Evolutionary Computation* **16**(1), 51–69.

Caterpiller (1996), *Caterpillar Performance Handbook*, 27 edn, Caterpillar Inc.

Chen, B., Zeng, W., Lin, Y. & Zhang, D. (2015), 'A new local search-based multiobjective optimization algorithm', *IEEE Transactions on Evolutionary Computation* **19**(1), 50–73.

Das, I. & Dennis, J. E. (1998), 'Normal-boundary intersection: A new method for generating the Pareto surface in nonlinear multicriteria optimization problems', *SIAM Journal on Optimization* **8**(3), 631–657.

Deb, K. (2001), *Multi-Objective Optimization using Evolutionary Algorithms*, first edn, Chichester, UK: Wiley.

Deb, K. & Agrawal, R. B. (1995), 'Simulated binary crossover for continuous search space', *Complex Systems* **9**(2), 115–148.

Deb, K. & Jain, H. (2014), 'An evolutionary many-objective optimization algorithm using reference-point-based nondominated sorting approach, part I: Solving problems with box constraints', *IEEE Transactions on Evolutionary Computation* **18**(4), 577–601.

Deb, K., Miettinen, K. & Chaudhuri, S. (2010), 'Toward an estimation of Nadir objective vector using a hybrid of evolutionary and local search approaches', *IEEE Transactions on Evolutionary Computation* **14**(6), 821–841.

Deb, K., Miettinen, K. & Sharma, D. (2009), A hybrid integrated multi-objective optimization procedure for estimating nadir point, *in* M. Ehrgott, C. M. Fonseca, X. Gandibleux, J.-K. Hao & M. Sevaux, eds, 'Evolutionary Multi-Criterion Optimization', Springer Berlin Heidelberg, Berlin, Heidelberg, pp. 569–583.

Deb, K., Pratap, A., Agarwal, S. & Meyarivan, T. (2002), 'A fast and elitist multiobjective genetic algorithm: NSGA-II', *IEEE Transactions on Evolutionary Computation* **6**(2), 182 –197.

Deb, K. & Srinivasan, A. (2006), Innovization: Innovating design principles through optimization., *in* 'Proceedings of the Genetic and Evolutionary Computation Conference (GECCO-2006)', New York: The Association of Computing Machinery (ACM), pp. 1629–1636.

Godwin, R. J. & Spoor, G. (1977), 'Soil failure with narrow tines', *Journal of Agricultural Engineering Research* **22**(22), 213–228.

Gupta, P. D., Gupta, C. P. & Pandey, K. P. (1989), 'An analytical model for predicting draft forces on convex-type wide cutting blades', *Soil and Tillage Research* **14**(2), 131 – 144.

Haimes, Y. Y., Lasdon, L. S. & Wismer, D. A. (1971), 'On a bicriterion formulation of the problems of integrated system identification and system optimization', *IEEE Transaction on Systems, Man, and Cybernetics* **1**(3), 396–297.

Hettiaratchi, D. R. P. & Reece, A. R. (1967), 'Symmetrical three-dimensional soil failure', *Journal of Terramechanics* **4**(3), 45–67.

Hettiaratchi, D. R. P. & Reece, A. R. (1974), 'The calculation of passive soil resistance', *Géotechnique* **3**(24), 289–310.

Ishibuchi, H. & Murata, T. (1996), 'Multi-objective genetic local search algorithm', *IEEE Transaction on Evolutionary Computation* **28**, 119–124.

Ishibuchi, H. & Narukawa, K. (2004), Some issues on the implementation of local search in evolutionary multiobjective optimization, *in* K. Deb, ed., 'Genetic and Evolutionary Computation – GECCO 2004', Springer Berlin Heidelberg, Berlin, Heidelberg, pp. 1246–1258.

Ishibuchi, H., Yoshida, T. & Murata, T. (2003), 'Balance between genetic search and local search in memetic algorithms for multiobjective permutation flowshop scheduling', *IEEE Transactions on Evolutionary Computation* **7**(2), 204–222.

Jack, E. & Liu, C. (1985), 'Unified soil classification system (USCS)', *Classification of Soils for Engineering Purposes: Annual Book of ASTM Standards* **08**(1), 395408.

Jaszkiewicz, A. (2002), 'Genetic local search for multi-objective combinatorial optimization', *European Journal of Operational Research* **137**(1), 50 – 71.
URL: *http://www.sciencedirect.com/science/article/pii/S0377221701001047*

Karmakar, S. & Kushwaha, R. L. (2006), 'Dynamic modeling of soil-tool interaction: An overview from a fluid flow perspective', *Journal of Terramechanics* **43**(4), 411 – 425.

Ke, L., Zhang, Q. & Battiti, R. (2014), 'Hybridization of decomposition and local search for multiobjective optimization', *IEEE Transactions on Cybernetics* **44**(10), 1808–1820.

King, R. H., Susante, P. V. & Gefreh, M. A. (2011), 'Analytical models and laboratory measurements of the soil-blade interaction force to push a narrow tool through JSC-1A lunar simulant and ottawa sand at different cutting depths', *Journal of Terramechanics* **48**(1), 85–95.

Knowles, J. & Corne, D. (1999), The Pareto archived evolution strategy: a new baseline algorithm for Pareto multiobjective optimisation, *in* 'Proceedings of the 1999 Congress on Evolutionary Computation-CEC99 (Cat. No. 99TH8406)', Vol. 1, p. 105 Vol. 1.

Knowles, J. D. & Corne, D. W. (2000), M-PAES: a memetic algorithm for multiobjective optimization, *in* 'Proceedings of the 2000 Congress on Evolutionary Computation. CEC00 (Cat. No.00TH8512)', Vol. 1, pp. 325–332 vol.1.

Knowles, J., Thiele, L. & Zitzler, E. (2006), A tutorial on the performance assessment of stochastic multiobjective optimizers, TIK Report 214, Computer Engineering and Networks Laboratory (TIK), ETH Zurich.

Kukkonen, S. & Lampinen, J. (2005), GDE3: The third evolution step of generalized differential evolution, *in* 'IEEE Congress on Evolutionary Computation (CEC'2005)', pp. 443 – 450.

Kumar, A., Sharma, D. & Deb, K. (2007), A hybrid multi-objective optimization procedure using PCX based NSGA-II and sequential quadratic programming, *in* '2007 IEEE Congress on Evolutionary Computation', pp. 3011–3018.

Kushwaha, R. L., chi, L. & Shen, J. (1993), 'Analytical and numerical models for predicting soil forces on narrow tillage tools', *Canadian Agriculture Engineering* **35**(3), 183–193.

Lara, A., Sanchez, G., Coello, C. A. C. & Schutze, O. (2010), 'HCS: A new local search strategy for memetic multiobjective evolutionary algorithms', *IEEE Transactions on Evolutionary Computation* **14**(1), 112–132.

Luengo, O., Singh, S. & Cannon, H. (1998), Modeling and identification of soil-tool interaction in automated excavation, *in* 'Proceedings. 1998 IEEE/RSJ International Conference on Intelligent Robots and Systems. Innovations in Theory, Practice and Applications (Cat. No.98CH36190)', Vol. 3, pp. 1900–1906.

McKyes, E. (1985), *Soil Cutting and Tillage*, Elsevier, New York.

McKyes, E. & Ali, O. S. (1977), 'The cutting of soil by narrow blades', *Journal of Terramechanics* **14**(2), 43–58.

Miettinen, K. (1998), *Nonlinear Multiobjective Optimization*, Vol. 12, 1 edn, Springer US, Springer Science Business Media New York. International Series in Operations Research & Management Science.

Murata, T., Nozawa, H., Tsujimura, Y., Gen, M. & Ishibuchi, H. (2002), Effect of local search on the performance of cellular multiobjective genetic algorithms for designing fuzzy rule-based classification systems, *in* 'Proceedings of the 2002 Congress on Evolutionary Computation, 2002. CEC '02', Vol. 1, pp. 663–668.

Nebro, A. J., Durillo, J. J., Garcia-Nieto, J., Coello, C. A. C., Luna, F. & Alba, E. (2009), SMPSO: A new PSO-based metaheuristic for multi-objective optimization, *in* '2009 IEEE Symposium on Computational Intelligence in Multi-Criteria Decision-Making(MCDM)', pp. 66–73.

Obermayr, M., Dressler, K., Vrettos, C. & Eberhard, P. (2011), 'Prediction of draft forces in cohesionless soil with the discrete element method', *Journal of Terramechanics* **48**(5), 347 – 358.

Perumpral, J. V., Grisso, R. D. & Desai, C. (1983), 'A soil-tool model based on limited equilibrium analysis', *Transactions of the American Society of Agriculture Engineers* **26**(4), 991–995.

Qinsen, Y. & Shuren, S. (1994), 'A soil-tool interaction model for bulldozer blades', *Journal of Terramechanics* **31**(2), 55–65.

Reece, A. R. (1964), 'The fundamental equation of earth-moving mechanics', *Proceedings of the Institution of Mechanical Engineers* **179**, 16–22.

Ren, L., Han, Z., Li, J. & Tong, J. (2002), 'Effects of non-smooth characteristics on bionic bulldozer blades in resistance reduction against soil', *Journal of Terramechanics* **39**(4), 221 – 230.

Ren, L., Tong, J., Zhang, S. & Cheng, B. (1995), 'Reducing sliding resistance of soil against bulldozing plates by unsmoothed bionics surfaces', *Journal of Terramechanics* **32**(6), 303 – 309.

Sharma, D. (2010), On the flexible applied boundary and support conditions of compliant mechanisms using customized evolutionary algorithm, *in* 'Proceedings of Simulated Evolution and Learning - 8th International Conference, SEAL 2010', Springer, pp. 105–114.

Sharma, D. & Deb, K. (2014), 'Generation of compliant mechanisms using hybrid genetic algorithm', *Journal of The Institution of Engineers (India): Series C* **95**(4), 295–307.
URL: *https://doi.org/10.1007/s40032-014-0127-z*

Sharma, D., Deb, K. & Kishore, N. (2008), Towards generating diverse topologies of path tracing compliant mechanisms using a local search based multi-objective genetic algorithm procedure, *in* 'Evolutionary Computation, 2008. CEC 2008. (IEEE World Congress on Computational Intelligence). IEEE Congress on', IEEE, pp. 2004 –2011.

Sharma, D., Deb, K. & Kishore, N. N. (2011), 'Domain-specific initial population strategy for compliant mechanisms using customized genetic algorithm', *Structural and Multidisciplinary Optimization* **43**(4), 541–554.

Sharma, D., Deb, K. & Kishore, N. N. (2014), 'Customized evolutionary optimization procedure for generating minimum weight compliant mechanisms', *Engineering Optimization* **46**(1), 39–60.

Sharma, D., Kumar, A., Deb, K. & Sindhya, K. (2007), Hybridization of SBX based NSGA-II and sequential quadratic programming for solving multi-objective optimization problems, *in* '2007 IEEE Congress on Evolutionary Computation', pp. 3003–3010.

Shmulevich, I., Asaf, Z. & Rubinstein, D. (2007), 'Interaction between soil and a wide cutting blade using the discrete element method', *Soil and Tillage Research* **97**(1), 37 – 50.

Shukla, P. K. & Deb, K. (2007), 'On fnding multiple Pareto-optimal solutions using classical and evolutionary generating methods', *European Journal of Operational Research* **181**, 1630–1652.

Sindhya, K., Deb, K. & Miettinen, K. (2008), A local search based evolutionary multi-objective optimization approach for fast and accurate convergence, *in* G. Rudolph, T. Jansen, N. Beume, S. Lucas & C. Poloni, eds, 'Parallel Problem Solving from Nature – PPSN X', Springer Berlin Heidelberg, Berlin, Heidelberg, pp. 815–824.

Sindhya, K., Miettinen, K. & Deb, K. (2013), 'A hybrid framework for evolutionary multi-objective optimization', *IEEE Transaction on Evolutionary Computation* **17**(4), 495–511.

Sindhya, K., Sinha, A., Deb, K. & Miettinen, K. (2009), Local search based evolutionary multi-objective optimization algorithm for constrained and unconstrained problems, *in* '2009 IEEE Congress on Evolutionary Computation', pp. 2919–2926.

Swick, W. & Perumpral, J. (1988), 'A model for predicting soil-tool interaction', *Journal of Terramechanics* **25**(1), 43 – 56.

Terzaghi, K. (1943), *Theoretical Soil Mechanics*, John Wiley and Sons Inc.

Tsuji, T., Nakagawa, Y., Matsumoto, N., Kadono, Y., Takayama, T. & Tanaka, T. (2012), '3D DEM simulation of cohesive soil-pushing behavior by bulldozer blade', *Journal of Terramechanics* **49**(1), 37 – 47.

Wislicki, A. (1969), 'The influence of soil condition on the performance of a tracklayer operating a bulldozer', *Journal of Terramechanics* **6**(2), 35 – 45.

Xia, K. (2008), 'A framework for earthmoving blade/soil model development', *Journal of Terramechanics* **45**(5), 147 – 165.

Zhang, Q. & Li, H. (2007), 'MOEA/D: A multiobjective evolutionary algorithm based on decomposition', *IEEE Transactions on Evolutionary Computation* **11**(6), 712–731.

Zhang, R., Chen, B., Li, J.-Q. & Xu, S.-C. (2008), 'DEM simulation of clod crushing by bionic bulldozing plate', *Journal of Bionic Engineering* **5**, 72 – 78.

Zitzler, E., Laumanns, M. & Thiele, L. (2002), SPEA2: Improving the strength Pareto evolutionary algorithm for multiobjective optimization, *in* K. Giannakoglou et al., eds, 'Evolutionary Methods for Design, Optimisation and Control with Application to Industrial Problems (EUROGEN 2001)', International Center for Numerical Methods in Engineering (CIMNE), pp. 95–100.

Zitzler, E., Thiele, L., Laumanns, M., Fonseca, C. M. & Fonseca, V. (2003), 'Performance assessment of multiobjective optimizers: An analysis and review', *IEEE Transactions on Evolutionary Computation* **7**(2), 117–132.